University of Southern Queensland

Faculty of Engineering and Surveying

THE PRELIMINARY STUDY ON THE MECHANICAL PROPERTIES OF HEAT-TREATED BOVINE BONE USING EXPERIMENTAL AND SIMULATIONS APPROACHES

A dissertation submitted by

Mei-ling Lau

For the award of
DOCTOR OF PHILOSOPHY

2013

ABSTRACT

A critical factor that leads to bone fracture is the deterioration of bone quality. For a severe bone fracture that incurs a loss of volume, bone is unable to recover and bone grafting may be needed. Heat-treatment of bone is proposed as one of the most reliable and simple sterilisation methods to overcome the risk of rejection and disease transfer during transplantation.

The mechanical properties of bone at the micro-structural level after heat-treatment are not well characterised. To address this, this study investigated the localised mechanical properties of micro-structural tissues with the global structural level at different pre-set temperature ranges. Bovine cortical bone was used in this study as it has similar structure and morphology to human bone.

The results of the nanoindentation test demonstrated that heat-treated cortical bones can maintain relatively high elastic modulus (E) and nanoindentation hardness (H) among values between of 90^0C to 150^0C as compared to those of pristine bone. A significant increase of 44% (longitudinal) and 23% (transverse) of E values were found when compared to pristine bone. Also, an increase of 43% and 38% of H values in longitudinal and transverse directions respectively were found when compared to pristine bone. Furthermore, the E and H values of interstitial lamellae in this study at various temperatures are from 18.4 to 30.5 (GPa) and 0.84 to 1.27 (GPa),

respectively. The E and H values of osteon are from 18.6 to 28.8 (GPa) and 0.83 to 1.25 (GPa), respectively.

In the current study, compressive testing was employed to measure the global stiffness (E) of the bone samples. When heated at 150°C, the bone specimens showed an increase of 60% in stiffness (E) and an increase of 26% in yield stress. On the other hand, when heated at 90°C, a slight increase of 11.4% in stiffness (E) and 21.5% in yield stress was recorded.

Backscattered Electron (BSE) imaging was conducted to examine the relationship between mineral content and mechanical strength within the nanoindentation regions. The data demonstrated that the non heat-treated bones obtained the highest calcium wt% amongst the three groups. As temperature increased, there was a slight decrease in calcium wt%; however, the changes were not severe in this study.

Thermal gravimetric analysis (TGA) was used to investigate the condition of organic constituents of the bovine cortical bone. The TGA results demonstrated that heat-treated bones had three stages of weight loss. The first stage was the loss of water, which started from room temperature to 160°C. The second stage included a weight loss of organic constituents starting from 200°C to 600°C. Upon reaching 600°C, the organic constituents were decomposed and mineral phase loss started taking place until 850°C.

Computational modeling – finite element analysis (FEA) was conducted to investigate the relationship between the porosity and the mechanical properties of two main components of the cortical bone. Varying the diameters of the Haversian canal and the distribution of Volkman's canals in osteonal bone models showed a significant difference. This means that the increase of the porosity apparently affected the elastic modulus of cortical bone. This validated FE model is able to simulate the bone properties with the consideration of different bone porosity and its heterogeneous mechanical properties in osteonal and interstitial bone's longitudinal and lateral directions.

Suggestions for further study of the mechanical and chemical properties of heat-treated cortical bone for clinical applications are presented.

ASSOCIATED PUBLICATIONS

The following publications were produced during the period of candidature:

Journal Papers:

Mei-Ling Lau, Kin-Tak Lau, Yan-Dong Yao Yeo, Chi-ting Au Yeung, and Joong-Hee Lee, "Measurement of Bovine Bone Properties through Surface Indentation Technique", *Materials and Manufacturing Processes*, No. 25, 2010, pp 324–328.

Mei-Ling Lau, Kin-Tak Lau, Harry Ku, Debes Bahattacharyya and Yan-Dong Yao, "Measurements of Heat treatment Effects on Bovine Cortical Bones by Nanoindentation and Compression Testing", *Journal of Biomaterials and Nanobiotechnology*, No. 3, 2012, pp 105-113

Mei-Ling Lau, Kin-Tak Lau, Harry Ku, Francisco Cardona and Joong-Hee Lee, "Analysis of Heat-treated Bovine Cortical Bone by Thermal Gravimetric and Nanoindentation", *Composites B (Accepted)*

Mei-Ling Lau, Kin-Tak Lau, Harry Ku, "Mechanical Properties of Heat-treated Bovine Cortical Bones by Nanoindentation", *Bones* (*Under reviewing*)

Mei-Ling Lau, Kin-Tak Lau, Yan-Sheng Yin, Lan Li, May Wong, Kevin Chan, and William Chen, "A Shape Memory Alloy Energy Absorber for Backpack Design", *Materials and Manufacturing Processes*, No.25, 2010, pp 281–286.

Conference Paper:

Mei-Ling Lau, Kin-Tak Lau and Yan-Dong Yao Yeo, "Experimental Measurement of Cortical Bone Properties", *The 17th International Conference on Composites or Nano Engineering (ICCE-17), Hawaii, U.S.*, July 2009.

Mei-Ling Lau, Kin-Tak Lau, Yan-Dong Yao and Debes Bahattacharyya, "A Study on Bone Properties using Nanoindentation Technique", *Processing and Fabrication of Advanced Materials XIX (PFAM-19)*, New Zealand, January 2011.

Mei-Ling Lau, Kin-Tak Lau, Harry Ku, Debes Bahattacharyya and Joong-Hee Lee "Assessing Heat-treatment Effects on Bovine Cortical Bones by Nanoindentation", *Processing and Fabrication of Advanced Materials XX (PFAM-20)*, December 2011.

CERTIFICATION OF DISSERTATION

I certify that the ideas, designs and experimental work, results, analyses and conclusions set out in this dissertation are entirely my own effort, except where otherwise indicated and acknowledged.

I further certify that the work is original and has not been previously submitted for assessment in any other course or institution, except where specifically stated.

Sindy, Mei Ling Lau

0061014581

_____

Signature of Candidate

_____

Date

ENDORSEMENT

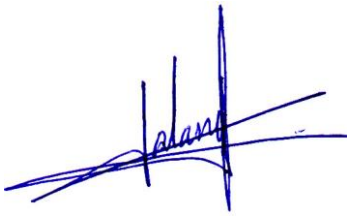

_____ _____

Signature of Principle Supervisor Signature of Associate Supervisor

_____ 27/02/2013

Date Date

ACKNOWLEDGEMENTS

I would like to express my most sincere appreciation to my PhD project supervisors Dr. Harry Ku and Prof. Alan Kin-Tak Lau for all their support, encouragement, valuable inputs and guidance provided at every stage of this thesis. I would also like to extend my gratitude toward the entire departmental and technical staffs, including Dr. Francisco Cardona and Mohan Trada for their assistance and support in using facilities and materials for conducting the experimental work. Special thanks to Annmaree Jackson for her contribution to edit the thesis and to all people who have been actively involved in carrying out this thesis and those who have given me this opportunity to do this thesis.

In addition, I wish to express my deepest appreciation to my family and sisters Kit Hing, Mei Lan and Mei To for their constant support throughout the study. I would like to extend my appreciation to my friends for their encouragement. Special thankful and grateful to Ahmed Naji for his supported and encouraged me all these days.

A particular appreciation is also extended to the University of Southern Queensland and the Centre of Excellence in Engineered Fibre Composites for financial support.

TABLE OF CONTENTS

LIST OF FIGURES

LIST OF TABLES

LIST OF ABBREVIATIONS

2-D	Two-dimensional
3-D	Three-dimensional
AFM	Atomic force microscopy
ANOVA	Analysis of variance
BMU	Basic multicellular unit
BSE	Backsattered electron
Ca	Cacium
Co-Cr	Cobalt-chromium alloy
CT	Computed tomography
d	Gauge diameter
DOF	Degree of Freedom
E	Young's modulus or modulus of elasticity
EDX or EDS	Energy dispersive X-ray spectroscopy
FEA	Finite element analysis
FEM	Finite element modeling
GH	Growth hormone
H	Hardness
HA	Hydroxyaptite
HIV	Human immunodeficiency virus
IOF	International Osteoporosis Foundation
L	Longitudinal

MR	Magnetic resonance
NI	Nodal interpolation
OI	Osteogenesis imperfect
P	Phosphorous
PBS	Phosphate-buffered Saline
PCL	Polycaprolactone
PE	Polyethylene
PGA	Poly (glycolic acid)
PLA	Poly (lactic acid)
PLGA	Poly (lactic-*co*-glycolic acid)
PLLA	Poly- L-lactic acid
PMMA	Polymethyl methacrylate
pQCT	Peripheral quantitative computed tomography
PTH	Parathyroid hormone
QCT	Quantitatively computed tomography
R-curve	Propagation toughness
RT	Room temperature
SD	Standard deviation
SEM	Scanning electron microscope
SHPB	Split Hopkinson Pressure Bar
T	Transverse
Ti	Titanium alloy
TCP	Tricalcium phosphate
TEM	Transmission electron microscopy

TFB	Treated femur bone
TRB	Treated rib bone
TGA	Thermal gravimetric analysis
UFB	Untreated femur bone
URB	Untreated rib bone
USA	United States of America
XRD	X-ray diffraction

Equation parameters:

A	Area
Ac	Projected contact area
Er	Reduce modulus
Ei	Elastic modulus of indentor
Es	Elastic modulus of specimen
νi	Poisson’s ratio of indentor
νs	Poisson’s ratio of specimen
Pmax	maximum indentation force
σ	Compressive stress
ε	Compressive strain
P	Applied force
S	Contact stiffness
ξ, η, ζ	Global degree of freedom
u,*v*,*w*	Local degree of freedom

Unit:

%	Percent
^{o}	Degree
^{o}C	Degree Celsius
cm	Centimeter
cm^3/min	Cubic centimeter per minute
GPa	Giga pascal
kN	Kilo-newton
mg/dl	Milligrams per deciliter
mm	Millimeter
mm^3	Cubic millimeter
mN	Millinewton
µm	Micron-meter
MPa	Mega pascal
Nm	Nanometer
wt%	Weight percent

Chapter 1

Introduction

Bone is defined as a special connective tissue. Its principal biological role is devoted to fundamental physiological functions with limited amounts of deformation during loading activities such as jumping or running. Similar to other engineering structures, the skeleton system has engineered a functional structure with unique material to respond to the intensive loading applied continuously (vertebral spine to support the body when sitting) and cyclically (femur and tibia when walking) during daily activities (Martin et al. 1998). Under the continuing loading or cyclic loads; some micro-cracks can be easily observed, even within the healthy bone. As these micro-cracks grow faster than bone remodeling, the eventual consequence is the complete fracture of bone. Other common causes of bone fracture are developmental deformities, resorption disturbance, trauma, poor diet, and lack of exercise (Kenley et al. 1993; Gupta et al. 2008).

Murugan et al. (2005) reported that approximately 6.3 million bone fractures occur in the United States of America (USA) every year. Among them, approximately

550,000 cases need bone grafting. It also expected that the number of hip replacements required in the United States of America (USA) will increase to around 272,000 cases by the year of 2030 compared to 152,000 in the year 2000. It has also been reported there were about 2.2 million bone graft procedures globally with the estimated cost approaching $2.5 billion per annum (Laurencin et al. 2009). A report published by the International Osteoporosis Foundation (IOF-2009) on osteoporosis issues within Asian country populations found that over the past decades, the number of reported hip fractures increased by 300% in Hong Kong; and by 500% in Singapore. A dramatic increase in the number of bone fractures in people over 75 years of age was found in Japan over past 12 years. In mainland China, it was found that 687,000 people aged over 50 years of age who incurred a hip fracture within a year period, had also been diagnosed with osteoporosis. Treatment of bone fractures has increased its significance in health concern among countries and continues to be a major burden as the population ages (Ritchie et al. 2004; IOF 2009).

A critical factor involved in bone fracture is the deterioration of bone quality in bone tissues. Osteoporosis is a bone resorption disturbance which mainly affects women after menopause. It is developed when the equilibrium of bone resorption and formation is difficult to maintain (Lau et al. 1997; Massaro et al. 2004). Low bone mass and deterioration of bone are characteristic of this skeletal disease, leading to bone fragility. Osteoporosis is also associated with a high risk of bone fractures of the hip, spine, tibia, fibula, wrist and ankle (Lau et al. 1997; Massaro et al. 2004; Murugan et al. 2005). Apart from the deterioration of bone mass that is associated to

bone fracture, a genetic disorder called Osteogenesis inperfect (OI) results in the decrease of type 1 collagen or the production of abnormal collagen and causes bones to break easily (niams.nih.gov, viewed on October, 2010). Osteogenesis imperfecta (OI) is characterised by varied degrees of skeletal fragility due to abnormalities caused by genetic defects in the supply of, and quality of type 1 collagen (orpha.net, viewed on October, 2010). As the genetic defects of lower levels of collagen affect the ability of the body to built strong bones, it is therefore difficult to provide mechanical support and results in a decrease to the load bearing strength. Osteoporosis and OI are diagnosed by examining the structural arrangements and material compositions of bone in determining the bone condition. Monitoring of mineral density and bone mass levels are effective in predicting the risk of fracture (Tatarinov et al. 2005).

It is important to understand the mechanics and mechanisms of bone fracture, both from materials and structural properties. The main motivation is to evaluate the fracture behavior of bone so that clinical diagnoses and therapy can be conducted, such as fractures fixation or reconstruction procedures (An et al. 2000). A complete understanding of hierarchical structure of bone from macroscopic to nanoscale dimensions is also important. Different hierarchical levels are contributed to distinct characteristics that influence the mechanical response (An et al. 2000). Extensive research has been conducted in the past decades to study the structural arrangements, material compositions and mechanical properties of bone (Rho et al. 1998a & 1999a; Catanese III et al. 1999; Jämsä et al. 2002; Shin et al. 2005; Tatarinov et al. 2005;

Fan et al. 2006; Ferreira et al. 2006; Hoc et al. 2006; Stanishevsky et al. 2008) in order to understand bone problems such as bone fracture, bone remodeling, and the design of bone-implant systems. Various methods have been used to visualise the internal architecture of the cancellous bone to create *in vivio* images of whole bone, such as quantitative computed tomography (QCT) and magnetic resonance (MR) (van Rietbergen et al. 1998). With the combination of finite element (FE) modelling, the elastic and failure properties of the cancellous bone can be quantified directly from high-resolution images of QCT and MR (van Rietbergen et al. 1998; Fan et al. 2004; Ural et al. 2006 & 2007). Mechanical testing (Bowman et al. 1996; Currey et al. 1998; Catanese III et al. 1999; Shin et al. 2005; Kotha et al. 2007) and nanoindentation testing (Rho et al. 1997; Rho et al. 1999b; Turner et al. 1999; Zysset et al. 1999; Oyen 2006; Wang et al. 2006) have been used to measure the elastic modulus and hardness of cortical and cancellous bone. For example, Ferreira et al. (2006) applied the Split Hopkinson Pressure Bar (SHPB) technique to measure the mechanical properties of bovine bones. The SHPB is composed by a gas gun and three lined up cylindrical slender bars; the second and third bars represent as an input and output bars, then the specimen is located between them and attached with strain gauges. They found that the Young's modulus ranged from 7.0 to 8.9 GPa and 4.9 to 9.9 GPa in longitudinal and transverse direction, respectively.

The local mechanical properties of extracellular matrix of bone are typically conducted by using the nanoindentation technique. Nanoindentation testing is one of the promising novel techniques used to quantify the mechanical properties of

microstructures of various materials. This technique evolves from conventional Vickers microhardness test allows for assessment of mechanical properties at the nanometer scale (Hengsberger et al. 2002). With the additional capability of making small indentations at precise positions on microstructural features while concurrently various parameters such as load and depth of penetration can be measured. The nanoindentation is well suited to examine the microstructual features of material surface to provide a spatial resolution which is less than 1μm (Rho et al. 1997 & 1999a; Akhtar et al. 2005; Hoc. et al. 2006). Since bone tissues vary at different structural levels (from microsturcture of 10 to 500μm to sub-nanostructure of 1 nm) (Akhtar et al. 2005), the mechanical properties of microstructural units of bone tissues down to the osteon level can be explored by using the nanoindentation technique.

By analysing the indentation load-displacement behavior, it is possible to obtain the measurements of the Young's modulus (E), and hardness (H) of the bone (Catanese III et al. 1999; Rho et al. 1999a & b; Wang et al. 2006). Rho et al. (1997) have employed the nanoindentaion technique to indirectly measure the Young's modulus of bone through the observation of the return path of the load-displacement curve. It has been reported that the Young's modulus, measured in the longitudinal direction are 22.5 ± 1.3 GPa for the osteons and 25.8 ± 0.7 GPa for the interstitial lamellae (Rho et al. 1997). Higher elastic moduli of 24.7 ± 2.5 GPa and 30.1 ± 2.4 GPa, for the osteons and the interstitial lamellae of cortical bone in the longitudinal direction, respectively, have been reported by Wang et al. (2006). Wang et al. (2006) also

found that the hardness values of the cortical bone in the longitudinal direction range from 0.41 to 0.89 GPa for the osteons and the interstitial lamellae.

Bone is an amazing nanocomposite which is capable of self healing within a few weeks for minor defects. However, if the fracture is severe and a loss of volume has occurred, then bone is unable to self healing and a bone graft maybe required. Studies have focused on investigating the mechanical properties of bone after heat-treatment (Catanese III et al. 1999; Shin et al. 2005). Autograft bones are the commonly used for human bone replacement, it allows patient to use their own tendons from hip, the ribs or the leg, however they are limited in volume and additional surgery is often needed (Catanese III et al. 1999). Heat-treated cortical bone has been proposed as a substitute for bone transplant material to overcome the risk of rejection and disease transfer of allograft and xenograft implantations (Shin et al. 2005). With advantages obtained in biological (sterilizing against HIV) and mechanical properties (the mechanical strength can be maintain after heat-treatment), it is believed that heat-treated bones can be an excellent alternative material for bone grafts and synthetic bone substitutes, since it maintain the microstructural and ultrastructural features of pristine bone and biocompatible (Catanese III et al.1999; Shin et al. 2005). Catanese III et al. (1999) reported the elastic modulus (mean ± SD) remained similar to that of an non-heated cortical bone along the bone axis, being 16.3 ± 2.2 GPa for compression and 16.3 ± 3.7 GPa for tension when a cortical bone was heated to 350^{o}C. Cortical bone was also found to have maintained 63% of its non-heated strength in compression after being heated to 350^{o}C. The maintenance of

this strength makes it well suited for compressive load-bearing applications such as shares load with (in parallel to) surrounding bone (Catanese III et al. 1999).

Heat-treatment of bone remains one of the most reliable and simple sterilisation methods to overcome the risk of rejection and disease transfer from allograft and xenograft, e.g. for the prevention of human immunodeficiency virus (HIV) infection (Shin et al. 2005). However, the mechanical properties of the micro-structural level after heat-treatment are not well characterised. This research was carried out to address this issue by specially investigating the localised mechanical properties of micro-structural tissues within the global structural level in different pre-set temperature ranges. Bovine cortical bone is employed to carry out the experimental study because its structure and morphology is similar to human bone, and it is a possible bone substitute material for transplantation under appropriate sterilisation methods.

1.1 Aim and Objectives

In recent years, the heat-treatment of banking bones has become one of the simple and practical sterilization methods to preserve bone graft as it has potential to enhance bone growth. It is therefore of a great interest to understand the mechanical properties of the bone's matrix after heat-treatment at various temperature ranges. This project aims to investigate the localised mechanical properties of bovine cortical bone at the micro-structural level after heat-treatment. Additionally, this research project also aims to provide a comprehensive understanding on the relationship

between the micro-structural levels of heat-treated cortical bone and the mechanical properties response.

Mechanical and thermal properties of two types of cortical bones will be tested under various pre-set temperature ranges. The surface nanoindentation technique will be employed to localise the mechanical properties, both elastic modulus and hardness values, of different heat-treated bovine cortical bones in longitudinal and transverse directions. In addition, compressive test will be conducted to characterise the global elastic modulus of bone specimens in longitudinal direction. This research will also examine the correlation between bone mineral content and mechanical strength by using backscattered electron (BSE) imaging. Thermal gravimetric analysis (TGA) will also be used to study weight loss of the cortical bones specimens. In view of the importance of the relationship between microstructural features and the mechanical response in cortical bone, finite element analysis (FEA) will be employed to simulate the microstructural level of the cortical bone.

The objectives of this project are:

- To measure the local mechanical properties of pristine and pre-heated bovine cortical bones in longitudinal and transverse directions;
- To measure the local and global mechanical properties of bovine cortical bone through experimental study by nanoindentation and compression testing;

- To examine the correlation between mineral content and mechanical strength of bovine cortical bones;
- To examine the organic and mineral phases loss through thermal experimental measurement ;
- To stimulate the micro-structural level of cortical bone by computational method in order to observe the effect of porosity and the response of localized mechanical properties

1.2 Outline of Thesis

Bone Structure, Composition and Mechanics

A background review of the skeletal system, such as bone structure, bone composition, and types of bone cells are addressed in Chapter 2. The complex structure of human bone provides distinctive functions for daily activities and bearing of loading. The mechanical properties of bone are highly related to the material properties of bone tissues and structural properties of the whole bone.

Literature Review

Literature on recent research will provide an overview on the difference of - material and structural properties of bone; together with the main factors that affected the bone strength will be reviewed in Chapter 3. Mechanical properties of bone had been under investigation throughout a number of decades. Various mechanical properties tests such as compressive, tensile, torsion, bending, and nanoindentation are

employed to measure the material and architectural properties of bone are presented in this section. The investigation of the correlation between mineral content and mechanical strength of bone will also be reviewed.

Experimental Study

This research attempts to measure the mechanical properties of bovine cortical bone through surface indentation in longitudinal and transverse directions with regard to heat-treated in different temperature ranges. Details of the experimental study are outlined in Chapter 4. Specially, compressive test was conducted in longitudinal direction to characterise the global elastic modulus of bone specimens. Correlation between bone compositions and mechanical strength was investigated by backscattered electron (BSE) imaging and energy dispersive X-ray spectroscopy (EDX or EDS). Preliminary studies on the preparation of bovine bone samples and their mechanical properties were tested in two directions with regard to various temperature ranges and the examination of mineral content.

Finite Element Analysis on Microstructure

Computational modeling is one of the novel techniques that has been used recently to simulate the fracture of bone and analyse tissue growth, remodeling and degeneration. Chapter 5 focused on the simulation of the micro-structural level of the cortical bone. The osteonal bone, composed of the Haversian canal and Volkman's canals, is represented as a cylinder tube. The influence of porosity, with regard to the increase in diameter of the Haversian and Volkman's canals, were identified. In addition,

simplified 3D models of interstitial bones with evenly distributed and randomly distributed Volkman's canals were generated to compare the differences.

Concluding Remarks and Suggestions for Future Research

The conclusions of this thesis are given in the last chapter. A review on further testing on the heat-treatment of cortical bone for transplantation is proposed.

Chapter 2

Bone Structure, Composition and Mechanics

2.1 Introduction

The skeletal system is composed of individual bones which are joined by connective tissue (Cowin 2001). This complex and multifunctional system provides unique mechanical, biological, protective and chemical functions in the body. Mechanically, bone provides connective points for muscles to allow movement and locomotion. It also provides support against the pull of gravity. Anatomic structures, such as the skull and ribcage, provide protection for soft tissue and vital organs. Bone provides chemical functions for the storage of marrow and excess calcium, almost 98% of total body calcium store in bone (Cowin 2001; Khan et al. 2001; Massaro & Rogers 2004). Bone also plays an important role in the maintenance of mineral homeostasis in the body. For example, if blood calcium levels in a human body decrease below normal level (ionized calcium is between 1.8 mg - 3.0 mg/dl), calcium will be released from bones to provide an adequate supply for metabolic needs (Khan et al. 2001). If blood calcium level increase, the excess calcium is stored in the bone

matrix, the process of releasing and storing calcium happens continuously (National Cancer Institute, viewed on January 2011).

Bone is a unique tissue which is produced inside our bod*y* during embryonic life and grows rapidly throughout childhood until growth peaks at around 20 years of age (Khan et al. 2001; Massaro & Rogers 2004). Throughout this period, new bone is formed faster than the removal of old bone (formation exceeds resorption). As a result, bones become larger, heavier and denser. The process of resorption and reformation (remodeling) of bone goes on continuously and concurrently from around 20 years of age to approximately 40 years of age. During this period, the growth of bone mass (bone density and strength) is relatively stable (Massaro & Rogers 2004). After 40 years of age, the equilibrium between resorption and reformation of bone is difficult to maintain. If bone resorption occurs too quickly or bone reformation occurs too slowly, it will lead to a bone resorption disorder (National Cancer Institute, viewed on January 2011), such as osteoporosis. Osteoporosis mainly affects women after menopause and is the most common bone resorption disorder (Massaro & Rogers 2004). According to International Osteoporosis Foundation (IOF), the risk of an osteoporotic fracture increases with age in both women and men. It is reported that, one in three women and one in five men will suffer from bone fractures globally (IOF, viewed on January 2013).

2.2 Bone Structure

This section will describe the shape and hierarchical levels of bone and their structure. Two main bone structures i) macrostructure and ii) microstructure will be outlined below.

2.2.1 Shapes of Bones

There are approximately 300 soft bones in our body when we born. From childhood to adolescence, some bones are slowly replaced by hard bone and later fused together, hence, an adult skeleton has approximately 206 bones (National Cancer Institute, viewed on January 2011). Bones vary in size and shape. Based on the architecture and location, each bone contributes toward structure, protection and mineral homeostasis in distinctive ways. There are four principal types of bones (based on their anatomical shape: i) long, ii) short, iii) flat and iv) irregular (Gray 1977).

i) Long Bones

Long bones are comprised of a long hollow cylindrical shaft (diaphysis) of compact bone. Each end has an extremity (the epiphyses) of spongy bone (refer Figure 2.1). Examples of long bones include the femur, tibia and fibula of leg, humeri, radii, and ulnas of arms. Long bones are appropriate for load-bearing and can oppose

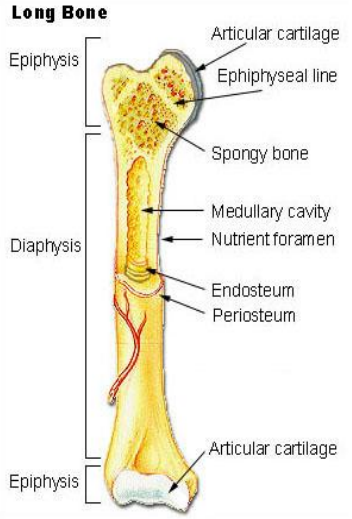

Figure 2.1 Internal structure of a long bone.

considerable stress. They also act as levers for sweeping and speedy movements (National Cancer Institute, viewed on January 2011; Gunn 2007).

ii) Short Bones

Short bones are club-liked in shape and are approximately equal in size vertically and horizontally. Short bones consist primarily of spongy bone which is covered by a thin layer of compact bone (refer Figure 2.2). The kneecaps (patellae), wrists (carpals) and some of the bones in the feet and ankles (tarsals) are examples of short bones. The short bones in the wrists and ankles are also known as sesamoid bones (National Cancer Institute, viewed on January 2011; Gunn 2007).

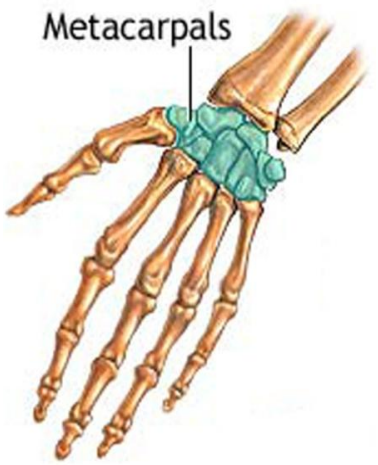

Figure 2.2 Metacarpals are an example of short bones.

iii) Flat Bones

Flat bones are thin, flattened, and usually curved (refer Figure 2.3). Flat bones consist mainly of spongy bone and are covered by protective layers of compact bone. The skull, ribs and scapula are typical examples of flat bones. Marrow is found inside the flat bones and produces more red blood cells than any other adult bone type (National

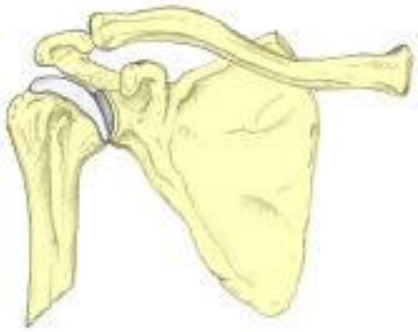

Figure 2.3 Scapular is an example of a flat bone.

Cancer Institute, viewed on January 2011; Gunn 2007).

iv) Irregular Bones

All other bones are classified as irregular bones. Vertebrae and the mandible are examples of irregular bones. Irregular bones are made up of mostly spongy bone with a thin layer of compact bone around them (refer Figure 2.4) (National Cancer Institute, viewed on January 2011; Gunn 2007).

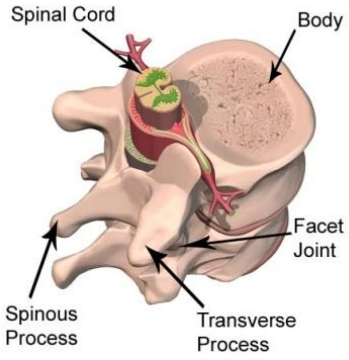

Figure 2.4 Vertebrae are examples of flat bones.

2.2.2 Hierarchical Structure of Bone

The material structure of a bone is complicated with integrated irregular arrangement and orientation of molecular components (Rho et al. 1998a). The composition of bone makes its material heterogeneous and anisotropic (Rho et al. 2002; Fan et al. 2002). The hierarchical structure of bone comprises of five levels. They are: i) the macrostructure: cancellous and cortical bone; ii) the microstructure (from 10 mm - 500 mm): Haversian systems, osteons, single trabeculae; iii) the sub-microstructure (1 mm – 10 mm): lamellae; iv) the nanostructure (from a few hundred nanometers to 1 mm): fibrillar collagen and embedded mineral; and v) the subnanostructure (below a few hundred nanometers): molecular structure of constituent elements, such as mineral, collagen, and non-collagenous organic proteins (Rho et al. 1998a; Fan et al., 2007). Figure 2.5 depicts the hierarchical structure of bone in various levels.

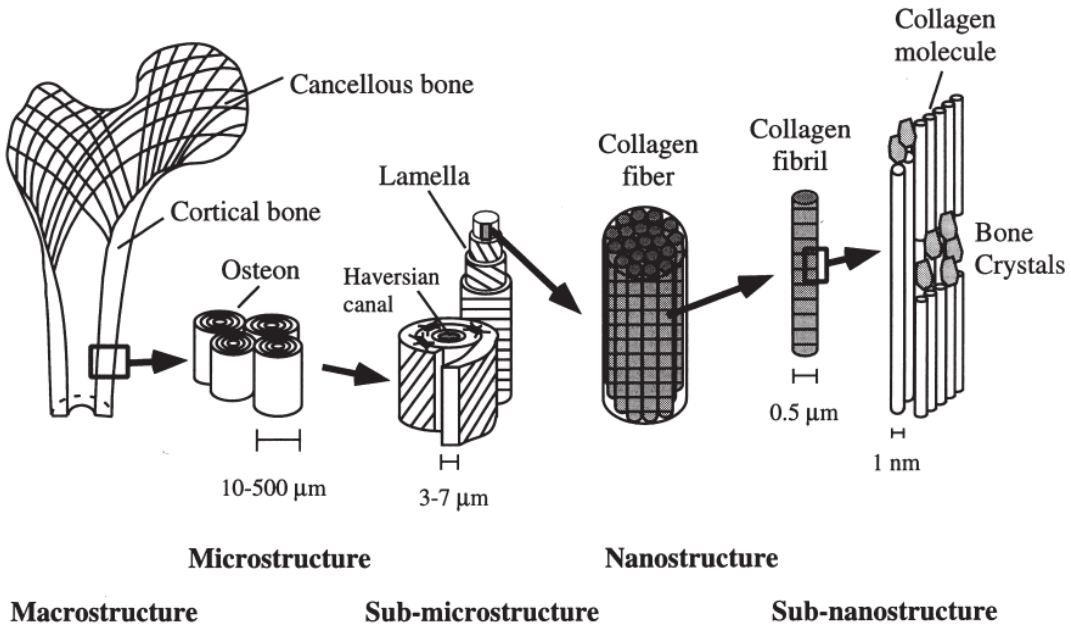

Figure 2.5 Hierarchical structure of bone in various levels: macrostructure, microstructure, sub-microstructure, nanostructure and sub-nanostructure (Rho et al., 1998a).

i) Macrostructure

Cortical Bone

Cortical (compact) bone and trabecular (cancellous) bone form the macroscopic tissue structure. Cortical bone is made up of dense and tough calcified tissues which form the surface layer. It accounts for 80% of the whole (1,400,000 mm^3) skeletal mass in adult humans and its surface area contributes to 33% of the total bone surface (Deng et al. 2005). Cortical bone accounts for 5% - 10% of porosity. The Haversian canals, Volkman's canals, and resorption cavities contains nervous tissues and blood vessels to form the porosity of the cortical bone (Martin et al. 1998). Figure 2.6 outlines the microstructure of cortical bone. The Haversian canal consists of blood vessels and is surrounded by lamellar of bone.

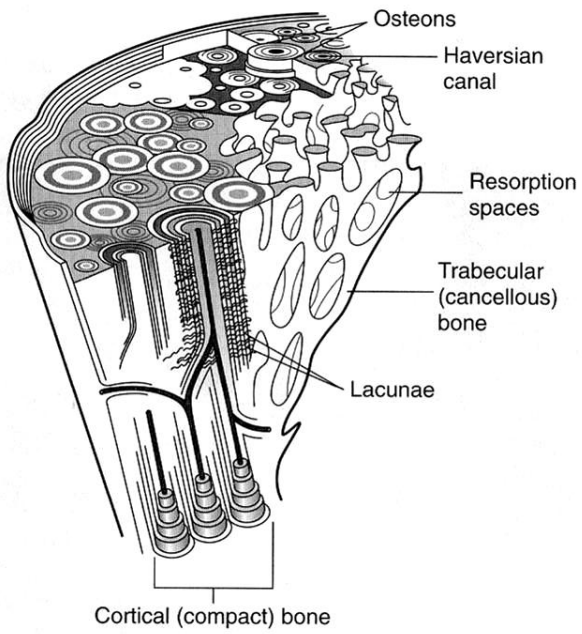

Figure 2.6 Diagram of some of the microstructure of cortical and trabecular bones (Khan et al. 2001).

Cortical bone has two types of surfaces: endosteum and periosteum. Endosteum is the inner surface of cortical bone that faces the bone marrow. It is active in bone formation and resorption. Periosteum is the outer surface of cortical bone. It faces the soft tissue, and contributes to bone growth. It also extends along the long bones diameter with aging (Khan et al. 2001). Renewing and remodeling constantly and continuously takes place in cortical bone to approximately 40 years of age in order to maintain balance (Deng et al. 2005).

Trabecular Bone

Trabecular (cancellous) bone is a sponge-like tissue comprising of rod or plate shaped trabeculae to form the internal support structure of bone. Contrary to cortical

bone, trabecular bone only accounts for 20% of the whole bone mass (350,000 mm^3). However, the surface area of a trabecular bone is large, which contributes around 75% of the total surface of the bone system (Rho et al. 1998a; Deng et al. 2005; Donnelly et al. 2006; Gunn 2007). Unlike cortical bone, trabecular bone accounts for 75% - 95% of porosity (refer Figure 2.7). The pores of trabecular bone are mainly filled with marrow and are interconnected by trabeculae. These trabeculae comprise plates or struts about 200 μm thick. A trabecular strut is about 50 μm - 300 μm in diameter. The trabeculae are not well organized. Sometimes they are arranged in an orthogonal array, but most often they are randomly arranged (Martin et al. 1998; Rho et al. 1998a).

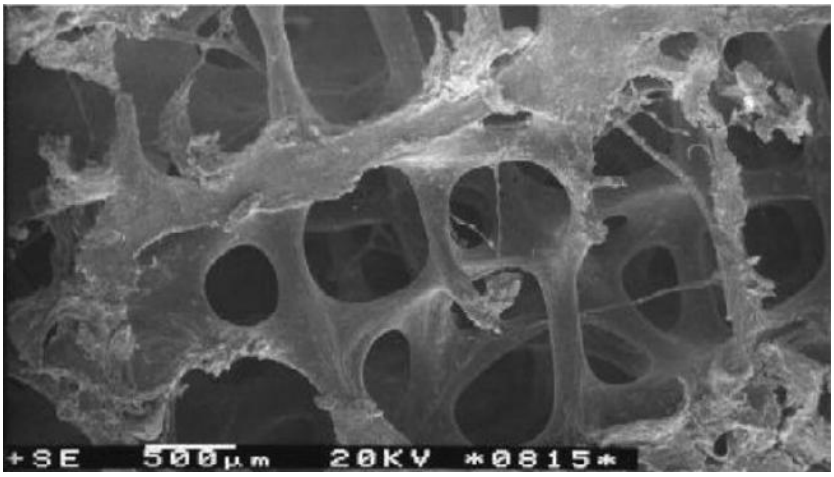

Figure 2.7 Trabecular structure in the calcaneus of a 24 years old man (feppd.org, viewed on February, 2011).

Some researchers characterise cortical and trabecular bones to be made of the same kind of material according to their porosity and density (Cater et al. 1977 & 1980; Keller et al. 1990). However, some researchers regard these two types of bones to

comprise different bone materials on the basis of the difference in bone matrix and cellular arrangements (Rice et al. 1988; Choi et al. 1990 & 1991; Rho et al. 1993). The material arrangement of trabecular bone allows bone marrow, blood vessels and connective tissue to come into contact with the bone. Trabecular bone is comparative metabolically active than cortical bone. Active metabolic activity means that bone is remodeled more often and is therefore considered "younger" than cortical bone (Rho et al. 1998a; Khan et al. 2001).

ii) Microstructure

Regular and concentric shaped lamellae form the microscopic structure of cortical bone. In contrast, the trabecular bone is formed by irregular lamellae (Rho et al. 1998a). Lamellae are formed by mineralised collagen fibers (3 μm - 7 μm wide). Usually several lamellae (4 - 20 lamellae of collagen fibers) wrap around a Haversian canal to form an osteon (10 μm - 500 μm in diameter) or a Haversian system (refer Figure 2.8) (Rho et al. 1998a).

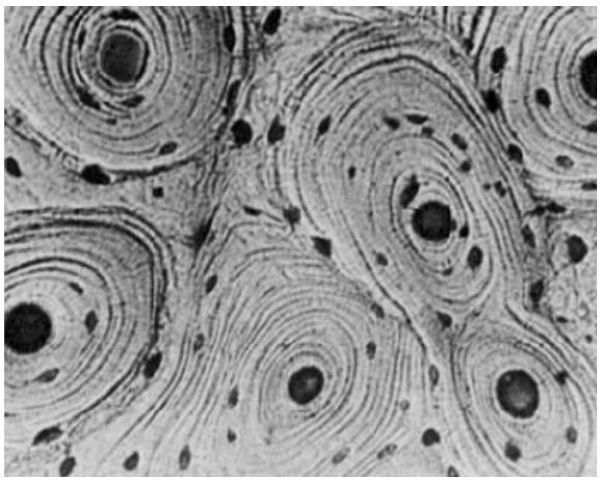

Figure 2.8 Lamellar structure of Haversian systems (osteons) in a cortical bone (feppd.org, viewed on February, 2011).

Lamellar and Woven Bone

Immature and randomly arranged collagen fibers and mineral crystals are considered to be a woven bone. Woven bone is highly mineralized than lamellar bone due to the quick formation; however, they are weak in mechanical response. Collagen fibers and mineral crystals are formed slowly and highly organised in parallel layers or tangential to the outer surface of bone, and formed plywood-like structures are called lamellar bone (Martin et al. 1998). Both woven and lamellar bone can be eventually organized into either cortical or trabecular bone (Khan et al. 2001).

Haversian Systems and Volkman's Canals

Haversian systems (osteons) form the basic structural unit of cortical bone. They usually align parallel to the long axis of bone to withstand tension, torsion, and bending, and compression (Rho et al. 1998a). In the center of each osteon is the Haversian canal which contains blood vessels, nerves and loose connective tissue. The Haversian canals are connected to each other and periosteum by Volkmann's canals. These canals are short and run perpendicular to the Haversian canals. Volkman's canals also contains blood vessels and nerves (Martin et al. 1998).

2.3 Bone Composition and Remodeling

Bone is a complex and unique connective tissue. The major bone tissues comprise (by weight) 20% - 25% organic component, 70% inorganic component, and 5% water (Khan et al. 2001).

The organic component, also called "osteooid", contains 98% of Type 1 collagen and noncollagenous protein. The remaining 2% includes osteoblasts, osteocytes, and osteoclasts (Khan et al. 2001). The organic component of bone provides tension properties and flexibility.

The inorganic component consists mainly of mineral-crystalline calcium hydroxyapatite. This component primarily contributes to compression and stiffness of bone (Martin et al. 1998; Khan et al. 2001; Behari 2009). For normal loading such as compression, load and deformation is converted to stress and strain by engineering equation, the elastic region obtained from the stress – strain curve is the elastic modulus or Young's modulus, which is the stiffness of a material (Martin et al. 1998; An et al. 2000).

2.3.1 Basic Components of Bone Matrix

The organic and inorganic bone matrix plays a significant role in structure, mechanical and biochemical properties of bone. Collagen, non-collagenous proteins and minerals will be introduced below.

Collagen

Collagen is the major structural protein in a bone matrix. The principal collagen molecule in bone is Type 1 collagen. This molecule consists of two identical alpha 1(I) chains and a single alpha 2(I) chain. Type 1 collagen is also found in tendons, ligaments and skin (Khan et al. 2001). Each collagen molecule is organised with the next in parallel order to form collagen fibril, and in turn are organised to form collagen fiber (refer Figure 2.9). Collagen not only provides bone flexibility and tensile strength, it also supports the nucleation of bone mineral crystals to give bone rigidity and compression strength (Martin et al. 1998; Khan et al. 2001; Behari 2009).

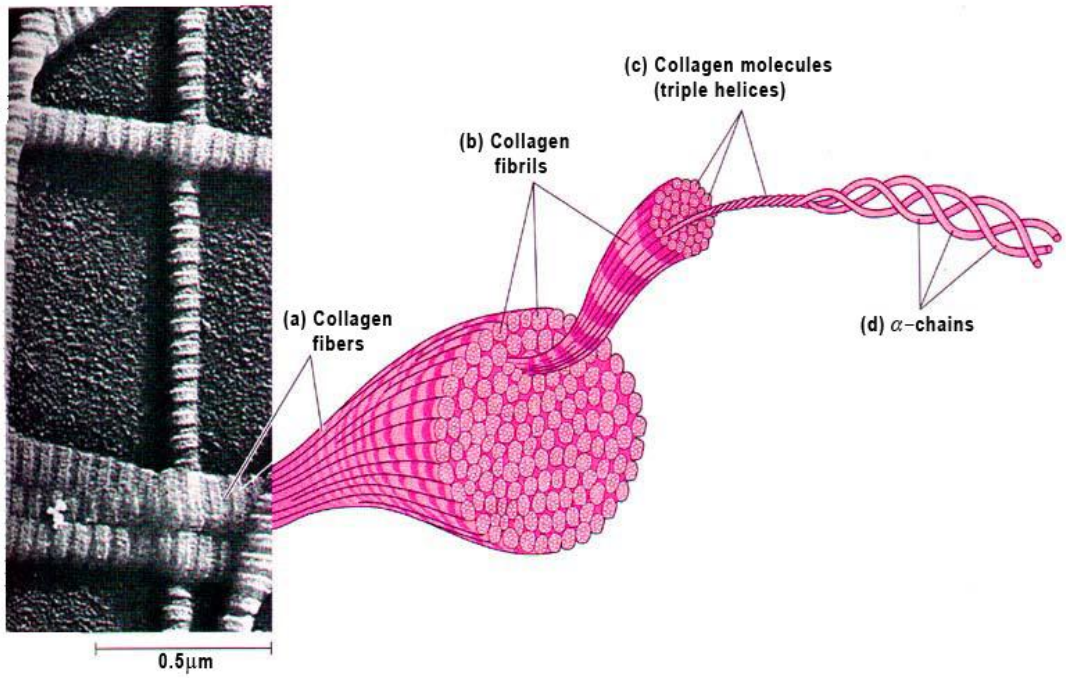

Figure 2.9 Schematic diagram of the assembly of collagen fibrils and fibers (http://hk.image.search.yahoo.com/search/images, viewed on February, 2011).

Non-collagenous Proteins

Although non-collagenous proteins account for a small percentage of the bone matrix by weight, they play a significant role in attracting osteoclasts to sites for bone resorption and forming new bones (Khan et al. 2001). Osteocalcin is one of the most abundant non-collagenous proteins secreted within bones and allows osteoclasts to attach to the surface for bone resorption. Other non-collagenous proteins in bone include osteopontin and osteonectin. These proteins are responsible for regulating calcium concentration and enhancing the mineralisation of new bone (Martin et al. 1998; Khan et al. 2001).

Mineral

The inorganic component of bone is mainly formed by hydroxyapatite crystals ($Ca_{10}(PO_4)_6(OH)_2$), and comprise two major constituents: calcium and phosphorous. These crystals are formed as rods or plates (20 nm – 80 nm long and 2 nm – 5 nm thick) in hexagonal symmetry, and are found in and around collagen fibers (Khan et al. 2001). Bone mineral also contains small amounts of other substances such as carbonate, fluoride, and chloride which are governed by the composition of body fluids (Martin et al.1998; Behari 2009). However, hydroxyapatite crystals may be replaced by these substances and influence the mechanical properties of bone. For example, bon crystals will increase in size and become more fragile when fluoride is found in excessive amounts (Khan et al. 2001).

2.3.2 Bone Cells

There are three types of bone cells: i) osteoblasts, ii) osteocytes, and iii) osteoclasts.

i) Osteoblasts

Osteoblasts are located on the outer surface of bone and also in the bone cavities. Osteoblasts work in teams to produce the organic component (osteoid), which mineralises to become new bone (Khan et al. 2001). Bone cells lay down osteoid (refer Figure 2.10A) at a rate of about 1 μm/day in concentric layers until the deposition of bone reaches the surface of the blood vessels. Bone apposition rate is refers to the rate of this process (Martin et al. 1998). Mineralisation takes place afterwards (refer Figure 2.10B). Hence, osteoblast is significant in bone formation.

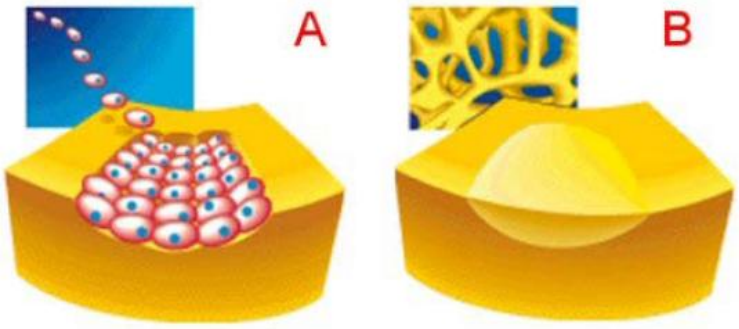

Figure 2.10 Bone deposition (feppd.org; viewed on February 2011).

ii) Osteocytes

Osteocytes are mature bone cells of osteoblasts that are embedded in bone cavities and are called lacunae. Osteocytes communicate with each other and with osteoblasts through calaliculi (gap junction). These interconnecting processes allow osteocytes

to perform complex networking throughout the bone matrix. These processes include facilitating mineral in and out of bone, matrix maintenance and calcium homeostasis, activation of bone turnover, and acting as mechano-sensory-receptors that regulate the mechanical stress of bone (Martin et al. 1998; Khan et al. 2001).

iii) Osteoclasts

Osteoclasts are responsible for bone resorption (removal of old bone to reduce bone volume). This large and multinucleated cell is located on the calcified bone surfaces and within the cavities named Howship's lacunae. When resorption takes place, osteoclast is attached to the bone surface (refer Figure 2.11A). Active lysosomal enzymes are then excreted via the ruffled border; usually eroding their path through bone at a rate of tens of micrometers per day by demineralizing bone with acid and digesting the collagen with enzymes (refer Figure 2.11 B) (Martin et al. 1998).

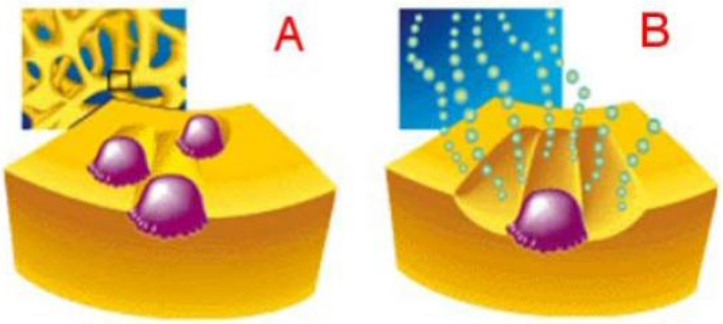

Figure 2.11 Bone resorption (feppd.org; viewed on February 2011).

Normally, the rate of bone deposition and absorption are in equilibrium with each other in order to maintain a constant total mass of bone. This process will continue

until about 40 years old. After this time, the activities of osteoblasts will slow down and equilibrium of bone mass is difficult to maintain (Massaro & Rogers 2004). As the osteoblastic activity (bone formation) is slower than osteoclastic activity (bone resorption), it means that the rate of bone deposition will diminish and bone becomes more brittle. The lowered osteoblastic activity leads to a bone-thinning disease called osteoporosis (Khan et al. 2001; Massaro & Rogers 2004).

2.3.3 Modeling and Remodeling of Bone

A major activity of bone cell is to organise the bone modeling and remodeling to allow bone growth and adjust the bone strength (Khan et al. 2001). During the process of modeling, bone strength is enhanced by adding mass. The growth of bone is also shaped in various ways by expanding the periosteal (outer) and endosteal (inner) diameters of bone, making the bone larger and thinner (Martin et al. 1998). Bone modeling is an important process which primarily occurs during growth. Each growing child loads his or her skeleton in a different way, thus requiring each skeleton to be "customised". This sculpting, involving the coupled activities of osteoclasts (resorption) in some regions and osteoblasts in other regions (formation) also occurs to some extent in an adult as well.

Bone remodeling is a more complex activity accomplished by the work of osteoclasts and osteoblasts together in basic multicellular units (BMU). About 10 osteoclasts and several hundred osteoblasts form a BMU (Martin et al. 1998). The total remodeling phase is about four months in which about three weeks are for resorption; then

formation or refilling is about three months. The particular characteristic of remodeling is not only a regularly occurring process throughout human life, it is also frequently associated with the replacement of damaged tissue with the same amount of new bone tissue in the same site. Eventually, the skeleton can increase its mechanical efficiency (Martin et al. 1998; Khan et al. 2001).

Although modeling and remodeling refer to the coupling activities of osteoclasts and osteoblasts, they differ from each other. Table 2.1 outlines some of these key differences:

Table 2.1 Modeling and remodeling of osteoclasts and osteoblasts (Martin et al. 1998)

	Modeling	Remodeling
Action	Independent action of two type of bone cells	Coupled and organized action between 2 types of bone cells
Result	Change of bone size, shape, or both	Normally does not affect size and shape
Rate	Greatly reduced after maturity of skeletal	Throughout life and essentially reduced after growth stops
Site	Continuous and sustained at a particular site	Non-continuous and have specific starting and ending
Strength	Maximize stiffness and minimize deformation	Replace fatigue damaged of bone

2.4 Bone Mechanics

Human bone is hard, rigid, and strong enough to withstand intensive physical activities and external force loading. For example, the diaphyses of the tubular long bone responds to torsion and bending loading; while the widened mataphyses of long and short bones are better for supporting and dissipating contact forces. The complex structure of cortical and trabecular bones are designed to fulfill the mechanical needs.

For example, the major function of cortical bone is for protection and structure, while the trabecular bone allows bone marrow, blood vessels, and connective tissues to contact with the bone and blood cell regeneration (Khan et al. 2001). The mechanical properties of bone are highly related to both material properties of bone tissues (mass, density, stiffness and strength) and structural properties of the whole bone (size, shape, cortical thickness, cross-sectional area, and trabecular architecture) (Khan et al. 2001).

When an applied force exceeds the withstanding limit of the bone structure, it leads to structural failure or bone fracture. However, as the applied force increases to the bone tissues, it will lead to permanent deformation or the yield of the material. Thus, the mechanical behavior of bone is not correlated to the bone structure - it is related to the material properties. The material properties of bones are determined by the organic and inorganic components. The organic component, mainly type 1 collagen, responds to tensile strength; whereas the inorganic components - mineral responds to compressive loading.

Various researchers studied the mechanical properties of cortical bone and trabecular bone in order to understand the mechanical strength (Hayyes et al. 1985; Martin et al. 1998; Turner et al. 1999; Rho et al. 1997, 1998b and c, 1999 b; Zysset el al. 1999; Donnelly et al. 2006; Wang et al. 2006). Cortical bone is defined as anisotropic and heterogeneous composite material which means that Young's modulus and the hardness of cortical bone in longitudinal and transverse direction vary. The

microstructure (Haversian system) of cortical bone is one of the factors that affect the strength of cortical bone. Some researchers consider cortical and trabecular are the same types of materials (Cater et al. 1997 & 1980; Keller et al. 1990). While others consider trabecular bone as different materials according to the bone matrix and cellular components (Rice et al. 1988; Choi et al. 1990 & 1991; Rho et al. 1993). Basically, the mechanical properties of bone involve a number of factors such as the porosity, density, distribution and degree of mineralization that can affects the bone strength.

Chapter 3

Literature Review

3.1 Bone Mechanical Properties

In providing structural and protective functions for our body, the mechanical properties of bone are vitally significant. Human bone starts to build as early as five to seven weeks in utero. From that time on, bone continues to grow and respond to its environment in order to form its genetic and "lifestyle" history (Khan et al. 2001). Bone strength and design are governed by various factors such as genetics, hormones, physical activity, and particularly important - mechanical loading activity. The mechanical properties of bone follow the same pattern of man-made load-bearing structures. However, due to the adaptive mechanisms in bone tissue, the mechanical properties and morphology respond to a given load or set of forces that are highly dependent on both structural properties and the material properties of the bone tissue itself (Martin et al. 1998; An et al. 2000; Khan et al. 2001).

3.1.1 Material and Structural Properties of Bone

When the whole bone experiences loads or forces during activities such as walking, jumping, or running, bone deformation will happen. As the applied load exceeds the limit the whole bone can withstand, it may lead to bone fracture, or structural failure (Khan et al. 2001). On the other hand, if a specimen of bone tissue is under an increased load, permanent deformation or yield will ultimately occur due to the increased stress applied upon it. Human bone is a heterogeneous composite material and complex in hierarchical structure. Hence the mechanical properties of bone include the material behavior of cortical and trabecular bone sections, bone tissues, single trabeculae or osteons, bone lamellae, collagen fibrils, fibrils, molecules, and mineral components (An et al. 2000; Khan et al. 2001). The mechanical properties of bone can be divided into two main aspects, i) the structural properties and ii) the material properties of the bone.

i) Structural (Geometric) Properties of Bone

The human skeleton is specially designed for intensive physical activity demands and adapts to respond to changes in these demands. For example, increasing the bone diameter allows the bone to be strong enough to withstand compression, tension, and shear stresses; yet the slightly curved shape in a long bone is able to resist impact loads (Khan et al. 2001). Bone size, bone geometry, cortical thickness, cross-sectional area and also microstructural properties such as trabecular architecture and cortical porosity are the main features of structural properties (Augat at.al. 2006). Up

to 70-80% of the whole bone strength can be predicted by geometrical measures (Augat at.al. 2006).

Structural properties are significant for analysing the global stress; while material properties are important in characterising bone pathologies, micro-level stress analyses, and bone adaption around implants (Rho et al. 1998b). Augat et al. (2006) suggests that the structural behavior of whole bone is highly dependent on the contribution of cortical bone as it carries a considerable share of the applied loads for the skeleton.

ii) Material Properties of Bone

The measure of material properties usually refers to the stiffness, static strength, toughness and fatigue resistance of the bone. The material stiffness (the force required to deform a structure) is represented by the slope of stress-strain curve which correlates with mechanical strength (yield or the failure point of a structure). Young's modulus of elasticity, denoted as "E" is usually referred to the stiffness of the material. Table 3.1 summarizes the major factors that determine bone strength according to a hierarchical structure (An et al. 2000). It has been shown that the porosity, density, orientation of osteons, and the degree of mineralisation of calcified bone can affect the mechanical properties of bone (An et al. 2000).

Table 3.1 Hierarchical level of bone (An et al. 2000)

Level	**Elements (Specimens)**	**Main Factors Determining Bone Strength**
Marcostructure (whole bone)	Femur, humerus, vertebrae, frontal bone, phalangeal bones, calcaneous, etc.	Macrostructure such as tubular shape, cross-sectional area, and porosity of long bone, cortical bone-covered vertebrae, or the irregular pelvic bone
Architecture (tissue level)	Compact bone or cancellous bone blocks, cylinders, cubes, or beams	Densities, porosity, the orientations of osteon, collagen fibers, or trabeculae
Microstructure (osteonal or trabecular level)	Osteons, trabeculae	Loading direction, with maximum strength along their long axis
Submicrostructure (lamellar level)	Lamella, large collagen fibers	Collagen-hydroxyapatite (HA) fibrils are formed into large collagen fibers or lamellar sheets with preferred directions. The orientations of the fibrils define directions of maximum and minimum strengths for a primary loading direction
Ultrastructure (nanostructure)	Collagen fibril and molecule, mineral components	HA crystals are embedded between the ends of adjoining collagen molecules; this composite of rigid HA and flexible collagen provides a materials which is superior in mechanical properties. More energy absorption is allowed and accepted a greater load bearing.

Rho et al. (1998b) reported that the mechanical properties of cortical bone are sensitive to the porosity, the mineralisation level and the organisation of the solid matrix. This means that the strength and elastic modulus are different in the longitudinal and transverse directions. The mechanical properties of trabecular bone are more sensitive to apparent density, ash density, trabecular connectivity, location

and function (An et al. 2000). The mechanical property differences in trabecular bone reported by Rho et al. (1998b) are much broader than cortical bone. According to Curry (2001), the Young's modulus of cortical and trabecular bones are roughly proportional to each other.

Organic and inorganic constituents of bone that affect the material properties of bone are also outlined in Table 3.1. As bone is a composite material which contains about 70% mineral (hydroxyapatite - HA), 22% proteins (type I collagen) and 8% water by weight (Augat et al. 2006), the quality and the spatial arrangement of these constituents highly contributes to the material properties. Type 1 collagen in organic constituents provides tensile strength, while the inorganic constituents and mineral give response to compressive loads. In contract to stiffness, toughness is not directly related to bending strength and Young's modulus. Most often it is related to fatigue fracture that resulted from mineralizsation of bone material. Fatigue may damage the bone material and reduce the stiffness of bone, however micro-cracking or damage under certain situation may strengthen the bone. Generally, micro-cracks or damaged bone tissue can be replaced by new bone tissue through remodelling of bone, eventually enhance the bone strength.

3.1.2 Measuring the Properties of Bone

Bone size and shape, bone strength, and the metabolic activity are the areas of interest for researchers (Rho et al. 1998b; Catanese III et al.1999; Cowin et al. 2001; Shin et al. 2005; Akhter et al. 2005). The methods that are used to determine the

mechanical properties of metal, composite materials, and other structural materials are also employed to measure properties of bones. These methods include i) compression, ii) torsion, iii) tensile, iv) bending and v) nanoindentation testing. The parameter for the mechanical properties testing is presented in Appendix 1.

i) Compression Test

Compression testing is one of the popular techniques used for assessing sectioned or whole bone specimens. According to Shin et al. (2005), the sectioned bone specimen needs to be aligned on its long axis and compression axis and placed between two parallel stainless steels platen. This technique is shown in Figure 3.1. Due to the friction and compressive end effects imposed between the specimen and the platen, compressive testing is less accurate then tensile testing. As the bone specimen is compressed, it will expand in a transverse direction. Induced friction between the specimen and platen, incur large stress concentrations and can produce result in measurement error (An et al. 2000). This particularly occurs when the load faces of bone specimen are misaligned with the loading platen.

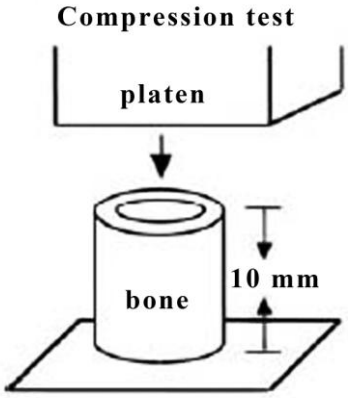

Figure 3.1 Schematic diagram of compression test for bone structure (Shin et al. 2005).

Despite of the difficulty in achieving accurate results using compression testing, it is considered a suitable measure of the mechanical properties of vertebral region because it simulates the vivo loading condition to which the bone is exposed (Cowin et al. 2001). With the addition of mechanical or optical extensometers a smaller bone specimens such as trabecular bone can be tested by the compression technique. Catanese III et al. (1999) report that the elastic modulus (mean ± SD) of intact specimens is 16.3±2.2 GPa, and yield stress is 170 MPa ±20 as measured using compression testing.

ii) Torsion Test

Torsion testing is normally used to measure the shear mechanical properties of whole bone. Both bone ends of the whole bone has to be embedded into a plastic block before it is mounted to the testing grips. When embedding the resin for fixation, perfect alignment is essential to reduce the potential error induced by bending moment (Cowin et al. 2001). The bone specimen is subjected to a torsion load with a rotation of 3.5^{o}/s until facture (refer Figure 3.2 (Shin et al. 2004)). Since load is applied at the ends of the bone during testing, the biomechanical effects of fracture, bone defects, or orthopaedic implants could be perfectly measured by torsion testing. This is because the vertebrate as well as the long bones are often subjected to torsional load during daily activities (An et al. 2000).

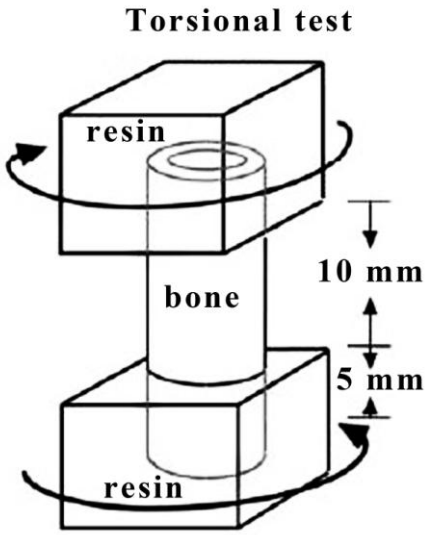

Figure 3.2 Schematic diagram of torsion test for bone structure (Shin et al. 2005).

iii) Tensile Test

Tensile testing is one of the accurate methods for measuring bone properties of large and carefully machined bone without inducing coupled bending moment (An et al. 2000). Tensile test is suitable for measuring both cortical and trabecular bone properties. Cortical bone specimens can be machined to a relatively small size (gauge diameter = $d \approx 3$ mm) (An et al. 2000) as a dog-bone shape (refer to Figure 3.3). However trabecular bone must be large enough to allow the trabecular structure to be treated as a continuum (Cowin et al. 2001). At least 4-8 mm of specimen width is suggested for trabecular bone specimen (An et al. 2000), the attachment method for tensile testing of the trabecular bone refer to Figure 3.4.

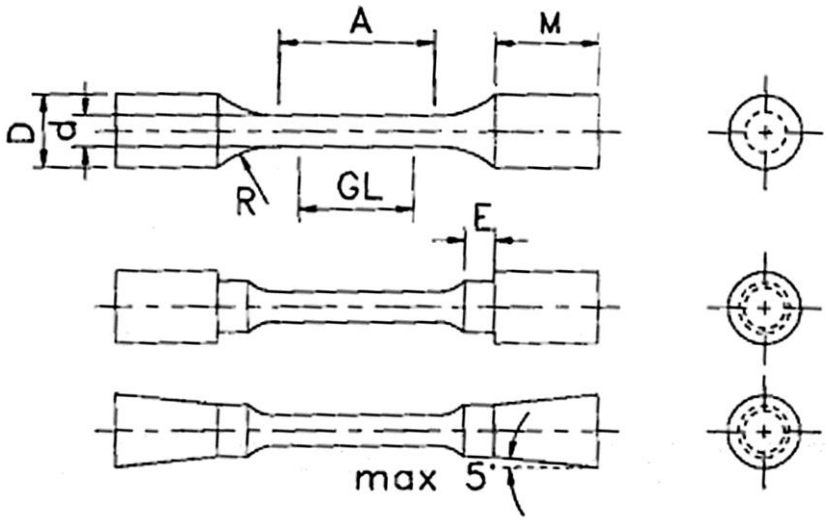

Figure 3.3 Schematic diagram of tensile test for cortical bone A=parallel length, GL=gauage length, M=grip length, R=curvature radius, D=specimen outer diameter, d=specimen gauage diameter (An et al. 2001).

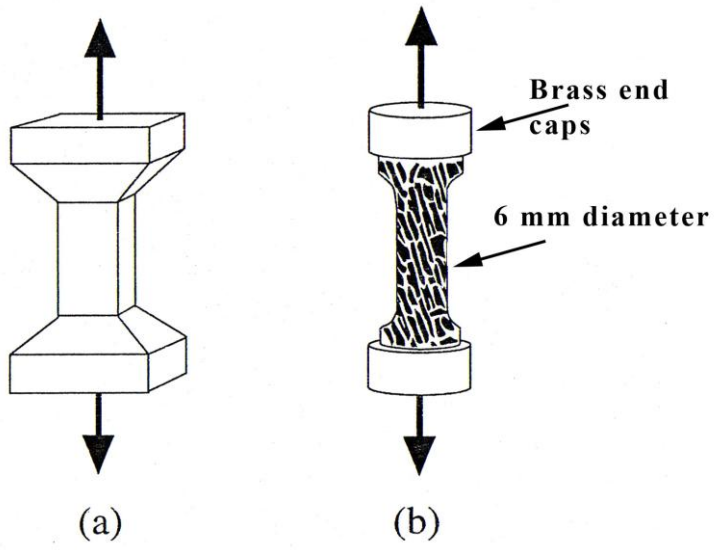

Figure 3.4 Schematic diagram of tensile test for trabecular bone (Cowin et al. 2001)

Extensometer is attached to the midsection of a specimen so that strain can be measured accurately. Stress can be calculated as the applied force divided by the bone cross sectional area in the midsection of bone specimen. Catanese III et al. (1999) has reported the elastic modulus (mean ±SD) of the intact specimens is 16.2±3.4 GPa, and yield stress is 46.8 MPa ±14.9 was obtained using tensile testing.

iv) Bending Test

Bending testing is preferable for measuring the mechanical properties of long bone, especially for some small animal bones that are difficult to machine for tensile or compression test specimens. Bending causes both tensile and compression stresses, therefore, bending failure usually occurs on the tensile side of bone. This is because bone is weaker in tension then in compression. Either three-point or four-point bending can be applied to rodent bone or machined bone specimens (refer Figures 3.5 (a) and (b), respectively).

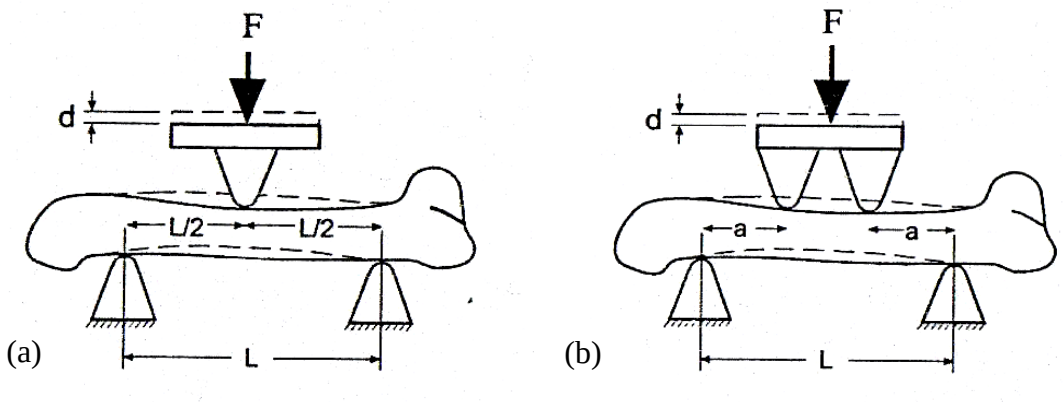

Figure 3.5 Schematic diagram of bending test for bone structure. (a) Three-point bending and (b) four-point bending test. F is the applied force and d is the resulting displacement (Cowin et al. 2001).

Three-point bending is a simpler technique but will create higher shear stress near the midsection of the bone. Four-point bending can produce pure bending and ensures that transverse shear stress is zero. However, the applied force needs to be equally distributed on two upper loading points. Four-point bending is usually utilised in regularly shaped specimens while three-point bending is most often used to measure a whole long bone. Akhter et al. (2005) attached a resistance strain gauge on the bone and found that the measured Young's modulus of the rat tibia is 29.4 GPa. This contrasted significantly with the calculated value of Young's modulus from displacement of the loaders at only 7.6 GPa. This difference was attributed to the span between the lower loader and the radius of curvature of the loading surface. The former determined the length-to-width ratio whilst the latter determined how much bone deformation occurred beneath the loaders.

Whether compression, tensile, bending, or other mechanical properties tests are used, two aspects of bone mechanics are considered significant for understanding the bone strength: the elastic modulus and ultimate strength. Table 3.2 summarises the aforementioned mechanical testing results of human bone.

Table 3.2 Compression and tensile test results from various researchers

Loading Mode	Bone Type	Region	Direction	Young's Modulus, GPa	Ultimate Stress, MPa
Compression	Cortical	Haversian (Martin et al.1998)	L	18.2± 0.9	105±17
			T	11.7±1.0	131±21
		Wet Femoral (Hayyes et al, 1985)	L	17.0	193
			T	11.5	133
	Trabecular	Proximal Tibia (Rohl at al. 1991)	-	0.489±3.31	2.22±1.42
Tensile	Cortical	Haversian (Martin et al.1998)	L	17.9±0.9	135±16
			T	10.1±2.4	53+11

v) Nanoindentation Test

Nanoindentation testing is one of the favorable novel techniques used recently to quantify the mechanical properties of microstructure of various materials. This technique evolved from the conventional Vickers microhardness testing. It is capable of making small indentations at precise positions on microstructural features whilst also monitoring the loads and displacements of the indenter on the specimen surface. The nanoindentation test is well suited to examine the microstructual features of material surfaces to provide a spatial resolution which is less than 1 μm (Rho et al. 1997 & 1999a; Akhter et al. 2005; Hoc et al. 2006). Since bone tissues vary at different structural levels (from microstructure: 10 to 500 μm to sub-nanostructure: 1 nm (Rho et al. 1999b), the mechanical properties of microstructural units of bone tissue down to the osteon level can be explored using the nanoindentation technique. By analysing the indentation load-displacement behavior, it is possible to obtain the measurement of the Young's modulus, E, and hardness, H, of the bone (Catanese III et al. 1999; Rho et al. 1999a; 1999b;Wang et al. 2006).

Nanoindentation testing is an indirect measurement of the contact area (refer to Figure 3.6) (TriboScratch®user manual). When a desired load is applied to an indenter and it is in contact with the specimen, the depth of penetration of the indenter below the specimen surface is measured in nanometers. Together with the known geometry of indenter, the area of contact at full load can further be determined (Fisher-Cripps 2004).

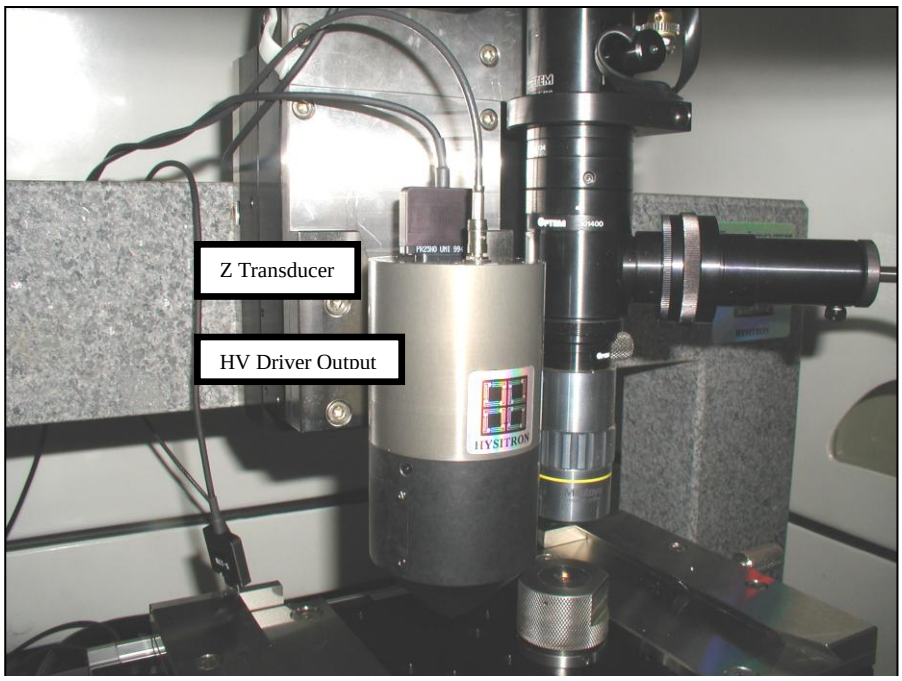

Figure 3.6 MultiRange NanoProbe head attached to the TriboScratch system (TriboScratch®user manual, 2006).

The hardness is determined by dividing the load by the area of contact; whereas, the elastic modulus is examined by the portion of the unloading curve (refer Figure 3.7).

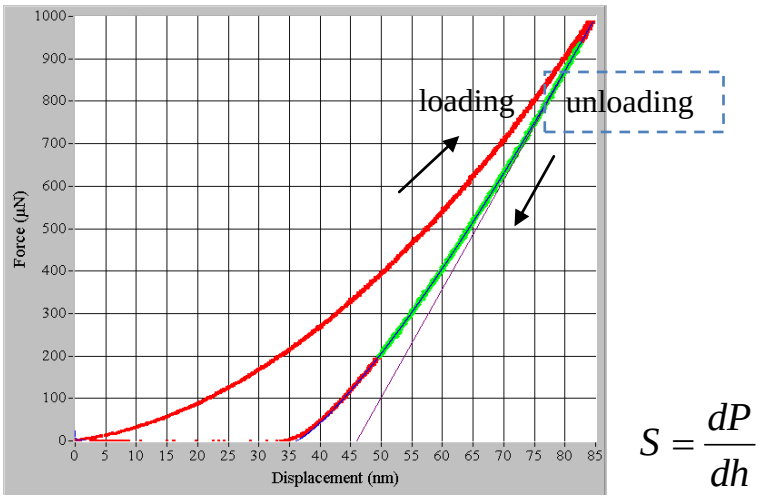

$$S = \frac{dP}{dh}$$

Figure 3.7 Load-displacement curve (TriboScratch®user manual, 2006).

Recently, nanoindentation has also been widely used to measure the elastic properties of the microstructural components of human and bovine bone (Rho et al. 1997 & 1998a & 1999a; 1999b; 1999c; Turner et al.1999; Zysset et al. 1999; Hoffler et al. 2000; Fan et al. 2002; Hengsberger et al. 2003; Akhtar et al. 2005; Donnelly et al. 2006; Oyen et al. 2006; Wang et al.2006). A summary of selected research is outlined in Table 3.3.

Differences in cortical bone between longitudinal and transverse directions have been observed by researchers (Rho et al. 1997 & 1998a & 1999a; 1999b; 1999c; Turner et al.1999; Zysset et al. 1999; Hoffler et al. 2000; Fan et al. 2002; Hengsberger et al. 2003; Akhtar et al. 2005; Donnelly et al. 2006; Oyen et al. 2006; Wang et al.2006). It is widely accepted that the modulus in longitudinal direction is significantly higher than in transverse direction. Hoffler et al. (2000), Rho et al. (1997) and Zysset et al. (1999) have also reported that the interstitial lamellae had greater elastic moduli and hardness than osteons. Many investigators have concluded that the elastic moduli of cortical bone are significantly higher than that of trabecular bone (Rho et al. 1999b and 1999c; Turner et al.1999; Wang et al.2006).

It should be noted that the difference of elastic moduli and hardness results between various researchers may have depended on the tissues type, the anatomical location, preparation of specimen and even the age of the donors.

Table 3.3 Summary of nanoindentation results from various researchers

Researchers	Bone Type	Location	Direction	Elastic Modulus, GPa (Average)	Hardness, GPa (Average)
Turner et al. 1999	Cortical bone	Femoral midshaft	L	23.45	-
			T	16.58	-
	Trabecular bone	Distal femur		18.14	-
Rho et al. 1998 b	Cortical bone	Tibiae	L	22.5	0.614
			T	25.8	0.736
	Trabecular bone	Thoracic vertebrae		13.4	0.468
Zysset et al. 1999	Cortical bone (Neck of fermur)	Osteonal	-	15.8	-
		Intersitial lamellae		17.5	
	Cortical bone (Diaphyseal Femoral)	Osteonal	-	19.1	-
		Intersitial lamellae		21.2	
	Trabecular bone (Neck of fermur)	Trabecular lamellae	-	11	-
Rho et al. 1999 b	Cortical bone	Osteonal	L	22.4	0.617
		Interstitial lamellae	L	25.7	0.736
		-	T	16.6	0.564
	Trabecular bone	-	L	19.4	0.618
			T	15.0	0.515
Rho et al. 1998 c	Cortical bone	Osteonal	L	21.7	0.63
			T	16.8	0.57
	Trabecular bone	Trabeculae	L	18.2	0.59
			T	16.2	0.56
Donnelly et al.2006	Trabecular bone (Vertebral)	Lamellar	-	22.9	0.85
		Interlamellar	-	19.2	0.73
Wang et al. 2006	Cortical bovine bone	Osteonal	L	24.7	0.811
		Interstitial lamellae	L	30.1	0.892
		-	T	19.8	0.647
	Trabecular bovine bone	-	L	20	0.528
			T	14.7	0.410

L = Longitudinal; T = Transverse

3.1.3 Evaluation for Architectural Properties of Bone

Extensive investigations have focused on the marco- and micro- levels of the mechanical properties of bones, including the studies on material properties (stress accumulation and bone mass) and structural properties (whole bone deformation) (Reilly et al. 1974; Schaffler et al. 1988; Bowman et al. 1996; Fantner et al. 2004; Ulrich et al. 2008).

Bone strength is a complex property which is highly related to the density, mineral content, organic matrix, as well as genetic components (Boskey et al. 1999). To understand how the matrix components interact (Yeni et al. 2001; Nalla et al. 2003), what the role of them is, and the influence they played on mechanical properties as the composition changes is significant to predict and prevent bone failure (Fantner et al. 2004).

Unlike the material and structural property tests outlined above, methods used for assessing the internal architecture of bone and mineral compositions are more accurate and noninvasive. Magnetic Resonance (MR) and peripheral Quantitative Computed Tomography (pQCT) can create high-resolution images and are widely used to examine the whole bones in vivo (van Rietbergen et al. 1998). X-ray Diffraction (XRD), Blackscatted Electron (BSE) Imaging, Transmission Electron Microscopy (TEM), Atomic Force Microscopy (AFM), Scanning Electron Microscope (SEM) and Thermal Gravimetric Analysis (TGA) are used to observe changes in surface morphology under loading, fractures modes of materials under

tensile, compression, and bending load. An example of trabecular bone captured by SEM (refer Figure 3.8) showing the multiple cracks that form the fractures (Fantner et al. 2004).

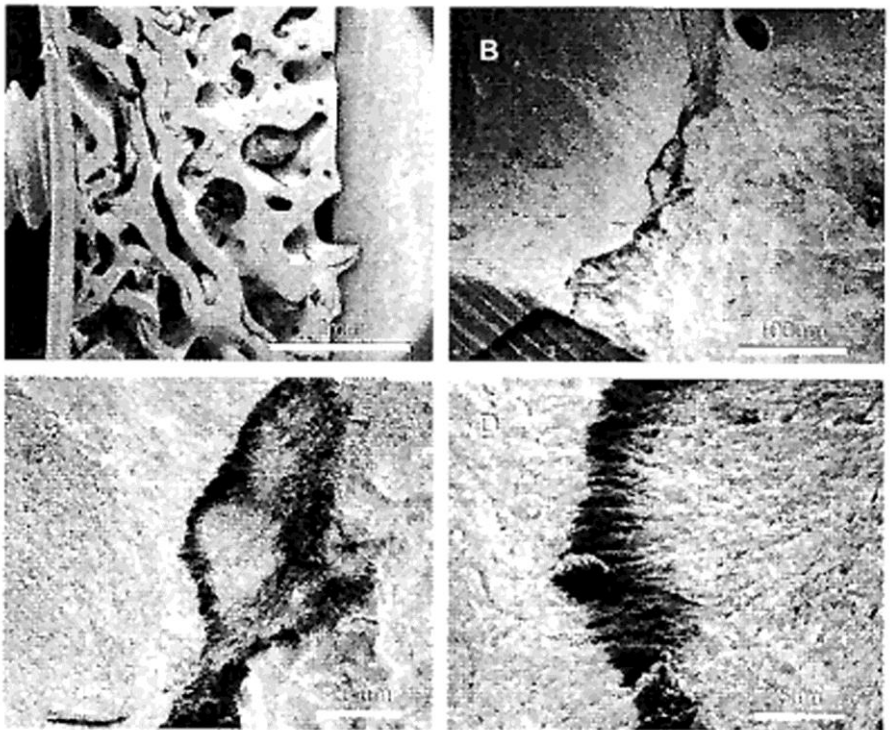

Figure 3.8 SEM images of partially crushed, boiled trabecular bone. (A) Low magnification view of the deformed trabeculae. The bone shows less breaks than the untreated or baked bone. (B) A crack formation seen from the surface and from the cross section, showing the multiple cracks that form the fractures. (C and D) High magnification view of the crack. Many filaments span the microcracks. The crack surface become hard to distinguish. (Fantner et al. 2004).

These methods have great potential to determine the mineral content of osteons, collagen fibril shear, crosslink scission, failure of collagen fibrils, crack formation and propagation, mineral displacement, and deformation and structural phase transformation (An et al.2000; Fantner et al. 2004; Tai et al. 2005). Detail description of i) BSE imaging and ii) TGA were outlined below.

i) Backscattered Electron (BSE) Imaging

Backscattered electron (BSE) imaging is a significant technique that is extensively used for the quantitative analysis of the mineral content of bones. BSE is a type of electron microscope which originates from a high-energy beam of electrons which are reflected from a sample by elastic scattering. BSE images are collected and converted by a detector to provide information, through the contrast of images to analyse the distribution of different chemical compositions within a sample. Figure 3.9 is an example of back-scattered scanning electron micrographs from Rho et al. (2002). BSE compares the darker and lighter regions. Darker regions indicate a lower mineral content and have been newly remodeled tissue. Lighter regions represent "older" interstitial tissues areas that are highly mineralized. A higher yield of electrons equates to a higher level of mineral density (Catanese III et al. 1999; Rho et al. 2002).

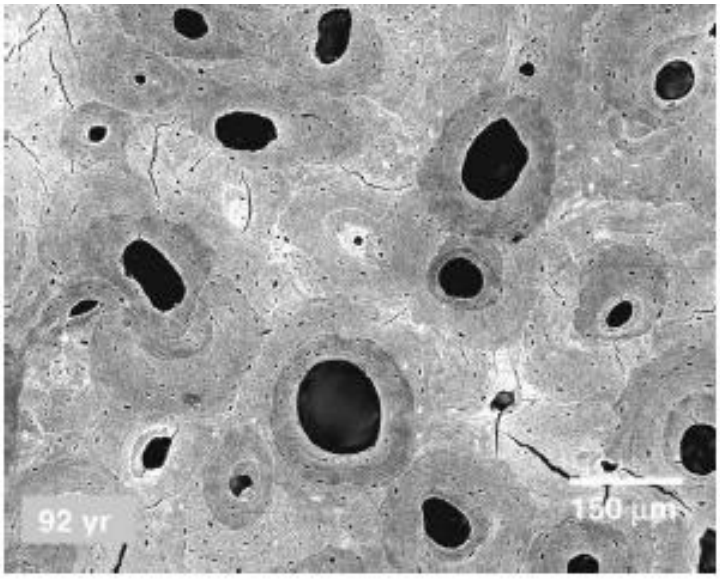

Figure 3.9 Backscattered scanning electron micrographs of 92-year-old male in carbon coated section (at 25kV) (Rho et al. 2002).

Hoc et al. (2006) and Bloebaum et al. (1997) strongly agreed that the intensity of BSE image has a close relation to mineral content. Hoc et al. (2006) suggests that the local Young's modulus to some extent is correlated to bone mineral content. However, the distribution of bone mineral content is not the only parameter to govern the local strain. Microstructures such as the porosity that may induce stress and strain concentrations also affect the mechanical behavior of bones.

ii) Thermal Gravimetric Analysis (TGA)

Thermal gravimetric analysis (TGA) is a monitoring system that determines how much weight (from bone) is lost as temperature changes. This technique involves heating a mixture with the testing substance to a temperature where one of the components can decompose into gas and dissociate into the air. If the compound in the mixture is known, then the percentage by mass can be determined by calculating the weight of what is left in the mixture and dividing it by the initial mass to obtain the percent mass of the substance in a sample. TGA is commonly used to determine characteristics of a material including polymers, absorbed moisture content of material, and level of inorganic and organic components in materials. Figure 3.10 shows the weight loss curve of different animal bones (Mkukuma et al. 2004).

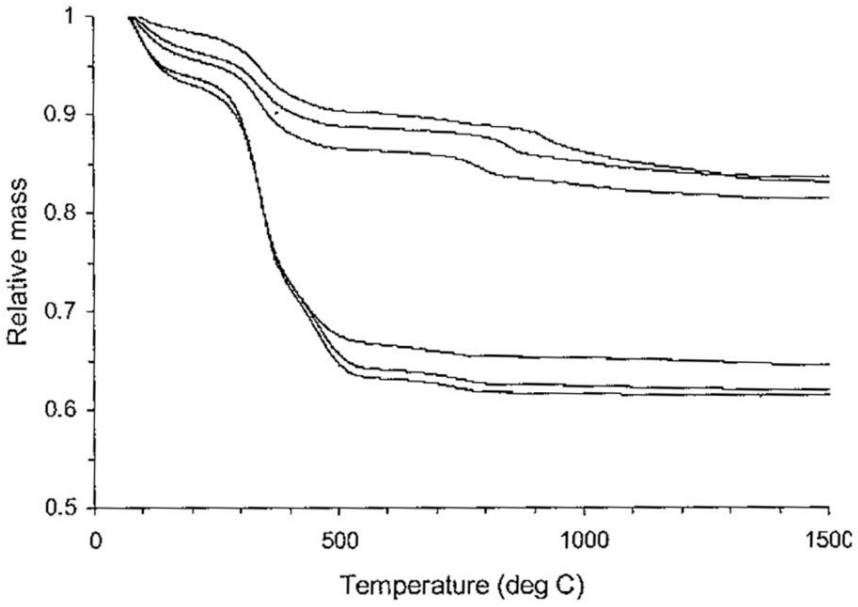

Figure 3.10 TGA results in air. Curves represent results in order (from top to bottom): porpoise ear bone, whale tympanic bulla, whale ear bone, whale periodic fin bone, deer antler, and cod clythrum. Masses were divided by the initial mass to give a relative mass, and are plotted against temperature (Mkukuma et al. 2004).

3.2 Computational Modeling of Bone

Extensive experimental and theoretical research had been undertaken looking at the correlation of physical properties (bone density, volume, and architecture, etc.) to bone mechanical properties (stiffness and strength) (An et al. 2000). The rapid development of computer technology combined with efficient microcomputed tomography or magnetic resonance imaging, makes it possible to perform three-dimensional (3-D) numerical modeling of bone. Finite element analysis (FEA) is one of the popular numerical analysis methods to investigate the stress and displacement of complex structures, such as whole bone (Ionescu et al. 2003; Taddei et al. 2007; Helgason et al. 2008; Yang et al. 2008; Chen et al. 2010), trabecular bone (van Rietbergen et al. 1995; Ulrich et al. 1998; Akhtar et al. 2006; Chevalier et al. 2007), collagen microfibril (Gupta et al. 2005; Buehler 2006; Dong et al. 2009) and to simulate the propagation of crack formation (Ortiz et al. 1999; Ural et al. 2006). The advantages of FEA are that it handles complex problems which are difficult to solve analytically, and is efficient for undertaking stress analysis in bones that are difficult to measure non-invasively in vivo (Yang et al. 2008).

3.2.1 Modelling of Whole Bone

Helgason et al. (2008) proposed and compared two different methods for assigning material properties to the right femur bone using FE models shown in Figure 3.11. One of the methods named V3 is a modification of Bone-Mat version V2 as described by Taddei et al. (2007).

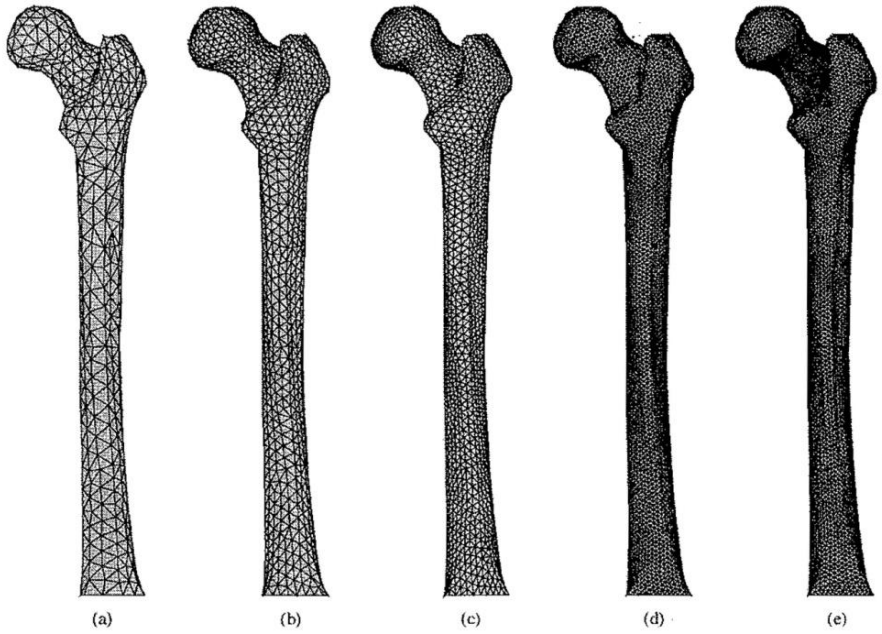

Figure 3.11 Five different FE meshes (10-node parabolic tetrahedral elements) of the femur used for convergence analysis. Models A-E are shown from left to right (Helgason et al. 2008).

Another new method is the nodal interpolation (NI). By modified material mapping strategy, a variable Young's modulus is introduced within each element against the systematic errors in the materials properties that are derived from the Computed Tomography (CT). Helgason et al. (2008) reported that both methods performed slightly better than the conventional method in predicting stress and strain. Chen et al. (2010) also used CT to scan a sheep tibia and combined this with FE modelling to analyse the bone structures (refer to Figure 3.12). Instead of modifying the dataset of the FE models, the researchers used the CT dataset to assign the material properties to a FE model in ABAQUS at each integration point. This improved the automation levels of the assignment procedure.

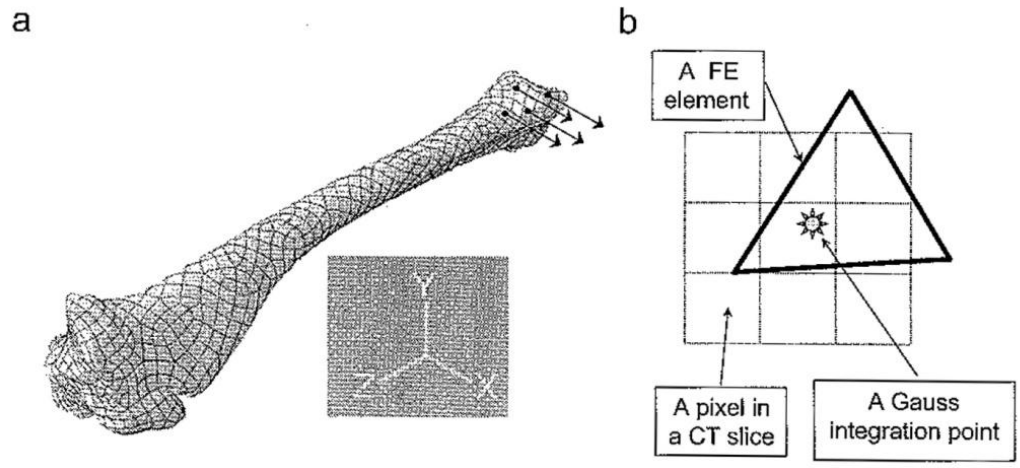

Figure 3.12 Assigning material properties from CT dataset to a Gauss integration point. (a) The FE geometry imported into ABAQUS. The arrows iindicate the four points where loading was applied and (b) an integration point in a pixel (Chen et al. 2010).

3.2.2 Modelling of Trabecular Bone

In order to enhance the accuracy of the finite element analysis results, researchers employed different meshing methods to model the trabecular bone structure. Ulrich et al. (1998) reported that by using a tetrahedron meshing method to model trabecular structure, it can dramatically reduce the loss of connectivity and maintain a better original geometry from micro-CT than with hexahedron elements. The tetrahedron meshing generated a smooth trabecular surface which provided an accurate calculation of the bone tissue loading. Figure 3.13 shows the FE models by using hexahedron and tetrahedron meshing methods.

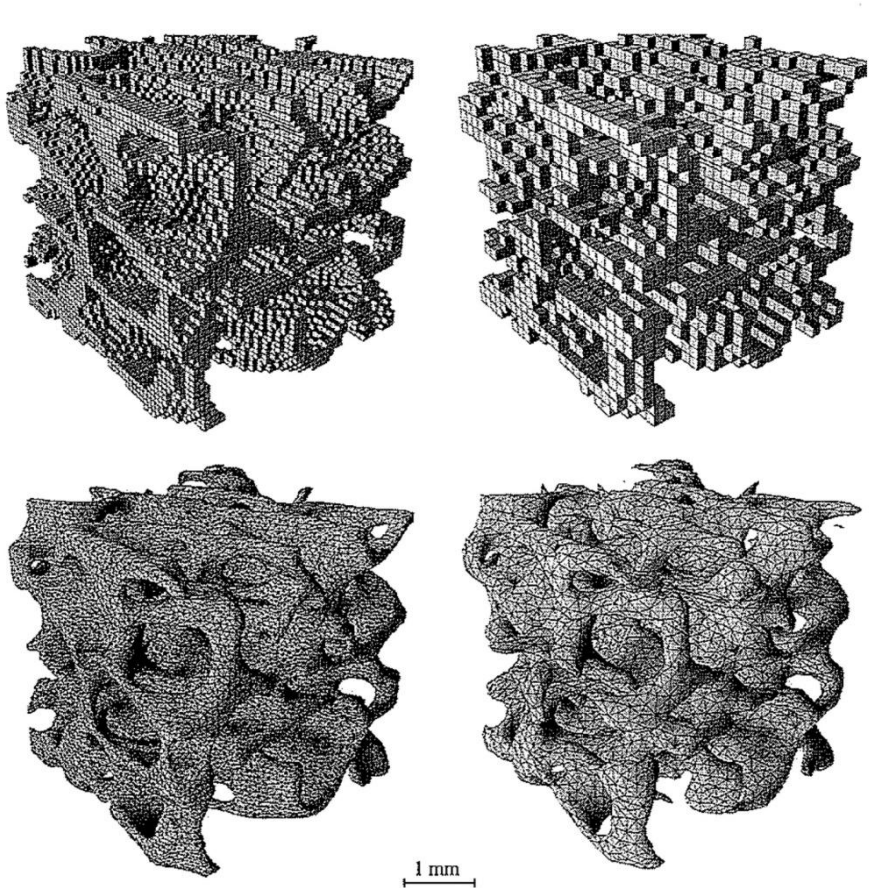

Figure 3.13 FE models of the femoral head specimen created at a voxel resolution of 84µm (left) and 168µm (right) using either the hexahedron (top) or the tetrahedron meshing approach (bottom) (Ulrich et al. 1998).

3.2.3 Prediction of Crack Propagation

Using computer modeling to predict crack propagation is essential and effective for the diagnosis and treatment of bone fractures. Ural et al. (2006) studied the FEM-based cohesive model to simulate crack growth behavior and age-related loss of bone toughness (refer Figure 3.14). Finite element simulation results show a rising R-curve (propagation toughness) with crack extension and also predict a greater age-related loss in propagation than initial toughness (Ural et al. 2006).

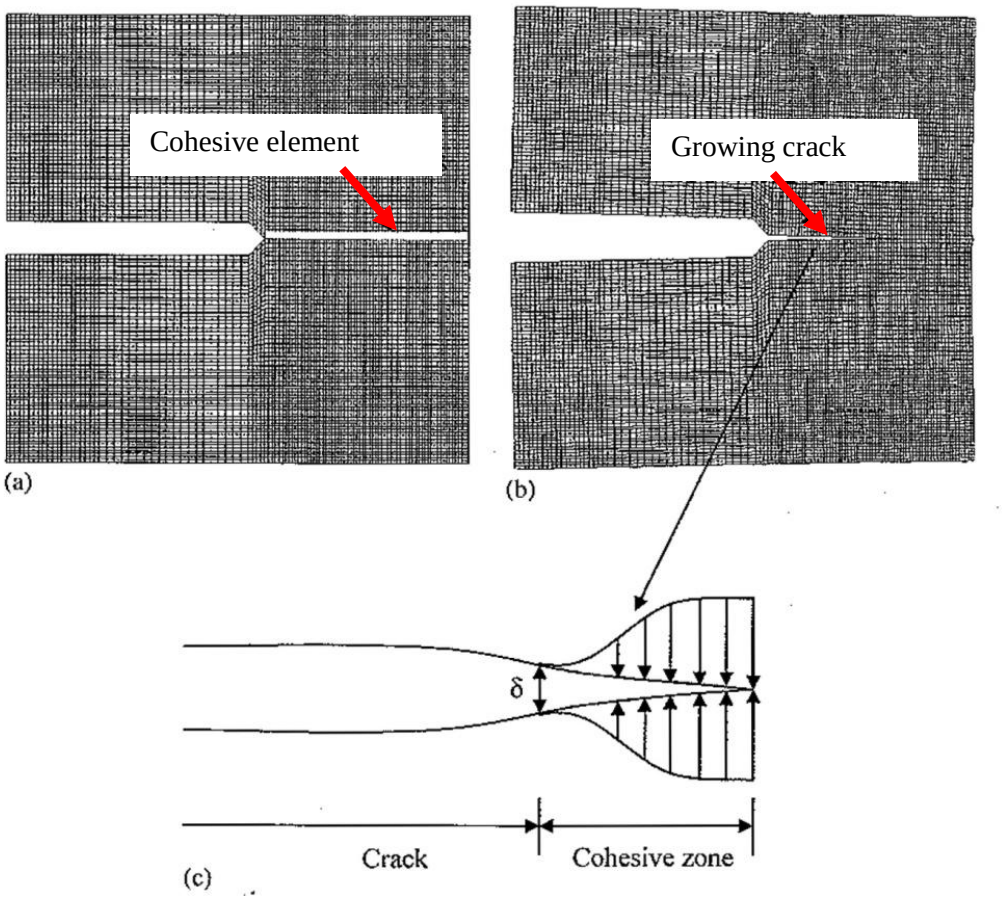

Figure 3.14 (a) An undeformed finite element mesh of CT specimen showing the location of the cohesive elements marked by the white line (b) a deformed mesh of CT soecimen with a propagation crack. Note that displacement magnification factor is 5. (c) A schematic representation of the cohesive zone (Ural et al. 2006).

3.3 Bone Grafting Technology

Bone that is transplanted from one region of the skeleton to another to aid the bone to heal, provide support, and strengthen and improve bone function is called a bone graft (Parikh 2002; Spine Org., viewed on May 2006). Most often, bone grafts are used to fill voids between the bones of the spine that are caused by disease, injury deformity or during surgical procedure (Spine Org. 2006). According to Murugan et al. (2005) approximately 6.3 million bone fractures occur every year in the United States of America (USA). Of these, approximately 550,000 cases require bone grafting. The hip, ankle, tibia and fibula bones of the skeleton are the most frequent regions where bone fractures occur. It was also reported that hip replacements in the year 2000 was approximately 152,000 cases. This represented an increase of around 33% from 1990 to 2000. It is also expected to increase to about 272,000 cases by the year 2030 (Murugan et al. 2005).

If a fracture is minor, bone is normally capable of self-healing within a few days to weeks. However, if the fracture is severe and incurs a loss of volume, the bone is unable to heal by itself. Bone grafting may then be required to restore function, without damaging any of the living tissue (Murugan et al. 2005). There are five major fracture healing phases as shown in Table 3.4 (Kenley et al. 1993).

Table 3.4 Phases in the normal fracture healing sequence

Phases	Time	Activities
Induction	0 - 2 days	- Hematoma formation - Release soluble inductive, growth, and inflammatory
Inflammation	2 - 14 days	- Polymorphonclear neutrophils - Macrophages
Soft callus	2 - 8 weeks	- Highly cellular and collagenous material in fracture gap - Chondeogenesis and angiogenesis
Hard callus	2 - 12 months	- Woven bone forms - Considered healed at this stage
Remodeling	1 or more years	- Lamellar bone forms

3.3.1 Bone Graft Materials

The function of graft materials is not only to replace bone, but also to stimulate the body to regenerate the loss of bone, reduce the healing time, and most importantly function is to strengthen the formation of new bone (Murugan et al. 2005). Ideal bone graft materials should be: i) osteoinductive and conductive; ii) biomechanically stable; iii) disease free; and iv) mineral antigenic (Finkemeier 2002). Bone grafting materials include i) autografts, ii) allografts, iii) xenografts, and iv) biocomposite materials, each with their own advantages and disadvantages (Murugan et al. 2005).

i) Autografts bone

Autografts bone is the most preferred bone grafting materials that are harvested directly from another part of the recipient's body. They are commonly used for human bone replacement because the autograft bone contains the greatest amount of the recipient's own growing bone cells and proteins such as osteogenicity,

osteoconductivity, and osteoinductivity properties help to simulate the bone growth (Finkemeier 2002; Spine Org., viewed on May 2006). Osteogenicity means the osteoblasts are able to produce minerals to calcify the collagen matrix for the formation of new bone. Osteoconductivity means the grafts provide an interconnection for the attachment of new osteoblasts and osteoprogenitor cells so that the new cells can migrate and new vessels can form. Osteoinductivity means graft should have the ability to induce non-differentiated stem cells or osteoprogenitor cells to differentiate into osteoblasts (Laurencin et al. 2009). Table 3.5 summarises osteogenic, osteoconductive, and osteoinductive materials that are currently approved for use in the United States of America (Kenley et al. 1993).

Table 3.5 Approved materials for bone grafting (Kenley et al. 1993)

Category	Material	Source*
Osteogenic, osteoinductive, and osteoconductive	- Autogenous bone graft - Allogeneic demineralised bone matrix	- Patient - *Osteotech*
Osteogenic and osteoinductive	- Autogenous bone marrow	- Patient
Osteoconductive	- Bovine bone mineral - Coralline hydroxyapatite	- *W. Lorenz* - *Interpore*

*** Italics indictate corporate source.**

Trabecular or cortical bone, demineralised bone matrix, and autologous bone marrow are suitable for autografts (Finkemeier 2002). Trabecular bone grafts are excellent space fillers as they can quickly adapt to the recipient site and revascularise easily. Moreover, cortical bone grafts are also a good choice for segmental fractures of bone less than 5 - 6 cm as they provide excellent structural support at the recipient site (Finkemeier 2002). The advantages of autografts are their excellent success rate, low

risk of disease transmission, preferable acceptance and effectiveness in the transplantation site, and they provide a strong frame work for the new bone growth (Spine Org., viewed on May 2006). However, autograft bone is limited in quantity. Additional surgery is often required which adds discomfort and pain to the recipient (Catanese III et al. 1998).

ii) Allografts bone

Allografts bone comes from bone banks that harvest from cadavers which provide an alternative to autografts. They have been used for the last three decades in periodontal therapy (American Academy of Periodontology 2001). Instead of harvesting bone from a recipient's own body, allograft bone can be obtained in large quantity from bone banks. This eliminates limited supply isues and adds another surgical site as autografts (Spine Org., viewed on May 2006). Allografts can derive from different types of bones in different forms. This inclues demineralised bone matrix, morselised and trabecular chips, and cortical bones from the pelvis, ribs, femur, tibia, and fibula (Finkemeier 2002).

Although allografts do not contain living cells, it is still suitable for surgeries that require large pieces of structural bone to be grafted. This is because the allograft bones are osteoconductive and stimulate the growth of new bone as well as providing mechanical support in compression (Finkemeier 2002; Parikh 2002). Despite of the advantages of allografts, they do present some drawbacks, such as the delay of healing due to the lack of living cells, and potential of disease transmission, such as

human immunodeficiency virus (HIV), during transplantation (Finkemeier 2002). Nevertheless, the risk can be greatly reduced by improving the tissue banking standards.

iii) Xenografts bone

Xenograft is another possible bone substitute material for transplantation from one species to another (animal bone tissue to human). Bovine bone mineral is commonly used due to the structure and morphology which are similar to human bone (Murugan et al. 2005). Again, the infrequent application in xenografts is due to the concern of the possibility of disease transmission during transplantation. In order to eliminate the risk of infection, the procurement, processing, and sterilisation of bone grafts is important. The most common sterilisation methods include autoclaving, gamma irradiation and ethylene oxide. However, most of these methods are associated with the destruction of collagen and affect the quality of the bone (Hamer et al. 1999; Dunsmuir et al. 2003).

iv) Biocomposites materials

Apart from the autografts, allografts and xenografts, researchers have investigated other materials that could be used for bone transplantation such as metal and alloys, ceramics, polymers, composites and nano-composites. Although most of these bone substitutes have similar positive properties of autograft, none have yet to demonstrate all the benefits of using a recipient's own bone. Table 3.6 summarises the advantages and disadvantages of the biomaterials for bone grafting.

Table 3.6 Classification of biomaterials for bone grafting (Murugan et al. 2005)

Biomaterials	Advantages	Disadvantages	Application	Examples
Metal and alloy	Too strong, tough, ductile	Dense, may corrode	Bone plates, load-bearing bone implants, dental arch wire, and dental brackets	Titanium, stainless steel, Co-Cr alloys, and Ti alloys
Ceramic	Bioinert Bioactive Bioresorabable High reistance to wear	Brittle, poor tensile, low toughness, lack of resilience	Hip joints and load-bearing bone implants Bone filler, coatings on bio-implants, orbital implant, alveolar ridge augmentation, maxillofacial reconstruction, and bone tissue engineering	Alumina, zirconia HA, bioglass TCP
Polymer	Flexible, resilient, surface modifiable, selection of chemical functional groups	Not strong, toxic of a few degraded products	Bone tissue scaffolds, bone screws, pins, bone plates, bone and dental filler, and bone drug delivery	Collagen, gelatin, chitosan, alginate, PLA, PGA, PLGA, PCL, PMMA, PE,
Composite	Strong, design flexibility, enhanced mechanical reliablility than monolithic	Properties might be varied with respect to fabrication methodology	Bone graft substitutesm middle ear implants, bone tissue ecaffolds, guided bone regenerative membranes, and bone drug delivery	HA/collagen, HA/PLGA, HA/PLLA, HA/PE
Nano-composite	Larger surface area, high surface reactivity, relatively strong interfacial-bonding, design flexibility, enhanced mechanical reliability than monolithic and /or microcomposite	No optimized technique for material processing	Major areas of orthopedics, tissue engineering, and drug delivery	Nono-HA/collagen, Nano-HA/gelatin, Nano-HA/chitosan, Nano-Ha/PLLA

3.3.2 Temperature-dependent Properties of Bone

Extensive research has been conducted in the past few years to investigate the mechanical properties of cortical and trabecular bones in order to understand the problems associated with bone structure and function under different conditions. The cortical bone is composed of mineral component (Hydroxyapatite) and organic matrix (mainly Type 1 collagen), thus is regarded as a composite material. Therefore, the procedure for preparing specimens in order to reduce the damage of polypeptide collagen is significant.

Typically bone is sectioned into appropriate sizes and removed of bone marrow under constant deionized water irrigation. The bone is then dehydrated at room temperature before it is embedded into a supportive fixture (Rho et al. 1997; Rho et al. 1999b & c; Turner et al. 1999; Wang et al. 2006). Dehydrated bone is commonly used for mechanical properties testing. Rho et al. (1999a) have reported that dried bovine bone has an increase in elastic modulus by 9.7% for interstitial lamellae and 15.4% for osteons. Moreover, the hardness of interstitial lamellae and osteons was increased by 12.2% and 17.6%, respectively. Heat-treated cortical bone has been proposed as a substitution for bone transplant material to overcome the risks of rejection and disease transfer of allograft and xenograft of implantation (Shin et al. 2005). With the advantages obtained in biological and mechanical properties, it is believed that heat-treated bone is an excellent alternative for bone graft and synthetic bone substitutes (Catanese III et al. 1999; Hengsberger et al. 2003; Shin et al. 2005; Todoh et al. 2008).

However, some researchers (Currey 1988; Hoc et al. 2006) argue that dehydrated bone would have a tremendous effect on strength. Bone specimens can therefore be deep-frozen and kept wet or immersed in saline solution throughout testing to alleviate these concerns. Shin et al. (2005) reported that heat treatment to 60^{o}C does not show significant effects in a bone's mechanical strength. However, heat treatment over 100^{o}C would lead to a decrease in a bone's mechanical strength. As temperature increased, there was a slight decrease of elastic modulus when measured by a torsion test. It is suggested that is due to the change of type 1 collagen. X-ray diffraction results obtained by Todoh et al. (2008) indicated that heat treatment below 200^{o}C had no significant changes in the crystal structure. Therefore the damage in the mineral phase is lower but did induce collagen degeneration.

Chapter 4
Mechanical Properties of Heat-treated Bovine Cortical Bone

4.1 Introduction

The mechanical properties of bone depend on the relationship between structural organisation in macroscopic scale and bone component in microscopic scale. Bone is regarded as a complex composite material consisting of hydroxyapatite mineral particles and organic matrix (mainly Type 1 collagen), which contributes to bone growth and strength, stiffness and tensile properties. In recent years, heat-treatment of banking bone has become one of the simple and practical sterilisation methods to preserve bone graft as it has potential to enhance bone growth. In addition, xenograft bone mineral is proposed as a bone substitute material because it has similar biological and mechanical properties to human bone. This chapter presents the localised mechanical properties of heat-treated bovine cortical bone measured by nanoindentation. Global stiffness was conducted by compressive test. Thermal gravimetric analysis (TGA) was used to investigate the condition of bone's organic

matrix after heat treatment. Furthermore, energy dispersive X-ray spectroscopy (EDX) which integrated with Backscattered Electron (BSE) imaging was conducted to examine the relationship between mineral content and mechanical strength within the nanoindentation regions.

4.2 Mechanical Properties of Heat-treated Bovine Cortical Bone by Nanoindentation Test

4.2.1 Fabrication Methodologies

Materials

Frozen ribs and a femur of bovine cortical bone (~3-4 years old) were procured from a local slaughterhouse. Three specimens from the rib bone were sectioned into 5mm thickness along its transverse plane direction, and another three specimens were sectioned into 3mm thickness along its longitudinal plane by a low-speed diamond saw (Metkon, resin bonded diamond cut-off wheels) under constant water application (refer Figure 4.1). Six specimens from ribs bovine cortical bone were randomly divided into three groups. Each group contained a longitudinal and transverse directions specimen. Group 1 contained pristine specimens of rib. The specimens were dried at room temperature (~23°C) for 24 hours as a control group. The bones in Group 2 and 3 were heat-treated in an oven for two hours at pre-set temperatures of 90°C and 150°C (refer Figure 4.2).

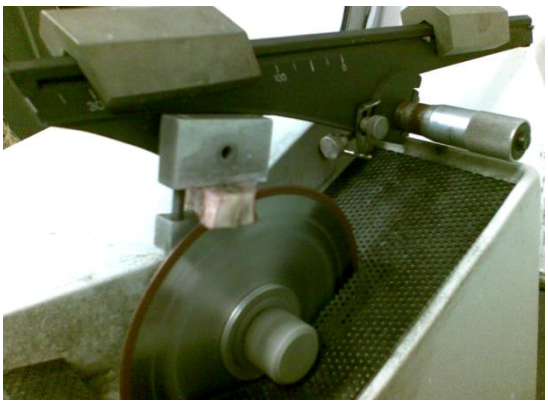

Figure 4.1 Metkon, resin bonded diamond cut-off wheels for machining the specimens.

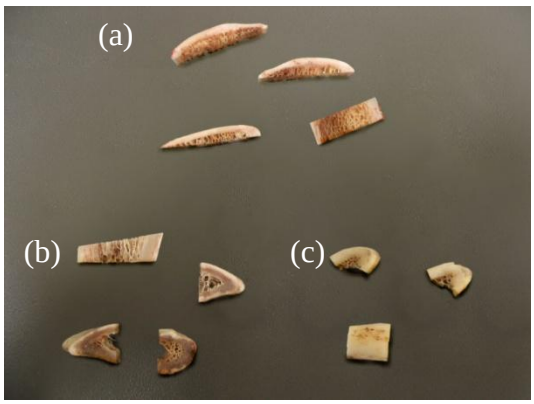

Figure 4.2 Bovine bones from ribs were machined and divided into 3 groups, (a) pristine, (b) heat-treated at 90°C, (c) heat-treated at 150°C.

Another 15 specimens from femur were sectioned into 5 mm thickness along its transverse plane direction by the same method and randomly divided into five groups containing three specimens each. Group 4 contained pristine specimens of femur that were dried at room temperatures (~23°C) as a control group. Specimens in Groups 5 to 8 were pre-heat treated in an oven for one hour at four distinct pre-set temperatures (refer Figure 4.3). Tables 4.1 and 4.2 summarise temperature ranges of the heat-treated bovine cortical bone of rib and femur. The temperature range selected in the experiment was based on studies conducted by Wang et al. (1999) and Todoh et al. (2008).

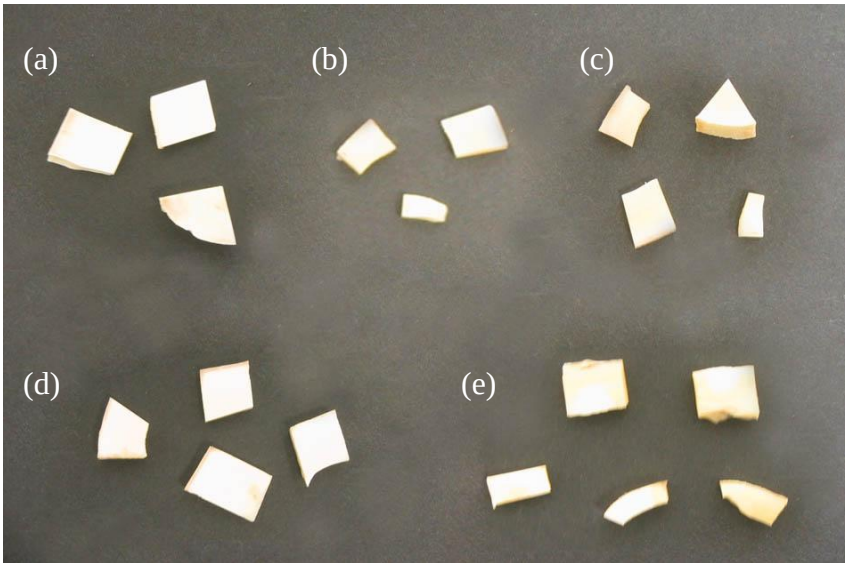

Figure 4.3 Bovine cortical bones from femur were machined and divided into 5 groups, (a) pristine, (b) heat-treated at 37°C, (c) heat-treated at 90°C, (d) heat-treated at 120°C, and (e) heat-treated at

A soft distilled water jet was used to remove marrow from inside each specimen. All specimens were also placed into an ultrasonic bath to remove any surface debris. Distilled water was used in an effort to reduce the formation of undesired minerals or bacteria on the specimen surface.

Table 4.1 Group and temperature ranges of bovine cortical bone from rib

Regions - Rib	Temperature Range	Heat-treated Time	Support	Cure Time and Temperature
Group1 (Pristine)	Dried at RT (~23°C)	24 hours	Embedded inside epoxy resin	24 hours at RT (~23°C)
Group 2	Heat-treated at 90°C	2 hours	Embedded inside epoxy resin	24 hours at RT (~23°C)
Group 3	Heat-treated at 150°C	2 hours	Embedded inside epoxy resin	24 hours at RT (~23°C)

Table 4.2 Group and temperature ranges of bovine cortical bone from femur

Regions - Femur	Temperature Ranges	Heat-treated Time	Support	Cure Time and Temperature
Group 4 (Pristine)	Dried at RT (~23°C)	24 hours	Embedded inside epoxy resin	24 hours at RT (~23°C)
Group 5	Heat-treated at 37°C	1 hour	Embedded inside epoxy resin	24 hours at RT (~23°C)
Group 6	Heat-treated at 90°C	1 hour	Embedded inside epoxy resin	24 hours at RT (~23°C)
Group 7	Heat-treated at 120°C	1 hour	Embedded inside epoxy resin	24 hours at RT (~23°C)
Group 8	Heat-treated at 160°C	1 hour	Embedded inside epoxy resin	24 hours at RT (~23°C)

RT = Room temperature

Sample Preparation

After cooling for 12 hours, bone specimens were embedded without being vacuumed into epoxy resin to provide support and allowed to cure for 24 hours at room temperature (refer Figures 4.4 and 4.5). Since Araldite GY251 epoxy resin (with hardener HY956 mixture ratio of 5:1) was used to provide support for the bone specimens, there was no need to use a vacuum container to remove excessive bubbles that may have occured by mixing the epoxy and hardener.

Studies by Fan et al. (2002) and Hoffler et al. (2000) suggest that the employment of epoxy resin only pervades into trabecular pores but not the tissue, thus, minimally influencing nanoindentation results. Rho et al. (1997) and Wang et al. (2006) suggested that all the indentations needed to perform away from the bone edge and mounting resin in order to reduce the inaccuracy of embedding on the measurements.

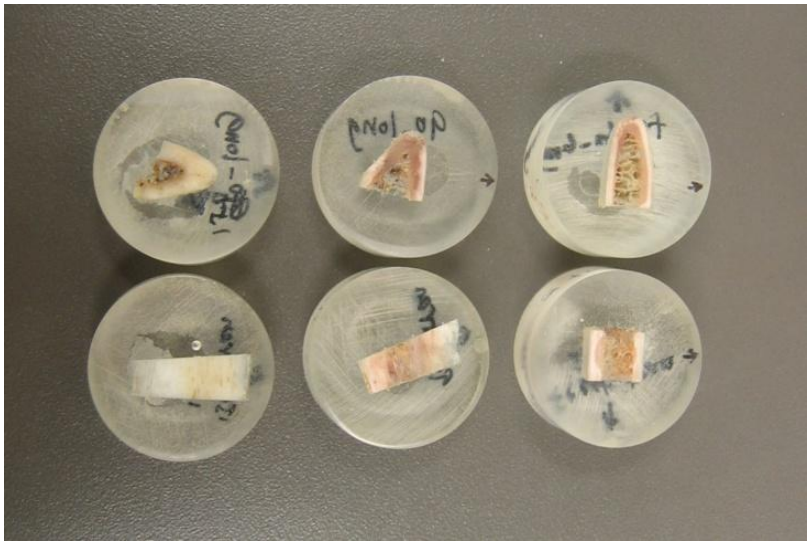

Figure 4.4 Bovine cortical bones from ribs were embedded into epoxy resin without being vacuumed to provide support.

Figure 4.5 Bovine cortical bones from femur were embedded into epoxy resin without being vacuumed to provide support.

Post-machining of the samples

In order to obtain a better nanoindentation test result, all surfaces of the embedded specimens were polished to generate a smooth surface. The specimens under constant water irrigation were ground using different grades of silicon carbide paper (60, 320, 800, 1200 and 2000 grit), and then further polished manually by soft synthetic flock polishing cloths with different grades of the diamond powder (15μm, 6μm and 1μm). After grinding and polishing, the specimens were washed by distilled water to clean up the surface debris. All specimen preparation was confirmed under an optical microscope (refer Figure 4.6) in order to obtain a clear lamellar microstructure of the bone and a smooth surface for nanoindentation (refer Figure 4.7).

Figure 4.6 Optical microscope (Nikon, Model EPIPHOT200).

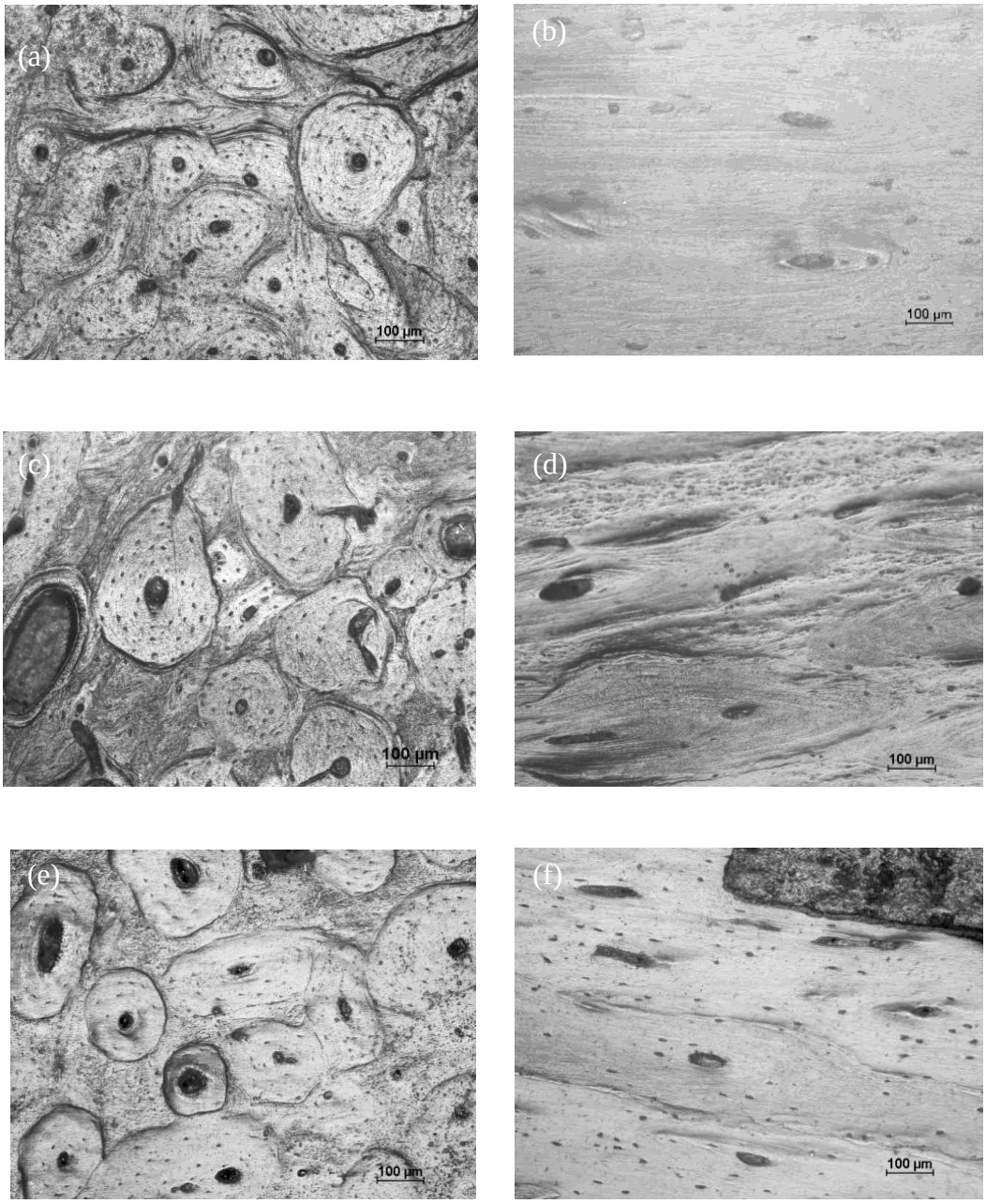

Figure 4.7 Optical micrographs of the rib cortical bone sample, (a, b) pristine bone in longitudinal and transverse directions respectively, (c, d) heat-treated at 90°C in longitudinal and transverse directions respectively, (e, f) heat-treated at 150°C in longitudinal and transverse directions respectively.

4.2.2 Nanoindentation Tests

A scanning nanoindenter comprised of a scanning probe microscope and a nanoindentation transducer was used at room temperature (~23°C) throughout the experimental study (refer Figure 4.8 (TriboScratch; Hysitron, Inc., Minneapolis, MN)). A sharp Berkovich (three-sided pyramid) diamond indenter tip was embedded in the transducer to measure the Young's modulus and hardness. The experimental specimen was glued on a stainless steel stage and the microstructure to be indented was located under the indenter and the optical microscope for continuous monitoring of the loads and indenter displacements. By using the x-y table and z height, the small indentations could be precisely positioned on the specimen surface with constant loading and displacement rate. (The distance between the indenter and specimen was remained constant during the test.)

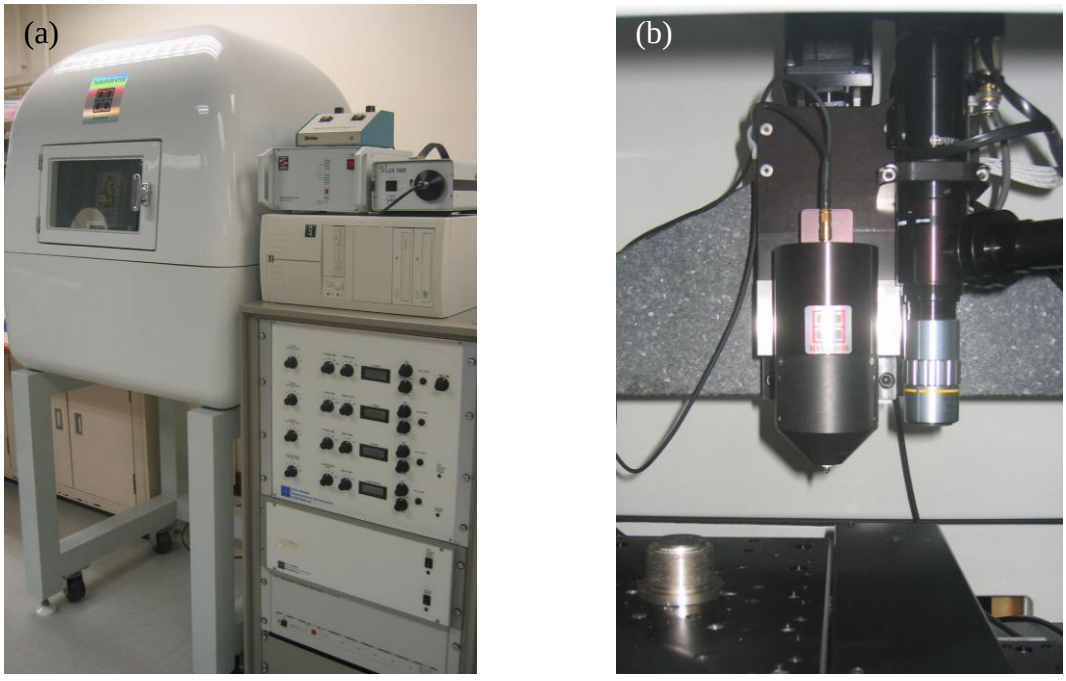

Figure 4.8 (a) Nanoindentater (TriboScratch; Hysitron, Inc., Minneapolis, MN) and (b) Berkovich diamond indenter tip attached to the TriboScratch system.

As the test started, the Berkovich indenter tip was slowly driven toward the specimen surface at a constant displacement rate and a permanent hardness impression was made after the surface contact. A maximum load of 30mN with a loading/unloading rate of 0.3mN/s produced a surface contact depth of 1000nm and the hardness impression was held for a period of 5s at the maximum load to eliminate any creep behavior.

The data obtained from indentation load-displacement tests were analysed to calculate the elastic modulus, *E*, and the hardness, *H*, using the method outlined by Oliver and Pharr, where the indenter area function has been well documented (Oliver et al. 1992). This method is based on the measurement of the contact stiffness *S*, and the upper portion of the unloading data to determine the relationship between contact stiffness and the elastic properties of the specimen.

The upper portion of the initial unloading contact stiffness *S* is defined as Equation 4.1

$$S = \frac{dP}{dh} \tag{4.1}$$

The relationship between contact stiffness and the elastic properties of the specimen is defined as Equation 4.2

$$S = \frac{dP}{dh} = \frac{2}{\sqrt{\pi}} E_r \sqrt{A} \tag{4.2}$$

Where *P* is the load, *h* is the depth, E_r is the reduce modulus, and *A* is the projected area of the elastic contact. The reduce modulus is related to the elastic modulus, *E* as per Equation 4.3

$$\frac{1}{E_r} = \left(\frac{1-\nu_s^2}{E_s}\right) + \left(\frac{1-\nu_i^2}{E_i}\right) \tag{4.3}$$

where, E_s and ν_s are the elastic modulus and Poisson's ratio for the specimen and E_i and ν_i are the same parameters for the indenter. For a standard diamond indentor probe, E_i is 1140 GPa and ν_i is 0.07. Bone is assumed to be isotropic, and elasto-plastic material, thus, the Poisson's ratio ν_s is assumed to be 0.3. As mentioned by Rho et al. (1997), the change measured value of E_s should not exceed 8% while ν_s ranges from 0.2 – 0.4.

The elastic modulus is derived by measuring the initial unloading stiffness and assuming that the contact area is equal to the optically measured area of the hardness impression. The hardness, *H*, is calculated as:

$$H = \frac{P_{\max}}{Ac} \tag{4.4}$$

where, P_{max} is the maximum indentation force and A_C is the projected contact area.

4.2.3 Nanoindentation Test Results

Cortical bone is formed by repeating units named Haversian systems (or "osteons") which are composed of regular, cylindrical layers of mineralised collagen fibers called lamellae (Rho et al. 1998a). Since bone remodeling is more active in a trabecular bone than cortical bone, cortical bone is deemed to be a mature bone even though they are well identified as the same kind of material. Mechanical properties at the microstructural level might be affected by the maturation of cortical bone, such as the degree of calcification and orientation of collagen fiber (Rho et al. 1998a; Wang et al. 2006).

In the rib specimens, a total of 642 indentations were produced within osteons and nearby interstitial regions along the longitudinal direction (perpendicular to the transverse axis). In the transverse direction (the perpendicular direction to the longitudinal axis), it was difficult to distinguish the osteons from interstitial lamellae, due to the structural arrangement of lamellae. The locations of indentations were therefore randomly chosen. Hence, the elastic modulus and hardness in transverse direction were averaged without regard to their exact location. A summary of the elastic moduli, E, and hardness, H of rib specimens in longitudinal and transverse directions is presented in Table 4.3. These results indicated the response of osteons and interstitial regions varied with temperature and direction. As temperature increased, the E and H also increased in both longitudinal and transverse directions. In addition, the E and H in the longitudinal direction were greater than in transverse direction due to the microstructural components.

Table 4.3 Average elastic moduli and hardness values of rib's cortical bovine bone in various temperatures

	Group 1 Pristine Specimen		Group 2 Heat-treated at 90^0C		Group 3 Heat-treated at 150^0C	
Direction	L	T	L	T	L	T
No. of Indentation	75	118	116	120	108	105
Young's Modulus, Average (GPa)	16.23±2.75	10.38±2.6	19.18±4.61	10.43±1.72	23.43±5.02	12.77±2.54
Hardness, Average (GPa)	0.51±0.15	0.39±0.11	0.67±0.23	0.44±0.11	0.73±0.25	0.54±0.17

L = Longitudinal direction; T = Transverse direction

As shown in Figure 4.9A, 75 indentations were produced in longitudinal direction of rib's specimens (Group 1), the average E value is 16.23±2**.75** GPa, and the average H value is 0.51±0.15 GPa. As shown in Figure 4.9B, 118 indentations were produced in the transverse direction, the average values of E and H are 10.38±2.6 GPa and 0.39±0.11 GPa, respectively.

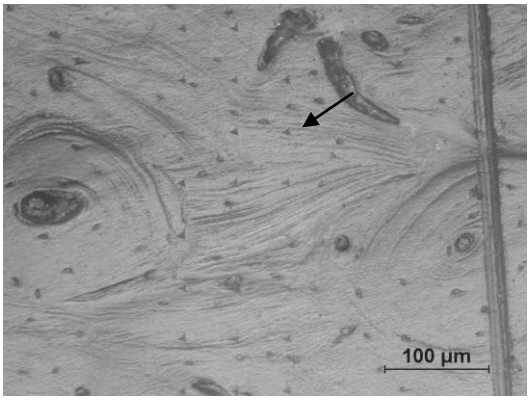

Figure 4.9A A total of 75 indentations were produced in longitudinal direction of an intact bovine cortical bone.

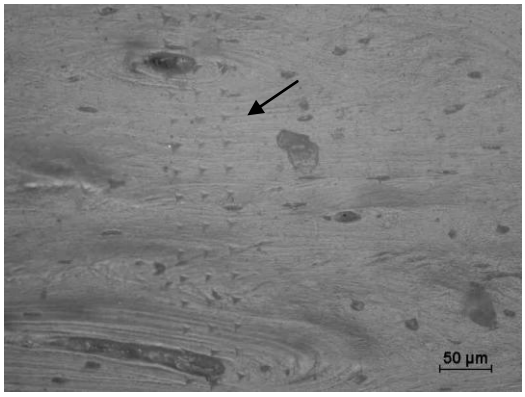

Figure 4.9B A total of 118 indentations were produced in transverse direction of an intact bovine cortical bone.

Figures 4.10A and B illustrate indentations produced in longitudinal (116 indentations) and transverse (120 indentations) directions, respectively. A moderate increase of 18% and 31% in E and H, respectively were found in Group 2 (heat-treated at 90°C) in the longitudinal direction as compared to Group 1. Whereas, only 0.4 and 12.8% increase in E and H, respectively are found in transverse direction.

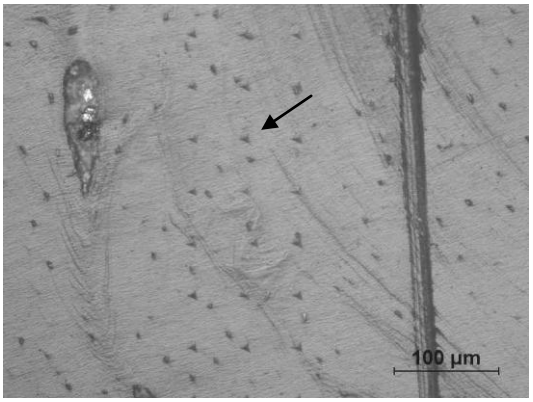

Figure 4.10A A total of 116 indentations were produced in longitudinal direction of heat-treated cortical bone at 90^0C.

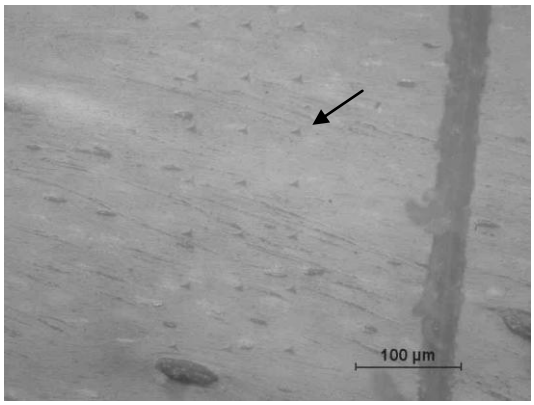

Figure 4.10B A total of 120 indentations were produced in transverse direction of heat-treated cortical bone at 90^0C.

As shown in Figure 4.11A, 108 indentations were made in longitudinal direction in Group 3. As shown in Figure 4.11B, 105 indentations were made in transverse direction. A significant increase of 44% and 43% in E and H, respectively were found in Group 3 (heat-treated at 150°C) in longitudinal direction as compared to Group 1. In addition, E and H in transverse direction also shows an increase of 23% and 38% as compared to Group 1. Figure 4.12 depicts the load-displacement curve of heat-treated rib bone specimen in longitudinal and transverse direction.

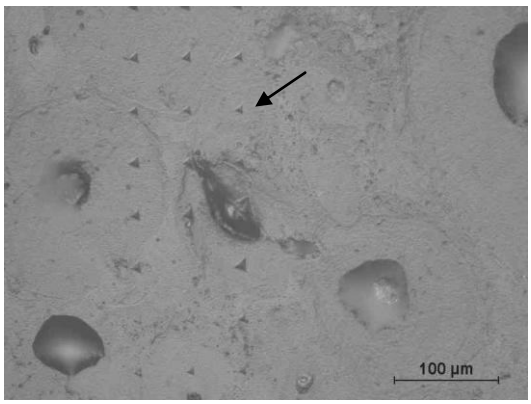

Figure 4.11A A total of 108 indentations were produced in longitudinal direction of heat-treated cortical bone at 150^{0}C.

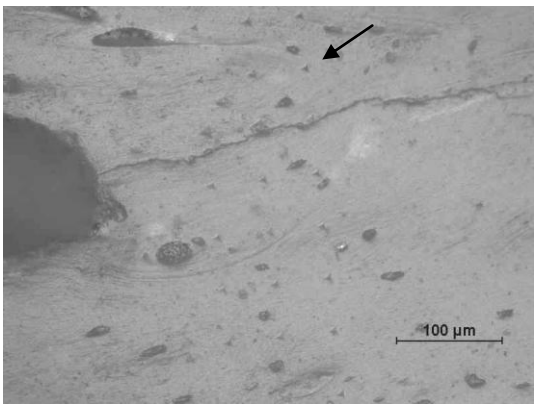

Figure 4.11B A total of 105 indentations were produced in transverse direction of heat-treated cortical bone at 150^{0}C.

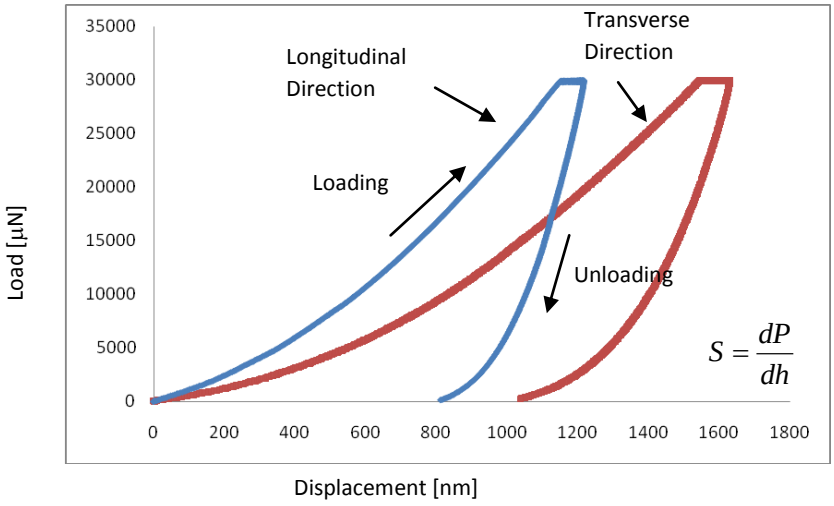

Figure 4.12 Load-displacement curve of heat-treated rib bone at 90^{0}C. S is the contact stiffness, P is the applied load and h is the depth. S, is the slope of the initial portion of unloading curve.

A total of 1200 indentations were undertaken in the femur specimens in this study. Among them, 600 indentations were made within 15 specimens in five different single osteonal lamellae in longitudinal direction (refer Figure 4.13A).

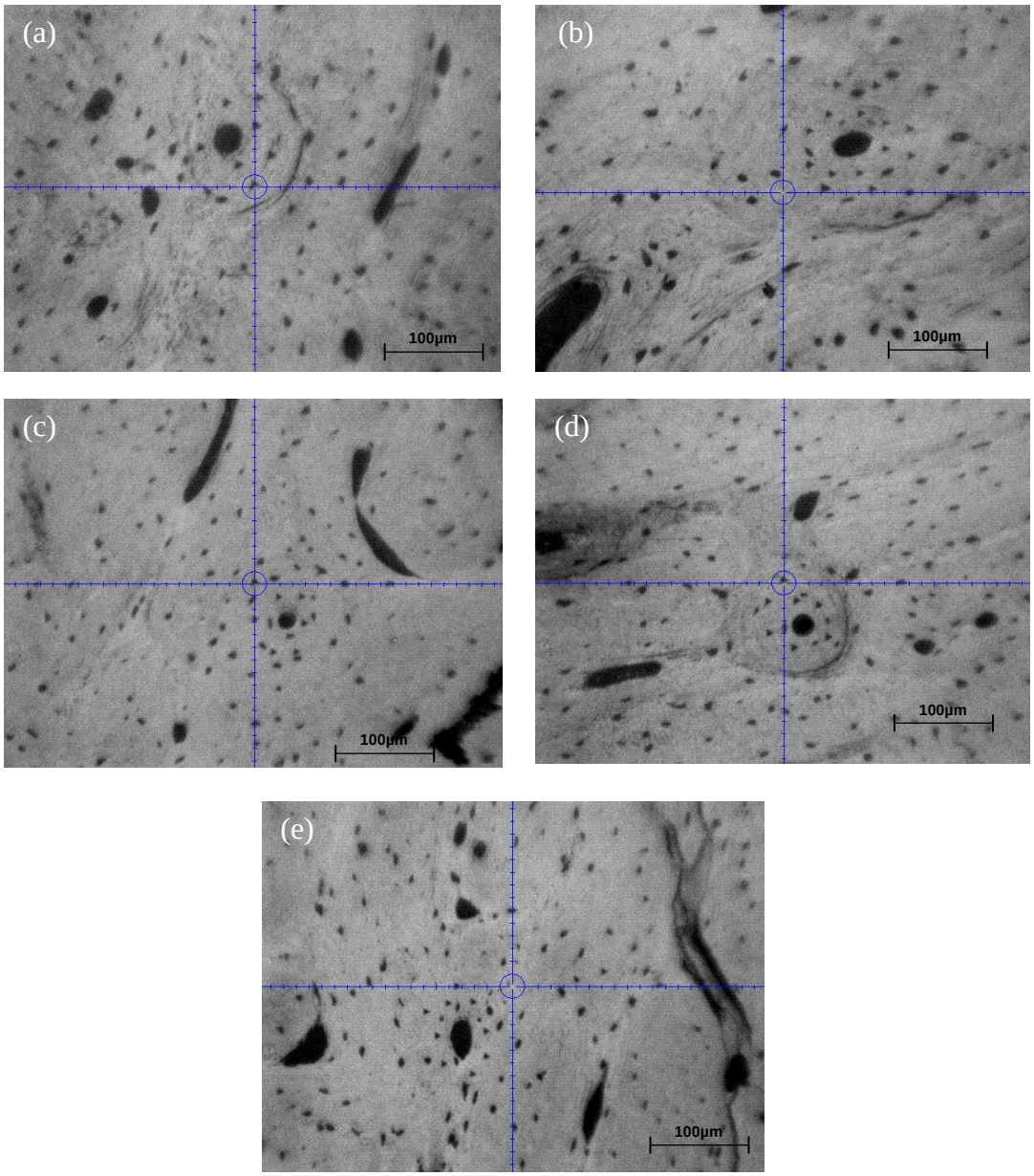

Figure 4.13A Specimens of bovine cortical bone from femur were heat-treated at five different temperature ranges from (a) pristine, (b) 37^0C, (c) 90^0C, (d) 120^0C and (e) 160^0C. Nanoindentation marks were impressed around Haversian canal.

Each single osteonal lamellae contained eight indentations which were made around Haversian canal. The approximate distance from Haversian canal was 0.02 mm and the distance between each indentation was set to between 0.025mm to 0.03mm. Another 600 indentations were made within 15 specimens in five randomly chosen interstitial lamellae regions (refer Figure 4.13B).

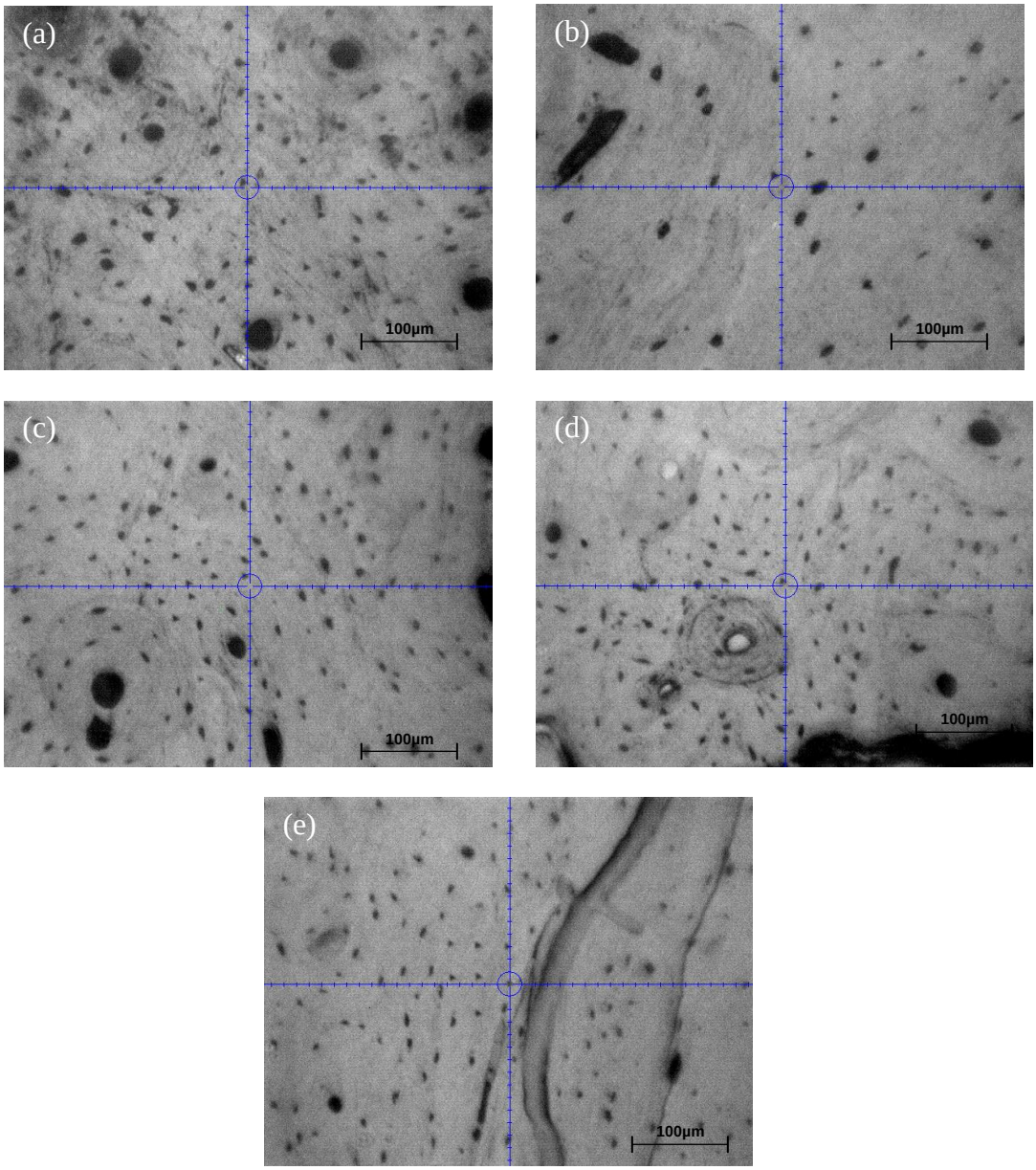

Figure 4.13B Specimens of bovine cortical bone from femur were heat-treated at five different temperature ranges from (a) pristine, (b) 37^0C, (c) 90^0C, (d) 120^0C. Nanoindentation marks were impressed around interstitial lamellae.

Each region contained eight indentations with an approximate 0.025mm to 0.03mm distance between each indentation. The E and H values of osteonal and interstitial lamellae are presented in Table 4.4.

Table 4.4 Average elastic moduli and hardness of femur's cortical bovine bone in various temperatures (Standard deviations are shown)

			Osteons		Interstitial lamellae	
Tempera-ture range (°C)	No. of Specimen	No. of Indentation	Elastic modulus, GPa (SD)	Hardness, GPa (SD)	Elastic modulus, GPa (SD)	Hardness, GPa (SD)
Pristine	3	40	26.13±1.61	0.96±0.06	28.89±2.11	1.07±0.09
37	3	40	18.59±1.28	0.83±0.08	18.38±1.53	0.84±0.06
90	3	40	26.32±2.46	1.06±0.08	28.50±1.69	1.17±0.06
120	3	40	28.77±2.33	1.11±0.11	30.54±2.57	1.24±0.11
160	3	40	28.65±2.07	1.25±0.11	29.14±1.70	1.27±0.10

The experimental results suggest that the E and H in osteonal lamellae are slightly lower than interstitial lamellae at different pre-set temperatures. For the pristine femur bone specimen (Group 4), the average values of E and H in osteona lamellae are 26.13 GPa and 0.96 GPa, respectively. While the average values of E and H are 28.89 GPa and 1.07 GPa in interstitial lamellae, respectively. For specimens heat-treated at 37°C, a significant decrease to 18.59 GPa and 0.83 GPa are observed in E and H, respectively in osteonal lamellae. The E and H in interstitial lamellae also followed the same pattern as osteonal lamellae, which showed a decrease to 18.38 GPa and 0.84 GPa, respectively in the specimens being heat-treated at 37°C. However, as bone specimens were heat-treated at 90°C, 120°C and 160°C, it showed a significant increase of E and H in both osteonal and interstitial lamellae.

An ANOVA, one-way analysis of variance method was used to calculate the mean values of the elastic moduli and hardness of osteonal and interstitial lamellae in the longitudinal direction. Results are shown in Table 4.5. The statistical difference in elastic moduli and hardness for osteonal are (p<0.03) and (p<0.06), respectively. For the interstitial lamellae, the statistical difference of elastic moduli and hardness are (p<0.08) and (p<0.2), respectively.

Table 4.5 ANOVA is employed to analysis the statistically differences of elastic moduli and hardness of osteonal and interstitial lamellae at various temperatures.

	p			
	Osteons		Interstitial lamellae	
Temperature range (°C)	Elastic modulus	Hardness	Elastic modulus	Hardness
Pristine	<0.000001	<0.00001	0.144	0.793
37	<0.000001	<0.000001	<0.000001	<0.000001
90	<0.00001	<0.00001	<0.00001	<0.00001
120	0.114	0.317	0.288	0.002
160	<0.000001	<0.000001	<0.000001	<0.000001

p= statistically significant difference

4.2.4 Nanoindentation Test Discussion

The nanoindentation results suggests that the elastic modulus (E) and hardness (H) of cortical bovine bone vary at different temperatures and is strongly dependent upon the anatomical region (rib or femur), orientations (longitudinal and transverse directions) and tissue types (osteons and interstitial lamellae) of the bone. As temperature increased, both rib and femur specimen results showed an increased in E and H. In addition, the values of E and H in femur specimens are higher than the rib specimens at the same temperature range. According to Zysset et al. (1999), the key

factor that may account for this difference is the turnover rate and osteon type in distinctive anatomical locations. That is, the mean age of osteons is diminished by the high turnover rate, hence, relieving mineralisation and affecting the elastic properties of bone.

Interestingly, a significant decrease in E and H was found in femur specimen heat – treated at 37^0C. This may be due to the presence of type 1 collagen molecules in bones. Leikina et al. (2002) stated that, the triple helices of type 1 collagen is unstable and easily melts at temperatures just several degrees above body temperature. However, the calcified collagen molecules, which composed of pyridinoline, are formed as hydroxypyridinium bonds and are very stable. Both rib and femur specimen results show that as temperature is increased to 90^0C, 120^0C and 150^0C respectively, the E and H values increase as compared to the pristine specimens. Where the temperature was increased to 160^0C in femur, the E and H values started to have a slight decreased as compared to the pristine specimens.

The nanoindentation results also show that, in the longitudinal direction, the E and H values of rib specimens are generally much higher than those in the transverse direction at any heat treated temperature. As shown in Figure 4.12, the load-displacement curves indicating the response of osteons varied with direction. This finding suggests that the structural orientation of the collagen networks has a significant influence on the mechanical properties of bones. According to Zioupos et

al. (1999) and Wang et al. (2001), collagen parameters are correlated to toughness and bone strength but have no significant impact on bone stiffness.

Another important finding in this study is the elastic modulus and hardness of the interstitial lamellae of femur is higher as compared to osteons lamellae. The modulus ratio (E1/E2) between osteons (E1) and interstitial lamellae (E2) observed here was approximately 0.9, which is similar to Rho et al. (1999c) results at 0.7. Rho et al. (1999c) also stated that osteons (22-24 GPa) were less stiff and mineralised than interstitial bone (24-26 GPa) due to the fact that interstitial bones is made from primary bone tissue whilst osteons are made of remnants of old osteons. The E and H values of interstitial lamellae in this study at various temperatures are from 18.4 to 30.5 GPa and 0.84 to 1.27 GPa, respectively. The E and H values of osteons are from 18.6 to 28.8 GPa and 0.83 to 1.25 GPa, respectively.

For specimens heated at 90^0C, a slight increase of 0.7% and 10% in E and H values was observed respectively in osteons compared to the pristine specimens. However, the E values in interstitial lamellae demonstrated a slight decrease of 1.3% and H values increase of 9.3% compared to the pristine specimens. Both osteons and interstitial lamellae have a moderate increase of 10% and 5.7% in E values, respectively when heat-treated at 120^0C; the H values also has a moderate increase of 15.6% and 15.8% in osteons and interstitial lamellae, respectively. For specimens heat-treated at 160^0C, a moderate increase of 9.6% in E values in osteons but the interstitial lamellae only has a slight increase of 0.85% compared to the pristine

specimens. The H values in both osteons and interstitial lamellae have a significant increase of 30.2% and 18.7%, respectively. These results correlate with findings reported by Wang et al. (2001). In the Wang et al. (2001) study, it was reported that non-calcified molecules in bone degenerated at about 43^0C while calcified collagen molecules started to degenerate at about 120^0C and completed the degeneration at 190^0C. The results also agree well with the findings of Catanese III et al. (1999) who reported that cortical bones heated up to 350^0C still maintained 63% of the elastic strength in compression compared to that of untreated bones. Catanese III et al. (1999) suggested that heat-treated bones at 350^0C could still be an excellent compressive load-bearing substitute in a human body.

4.3 Mechanical Properties of Heat-treated Bovine Cortical Bone by Compressive Test

4.3.1 Fabrication Methodologies

For the compressive test, an additional of nine specimens of frozen bovine bone from ribs in the longitudinal direction were machined and divided into three groups. The cross sectional dimensions were approximately 1.2 x 2.6 mm with 1 mm height (refer Figure 4.14).

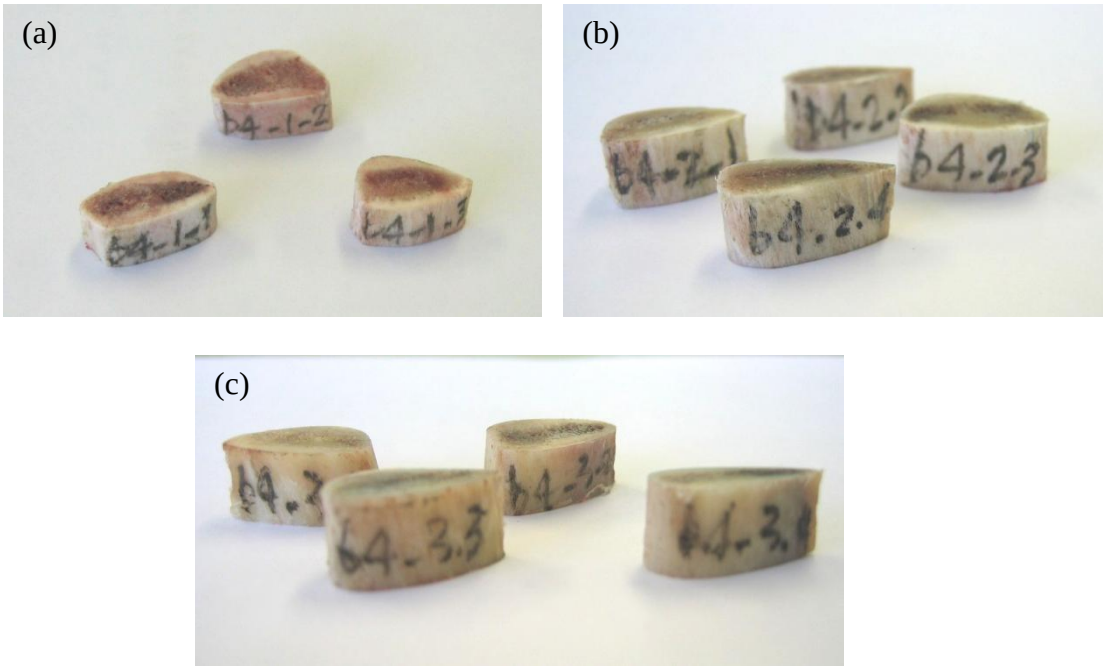

Figure 4.14 Specimens of bovine cortical bone from rib were machined for compressive test. (a) non-heat treated (pristine) as a control group; (b) heat-treated at 90°C; and (c) heat-treated at 150°C.

A soft distilled water jet was used to remove marrow from inside the specimens. All specimens were placed into an ultrasonic bath to remove any surface debris. Distilled water was used to reduce the formation of undesired minerals or bacteria on the specimen surface.

Bone specimens in Group 1 (control group) were non-heat treated (pristine) bone which was dried at room temperatures (~23°C). Groups 2 and 3 were heat-treated at pre-set temperatures in an oven at 90°C and 150°C, respectively for two hours. The tested specimens were cooled for 12 hours at room temperature. The specimens were not embedded into epoxy in order to avoid inaccurate results.

4.3.2 Mechanical Properties Measured by Compressive Tests

The compressive test was performed on an axial static testing (RT/50(50kN) , MTS Corp., Eden Prairie, Minnesota). The specimen was aligned on its bone axis and placed between two parallel stainless steel platen (refer Figure 4.15).

Figure 4.15 The specimen was placed between two parallel stainless steel platens to conduct compressive test.

The compressive strength of all specimens was tested to failure at a compression speed of 0.4 mm/s (refer Figure 4.16). Stress was determined from the measured applied force (P) divided by the cross-sectional area (A), ($\sigma = P/A$) whereas, strain (ε) was measured as length elongation (δ) divided by the original specimen length (L_0).

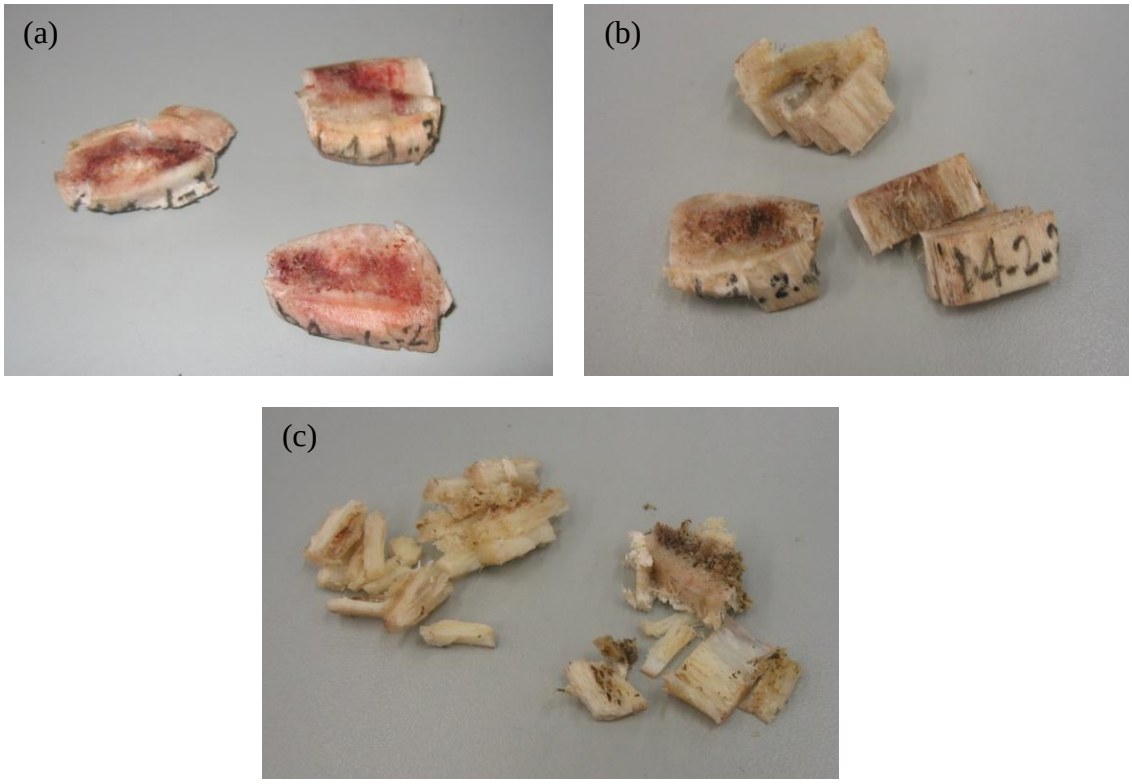

Figure 4.16 All specimens were tested to failure: (a) non-heat treated (pristine) as a control group; (b) heat-treated at 90°C; and (c) heat-treated at 150°C.

A program was created to obtain the data and an Excel file was used to plot the stress versus strain curve. The elastic modulus or Young's modulus ($E = \sigma/\varepsilon$) was generated from the slope of the stress-strain curve in the elastic region. Since it is often difficult to pinpoint the exact stress at which plastic deformation begins, the yield stress is often taken to be the stress needed to induce a specific amount of permanent strain, typically 0.2% (Roylance, 1999).

4.3.3 Compressive Test Results

The differences in the elastic properties of the non-heated and heat-treated samples were analysed using a one-way analysis of variance (ANOVA). The elastic modulus (obtained from the linear portion of the stress-strain curve) of the bovine bone varies with the increase of heating temperature (refer in Table 4.6). The compressive modulus of Group 1 specimen was 3.5 ± 0.6 GPa, whereas, the moduli of Group 2 and 3 were 3.9 ± 0.44 GPa and 5.6 ± 0.48 GPa respectively. The bone specimen, heat-treated at 90^0C showed a slight increase of 11.4% in stiffness (E). In addition, a significant increase of 60% in stiffness (E) was obtained in bone specimen heat-treated at 150^0C. The yield stress and yield strain for the heat-treated (90^0C and 150^0C) specimens (Groups 2 and 3), are outlined in Table 4.6. Figure 4.17 shows the typical stress strain curve of the non-treated group bovine specimen. Figure 4.18 shows the Young's modulus and yield stress (σ_y) versus heating temperature.

Table 4.6 Average elastic modulus, stress and stain at various temperature ranges

	Group 1 Pristine	Group 2 Heat-treated at 90^0C	Group 3 Heat-treated at 150^0C	*p* value
Average Elastic Modulus (GPa)	3.5±0.60	3.9±0.44	5.6±0.48	0.0047
Average Yield Stress (MPa)	72.84±3.8	88.51±18.15	91.85±9.36	0.200
Average Yield Strain (%)	3.18±0.42	2.45±0.48	1.67±0.08	0.016

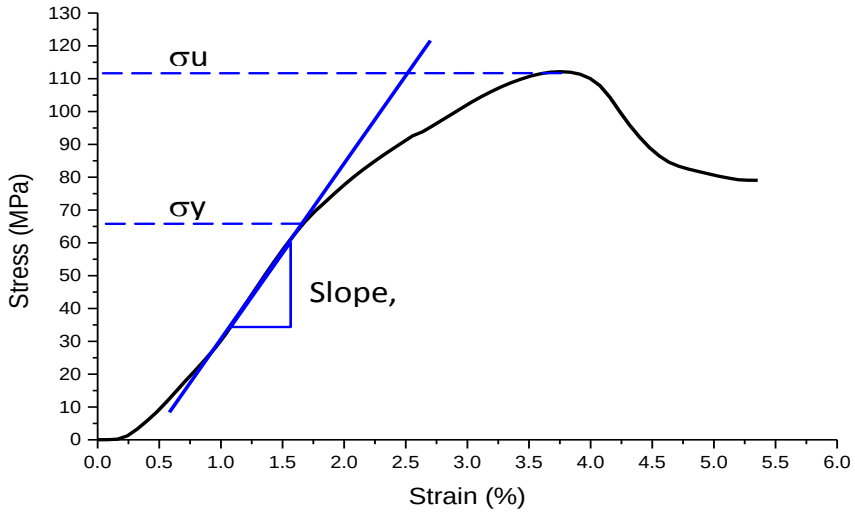

Figure 4.17 Stress-strain curve of heat-treated bone at 90°C.

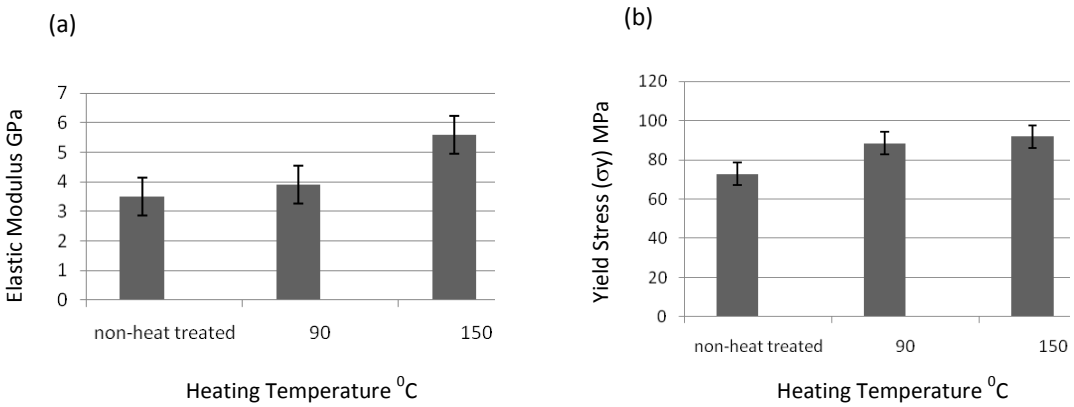

Figure 4.18 Compressive test results for mechanical properties: (a) Young's modulus vs heating temperature; (b) yield stress (σ_y) vs heating temperature.

4.3.4 Compressive Test Discussion

Compressive tests were conducted to further investigate the global mechanical properties of bovine cortical bone. It is interesting to note that the elastic modulus (E) of bone specimen in the compressive tests appear to have changed as much as those

of the localised mechanical properties measured in the nanoindentation tests. This indicates the resistance to deformation in heat-treated bovine specimens to be higher than that of pristine bone. Although the impact on stiffness is limited, the increased temperature might render the bones to become more brittle.

Various researchers have reported that the variation in bone strength is related to the change of bone collagen (Wang et al. 1999; Shin et al. 2005; Akhtar et al. 2005;). Wang et al. (1999) have stated that, the collagen molecule structure would be irreversibly changed (eg. unwinding of the triple helix) at specific temperatures (over 150°C), which plays an important role in the fracture properties of bone. In addition, Shin et al. (2005) also reported that the degeneration of collagen would most likely affect bone strength against torsion rather than compression. The results also agree well with the findings of CataneseIII et al. (1999), who reported that the cortical bones heated up to 350°C still maintained 63% of the elastic strength in compression compared to that of untreated bone.

4.4 Examine Mineral Content by Backscattered Electron (BSE) Imaging

In order to comprehensively investigate the potential correlations between mechanical strength and mineral content of bovine cortical bone, backscattered electron imaging (BSE) was applied to examine the mineral content of the indentation regions. As described by Bloebaum et al. (1997), the mechanical properties of bones are relatively determined by the mineral content of bone matrix, thus, it acts as an important role in turning bone strength to become stronger, tougher and stiffer until it reaches the optimum mineralisation (Rho et al. 2002; Roschger et al. 2008).

4.4.1 Fabrication Methodologies

The bovine rib cortical bone specimens used for nanoindentation tests were further used for BSE imaging to enable the images to be captured within the nanoindentation regions.

After the nanoindentation test, the surface of the bovine cortical specimens in the longitudinal direction were coated in a thin layer of carbon by vacuum evaporation (refer Figure 4.19). Carbon was used instead of gold because the images would be clearer. The coating method undertaken was in accordance with that used by Roschger et al.'s (2008) study.

Figure 4.19 The surface of the bone specimen was coated in a thin layer of carbon for BSE imaging.

4.4.2 Examination of Mineral Content by BSE Imaging

Conventionally, the microradiography technique is used to evaluate the variation of bone mineral content and mineralised tissues. However, due to the limitation of the volumetric resolution (estimated range was from 400-4000μm^3) and inaccuracy caused by projection errors effects, it was deemed that using BSE imaging would provide an advantage in obtaining a high volumetric resolution in bone (ranged from 0.07-137μm^3) (Bloebaum et al. 1997). Therefore, combining the nanoindentation mechanical properties test results with the BSE imaging results may explain the correlation between mechanical strength and mineral content of bone matrix.

Backscattered electrons were obtained by a detector that reflected the high-energy electrons after they collided with the surface of the specimens. The BSE signal was then converted into a black and white image, where the grey levels represent the mineral content (Roschger et al. 2008). BSE imaging (Scanning Electron Microscope

(Leica Stereoscan 440)) was operated with the accelerating voltage of 20 kV at a working distance of 10 mm to capture the images (refer Figure 4.20).

Fig. 4.20 Scanning Electron Microscope.

4.4.3 BSE Imaging Results

Six sites within the indentation regions were scanned. Figure 4.21 depicts the indentation marks can be clearly observed. Visual examination of the BSE images indicated that the light grey regions corresponded to tissues with higher mineral content and dark grey region with lower mineral content. The image results are consistent with those of Bloebaum et al. (1997), Hoc et al. (2006) and Roschger et al. (2008) in that the local variation of mineral content can be quantified by the frequency distribution of grey levels.

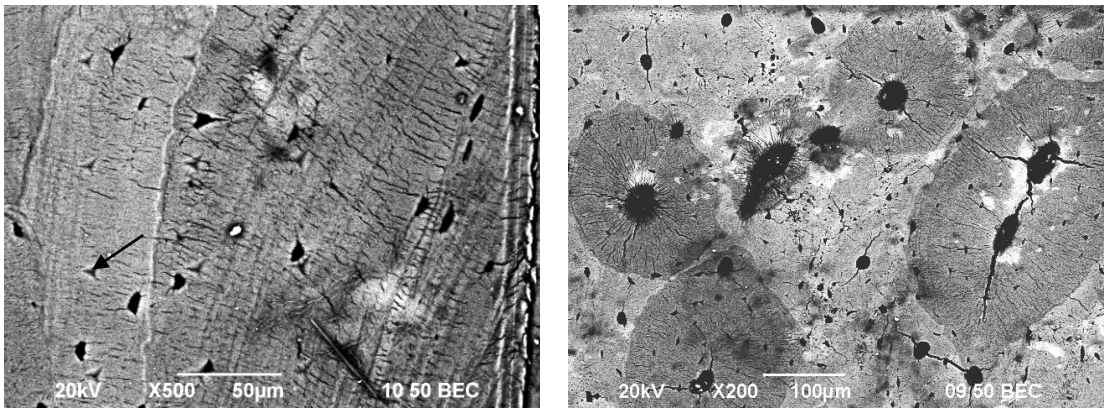

Figure 4.21 Backscattered scanning electron (BSE) images of bovine cortical bone. Light and dark gray regions represented the higher and lower mineral content respectively.

Electron diffraction x-ray (EDX) was performed to further examine the weight percent of calcium and phosphorous in each site (refer Figure 4.22). EDX results were used to conduct Ca/P molar ratios, which confirmed the compositional differences among the three groups of specimens. Results are summarised in Table 4.7. The data demonstrated the pristine bone contained the highest level of calcium (66.64%) among the three groups. As the bovine bone was heat-treated, the weight percentage of calcium decreased. Heat-treated bovine cortical bone to 90°C contained 64.91% of calcium on average. It only decreased 2.6% of calcium level as compared to pristine bovine bone. The average weight percentage of calcium in heat-treated bovine cortical bone to 150°C was 50.99%. This represented a significant decrease around 30.6% on average as compared to the pristine group.

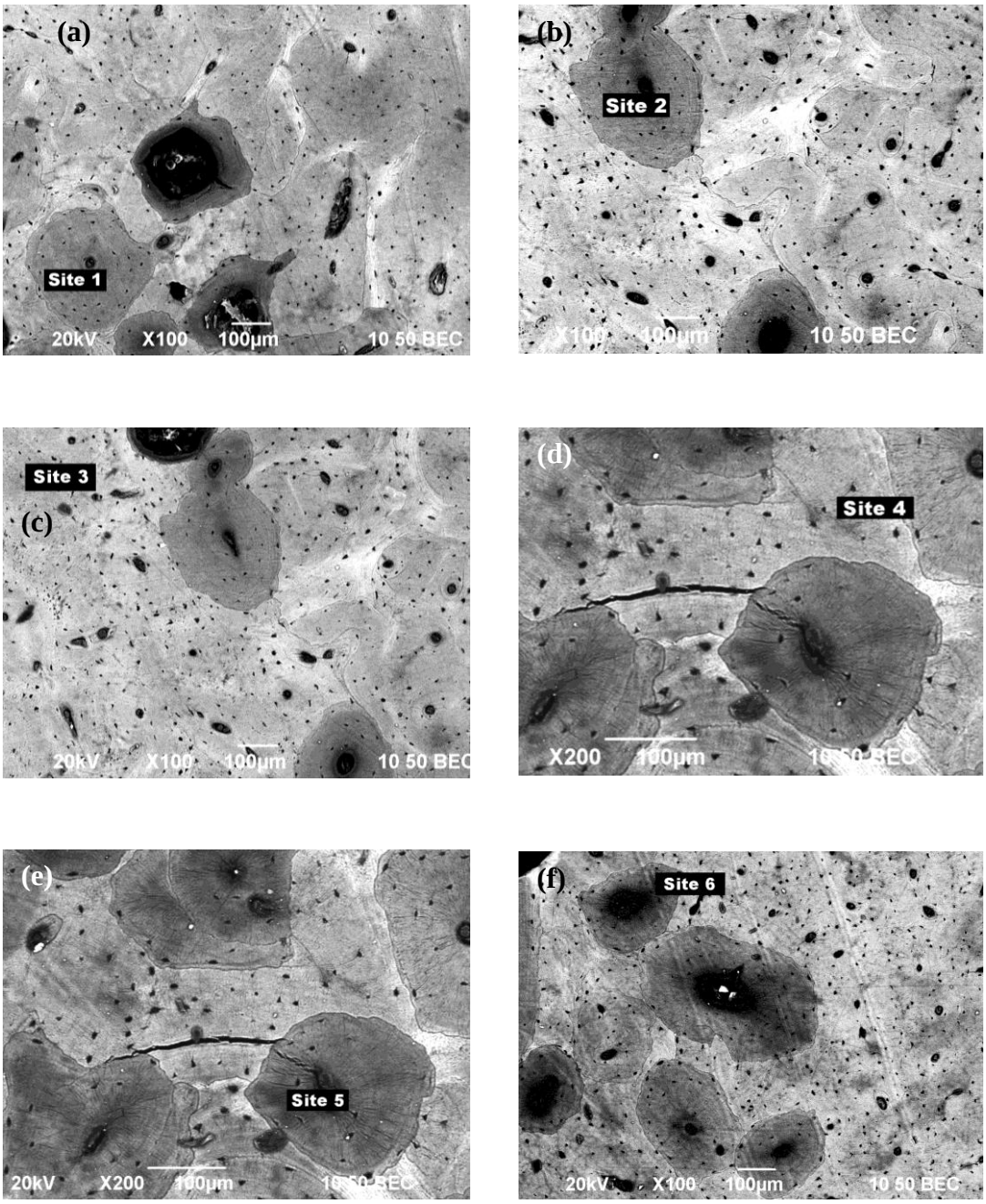

Figure 4.22 (a-f) is the BSE scanned regions of the pristine group.

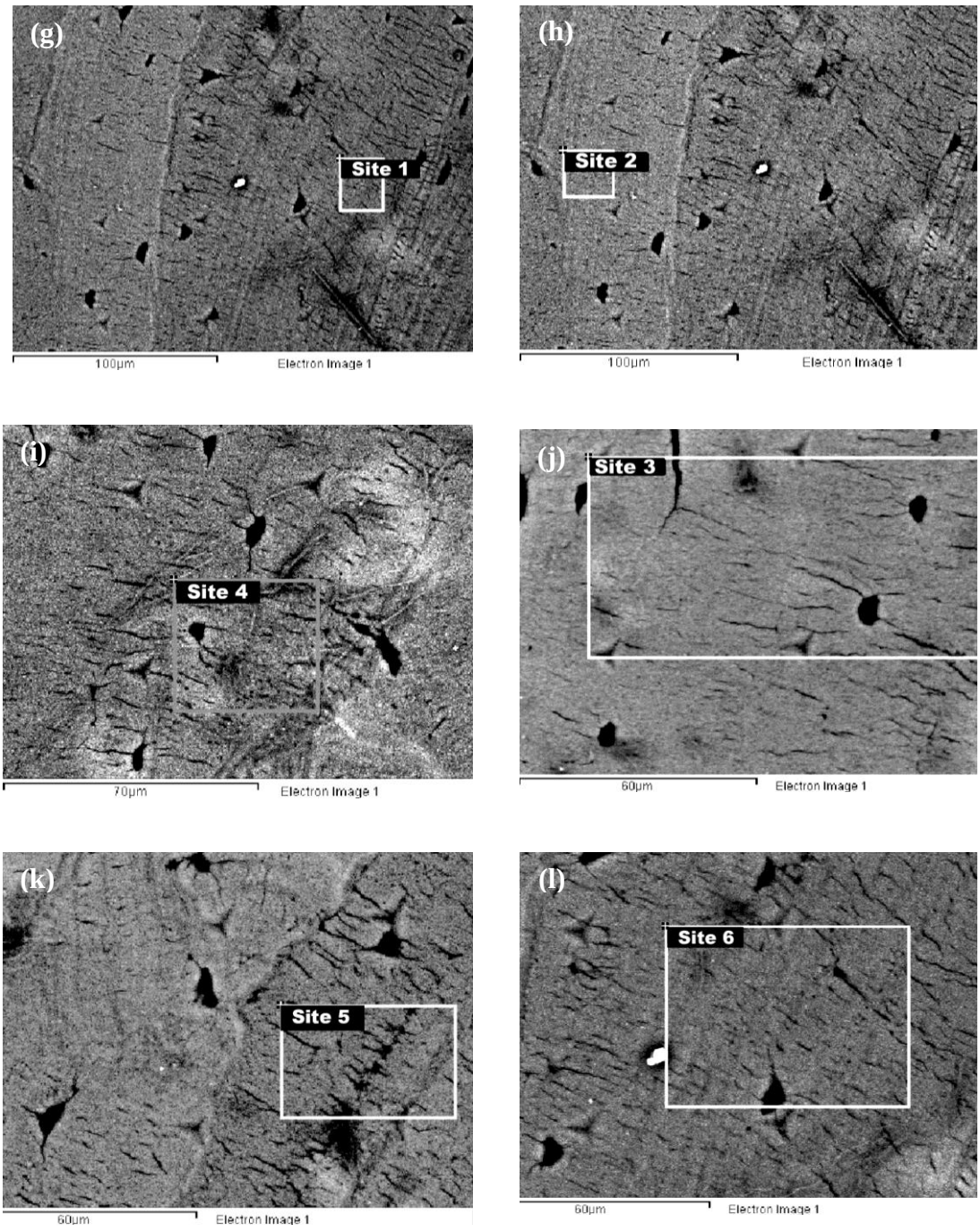

Figure 4.22 (g-l) is the BSE scanned regions of heat-treated in 90^0C.

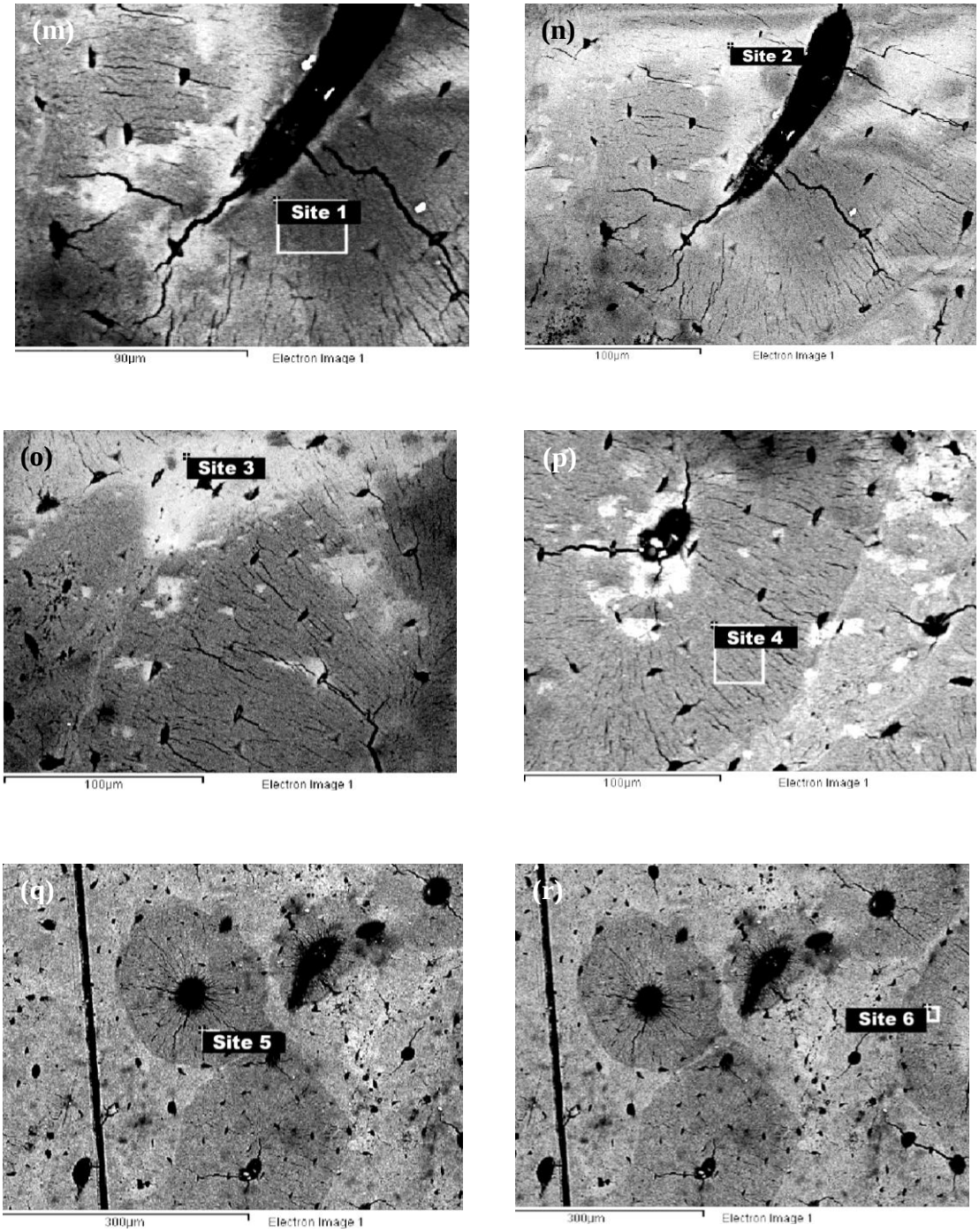

Figure 4.22 (m-r) is the BSE scanned regions of heat-treated in 150^0C.

Table 4.7 Summary of Ca/P ratios in different regions

	Group 1 Pristine			Group 2 Heat-treated in 90^0C			Group 3 Heat-treated in 150^0C		
	P(wt%)	Ca(wt%)	Ca/P	P(wt%)	Ca(wt%)	Ca/P	P(wt%)	Ca(wt%)	Ca/P
Site 1	33.4	66.6	2.0	33.4	65.2	2.0	34.1	63.5	1.9
Site 2	33.4	66.6	2.0	34.1	64.9	1.9	34.4	62.7	1.8
Site 3	32.9	67.1	2.1	33.6	65.5	2.0	34.5	62.6	1.8
Site 4	33.0	67.0	2.0	33.7	65.3	1.9	34.3	62.9	1.8
Site 5	33.6	66.4	1.9	33.0	64.2	2.0	34.3	62.8	1.8
Site 6	33.9	66.1	1.9	33.4	64.4	1.9	34.2	62.9	1.8
Average	33.5	66.6	2.0	33.5	65.0	1.9	34.3	62.9	1.8

4.4.4 BSE Imaging Discussion

Approximately 70% of bone tissue is composed of an inorganic component. This inorganic component is formed mainly by calcium and phosphorous which provide compression properties and stiffness. Although the heat-treated bone at 150°C obtained a higher elastic modulus and hardness among other groups, the EDX results of calcium was significantly lower than the other two groups. The heat-treated bone in 90°C contained 18% higher of mineral than the pristine bone, with the decrease of mineral content relatively lower. This means the ability to withstand compression and stiffness is high. As mentioned by Bloebaum et al. (1997) and Rho et al. (2002), mineral content is a significant factor that turns the bones stiffer and stronger when mineral content is increased. Therefore, it is believed that heat-treatment of the bone graft at 90°C is a more practical and effective way as far as biological and biomechanical aspects. By using the EDX results from BSE the Ca/P ratio of mineral content of heat-treated bone can be further understood.

4.5 Thermal Gravimetric Analysis (TGA) of Bovine Cortical Bone

4.5.1 Fabrication Methodologies

Materials and Sample Preparation

Frozen bovine cortical femur and rib bone (~3 - 4 years old) was procured from a local slaughterhouse for thermal gravimetric measurement. Bone pieces were machined to around 2mm x 3mm x 2mm dimension by a low-speed diamond saw (Metkon, resin bonded diamond cut-off wheels) with continuous deionized water irrigation to prevent thermal damage when machining the specimens.

Bone specimens were divided into four groups. Group 1 and 2 were untreated with phosphate-buffered saline (PBS), while Group 3 and 4 were treated with PBS. The preparation details are summarised in Table 4.8.

Table 4.8 Two groups of bone specimens were untreated with PBS; while 2 groups of specimens were treated with PBS

Group	Region of Bone	Fixation
Group1	Femur (UFB)	Untreated with Phosphate-buffered Saline (PBS)
Group 2	Rib (URB)	Untreated with Phosphate-buffered Saline (PBS)
Group 3	Femur (TFB)	Treated with Phosphate-buffered Saline (PBS)
Group 4	Rib (TRB)	Treated with Phosphate-buffered Saline (PBS)

4.5.2 TGA Tests

Thermal gravimetric analysis **(**TGA) was performed using TA instruments Q500 thermal analyser (refer Figure 4.23). Specimens were heated from room temperature to 850°C at a heating rate of 10°C/min in a stream of nitrogen (50cm^3/min).

Figure 4.23 TA instruments Q500 thermal analyser is used to perform the test.

4.5.3 TGA Measurement Results

Thermal gravimetric analysis (TGA) curves of untreated and treated femur and rib bovine cortical bone specimens from room temperature to 850°C are shown in Figures 4.24 and 4.25, respectively.

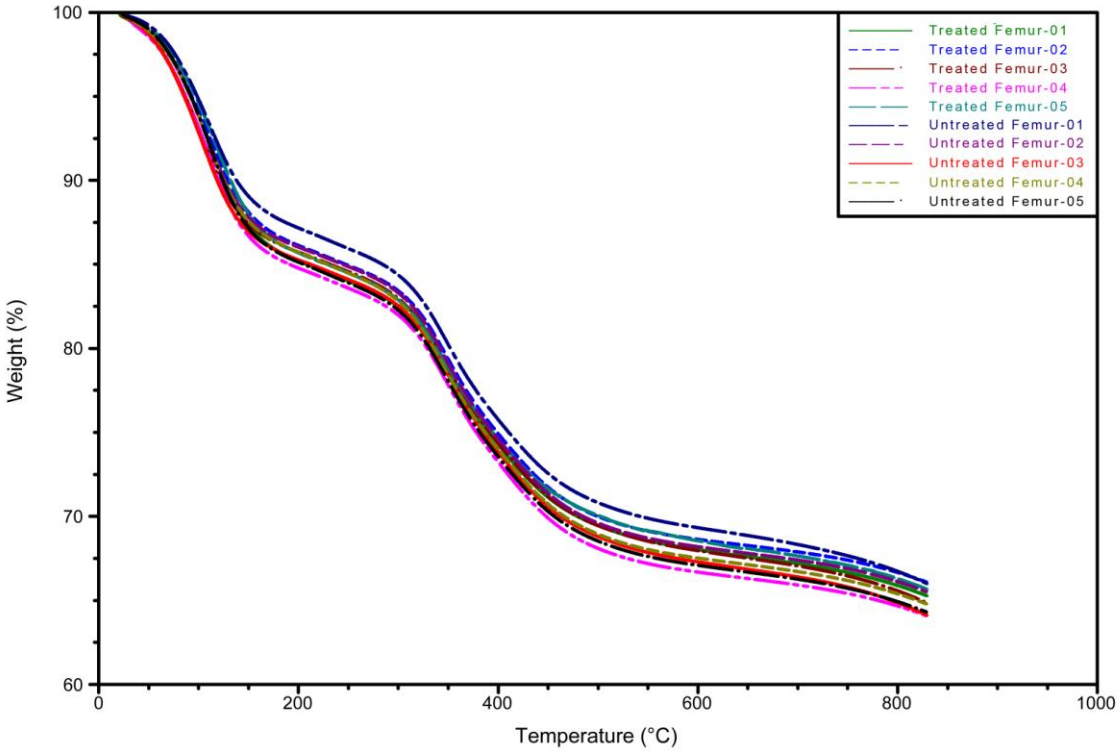

Figure 4.24 Untreated and treated with PBS of bovine cortical bone from femur.

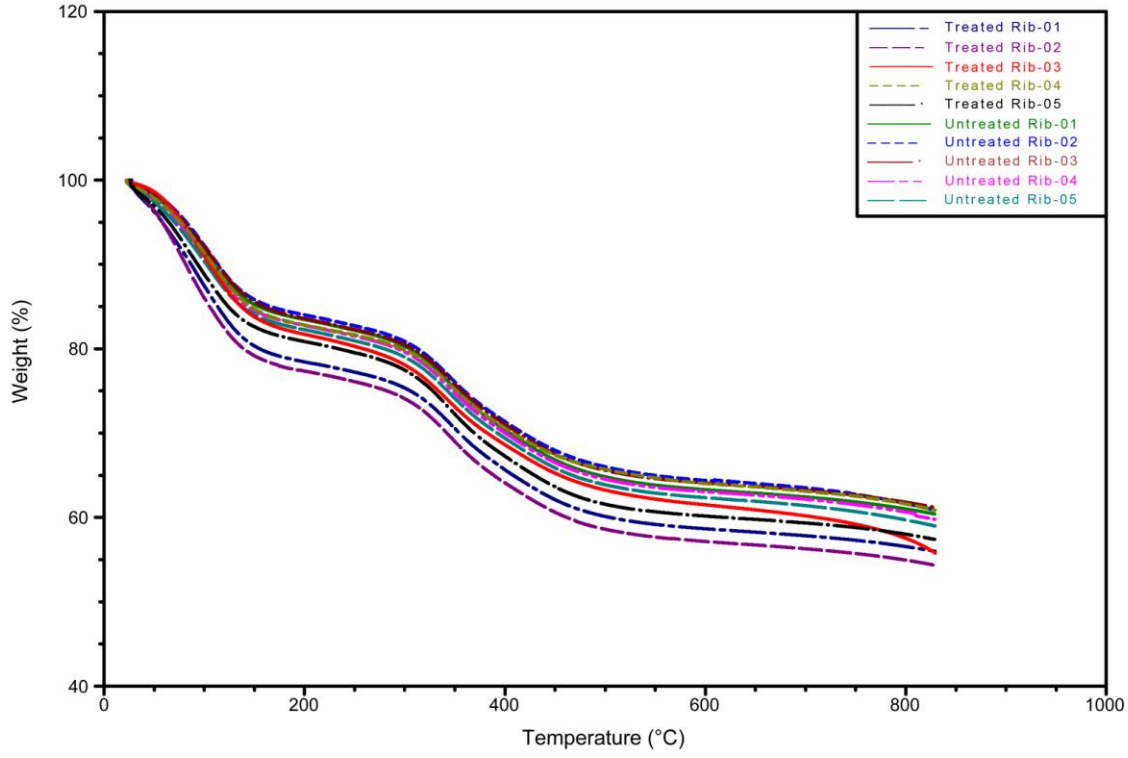

Figure 4.25 Untreated and treated with PBS of bovine cortical bone from rib.

Weight loss was observed when the specimens were heated from the room temperature (RT) to 160°C. This corresponds to the removal of water component. Continuous weight loss appeared between 200°C to about 600°C, which was due to the burning of the organic materials such as collagen and proteins. No significant weight loss is found after 600°C which indicates that the organic materials was removed completely and mineral phase (calcium phosphate) loss started to take place at 850°C.

The average amounts of water and organic materials lost during TGA measurements were calculated (refer Table 4.9). Approximately 12.8% and 13% of water was lost in the untreated femur bone (UFB) and treated femur bone (TFB) respectively when the specimens were heated from room temperature (RT) to about 160°C. A further approximately 32% of organic constituents was removed in both UFB and TFB specimens between 200°C to 600°C. Up to 850°C, around 35% of total loss was measured in both types of specimens.

Table 4.9 TGA results of femur and rib cortical bone as heated from room temperature to 850°C.

	Femur Cortical Bone		Rib Cortical Bone	
	Untreated-weight loss (%)	Treated with PBS-weight loss (%)	Untreated-weight loss (%)	Treated with PBS-weight loss (%)
Amount of water loss (25-160°C)	12.8%	13%	15.4%	18.4%
Amount of organic loss (200-600°C)	32%	32%	36.5%	39.6%
Total (25-850°C)	35%	35%	39%	43%

For the URB and TRB cortical bone specimens, the approximate average amount of water lost was 18.4% and 15.4%, respectively as they were heated from RT to about 160°C. As they were heated from 200°C to 600°C, there was around 40% and 36.5% of organics lost in URB and TRB specimens, respectively. Around 43% of total loss was found in URB specimens and 39% of total loss was found in TRB specimens as they were heated to 850°C.

4.5.4 TGA Measurement Discussion

A direct observation of the color change of specimens upon different temperature heating was made after TGA measurements. The colors of bovine cortical specimens were light ivory in both untreated and treated specimens from room temperature to 160°C. Upon heating to temperatures between 240°C and 300°C, the color of bone specimens changed to light - and dark - brown, respectively. When heated to 850°C, the specimens were black. These observations are consistent with that of Fantner et al. (2004) which mentioned that the baked sample changed from white to light brown as they were heated between 250°C and 500°C and believed that degradation of the organic materials appeared between this temperature range. However, these color changes were different from that of Ooi et al. (2007), who reported a black, dark grey and light grey images as the samples were heated to 400°C, 500°C and 600°C, respectively. Upon reaching 1200°C, the samples were white.

There was no significant difference in weight loss as compared to thermal gravimetric analysis (TGA) between untreated and treated specimens. However, the TGA result clearly shows a significant difference between femur and rib cortical bone specimens (refer Figures 4.26 and 4.27), Weight loss in rib cortical bone is higher than that in femur.

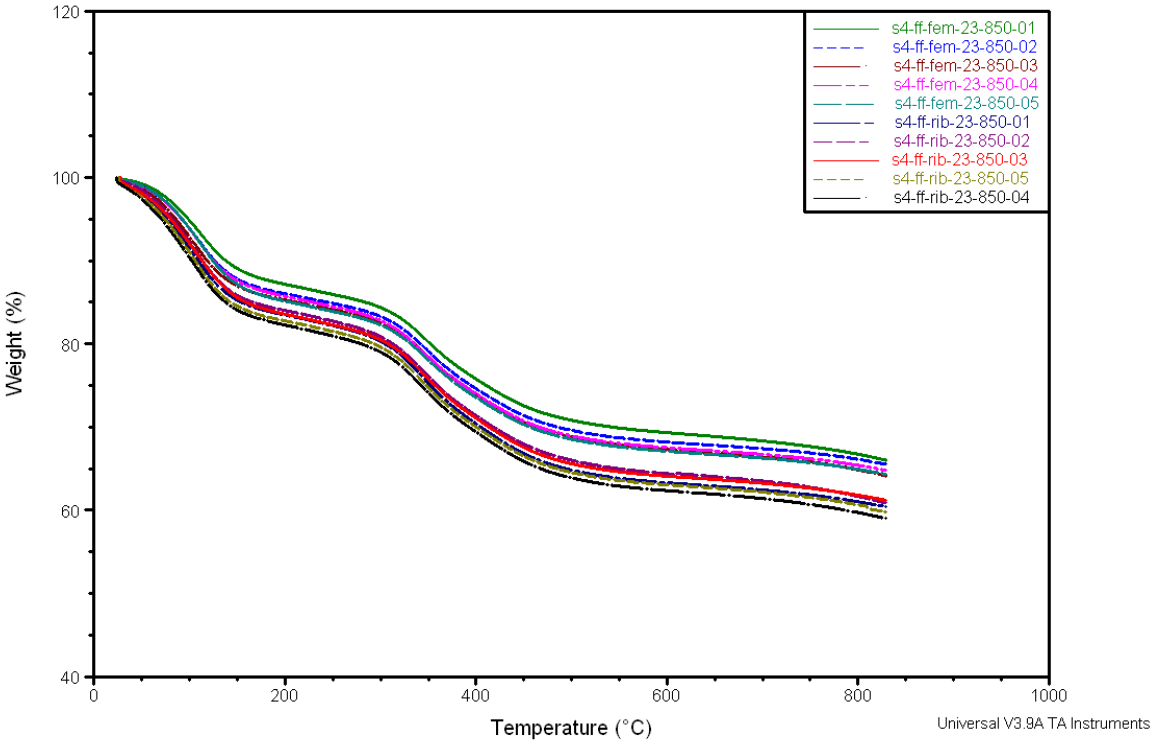

Figure 4.26 TGA results of femur and rib cortical bones treated without PBS as heated from room temperature to 850°C.

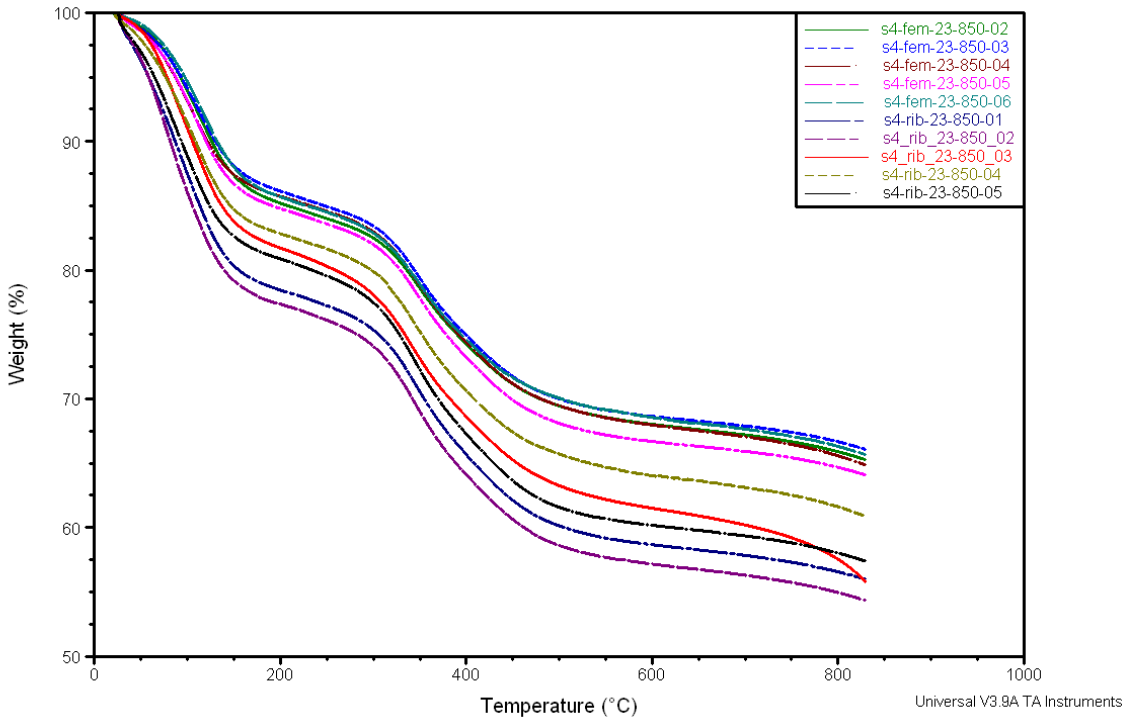

Figure 4.27 TGA results of femur and rib cortical bones treated with PBS as heated from room temperature to 850°C.

The TGA results in this study are in good agreement with findings of other researchers (Leikina et al. 2002; Lozano et al. 2003; Ooi et al. 2006; Labastida-Pólito et al. 2009), in which organic components such as collagen, fat tissues and proteins were removed as the samples were heated up to 200°C and completed at approximately at 600°C. Catanese et al. (1998) reported that around 85% of the organic material was removed upon heating the bone up to 350°C. Although different researchers have found different temperatures at which bone starts to lose organic material, most of the studies reported that there was an insignificant loss of organic material as the bone is heated up to 200°C.

The mechanical properties of bovine cortical bone tissue had been studied at different length scales: macrostructure (compressive test) and microstructure (nanoindentation test) at various heat-treated temperature ranges. In addition, BSE and TGA analysis also carried out to further investigate the changes of microstructure after heat-treatment. The local Young's modulus was measured at the microstructure level which contains osteonal and interstitial lamella by nanoindentation.

A significant increase in the mechanical properties was revealed in the microstructure level of the bovine cortical bone after being heat-treated at various temperature ranges (90°C to 160°C). These results were consistent with the global measurement in macrostructure level by compressive test. The elastic modulus and yield stress showed a slight increase as specimen heat-treated at 90°C and 150°C. It is known that the decrease of mechanical strength after heat-treatment is correlated to the degeneration of bone collagen (Shin et al. 2005) and the change of bone density (Carter et al. 1976). Burr (2002) also mentioned that the amount of collagen or its molecular stability and the degree of mineralization is associated to the mechanical properties.

The relationship between the weight loss and the heating temperature is obtained from the TGA measurement. As heating temperature increases, both types of specimens in this study showed an increase in weight. The weight loss indicates the amount of degeneration of collagen increase as temperature (Todoh et al. 2008).

Furthermore, the EDX results obtained from BSE in this study only showed a slight decrease of weight percentages of calcium and phosphorous as temperature increased. The changes were not severe and this indicated the overall effects of these changes on the mechanical properties appear to be not significant. According to Raspanti et al. (1994), the mineral phase structure of the bovine cortical bone remains unaffected when heated up to 500°C. However, contrary to this, Holden et al. [39] have found that as temperature exceeds 400°C, the mineral phase of human bone has significant changes, which can probably affect the bone stiffness and strength.

Therefore the preliminary study concluded that heat treatment at both 90°C and 150°C are deemed to be acceptable, from the biological and biomechanical points of view. However, for bone grafting the ultimate clinical decision regarding the usage of heat-treated bones have to be made after considering other non-mechanical factors.

Chapter 5

Finite Element Analysis (FEA) on Microstructure

5.1 Introduction

In this chapter, computational modeling incorporating detailed experimental data from nanoindentation, and compressive studies are used to identify the relationships among microstructural features and mechanical response in cortical bone.

Finite Element Analysis (FEA) has developed into significant and essential technology in the modelling and simulation in various fields, such as building and transportation (Liu et al. 2003a). FEA plays an increasingly important role in three principal areas of biomechanics, namely: (i) analysis of the skeleton; (ii) analysis and design of orthopaedic devices and (iii) analysis of tissue growth, remodelling and

degeneration (Boccaccio et al. 2011). FEA, is a powerful and widely used computational technique gain advantages in handling complex problems which are difficult to solve analytically. This technique has allowed researchers to measure local material properties to micron resolution (Mullins et al. 2007).

Although extensive experimental studies have been employed to measure and determine the mechanical properties of skeletal tissue, implementing the structural response into numerical simulation is still a great engineering challenge. Aforementioned, the hierarchical structure of human cortical bone consists of distinctly different structural levels from molecular to the macroscopic level (Gupta et al. 2005; Buehler 2006). Figure 5.1 provides a better understanding of the hierarchical structure of cortical bone (Hambli et al. 2012.). The different levels are treated as their own continuum, however also link with both higher level and lower levels (Mullins et al. 2006).

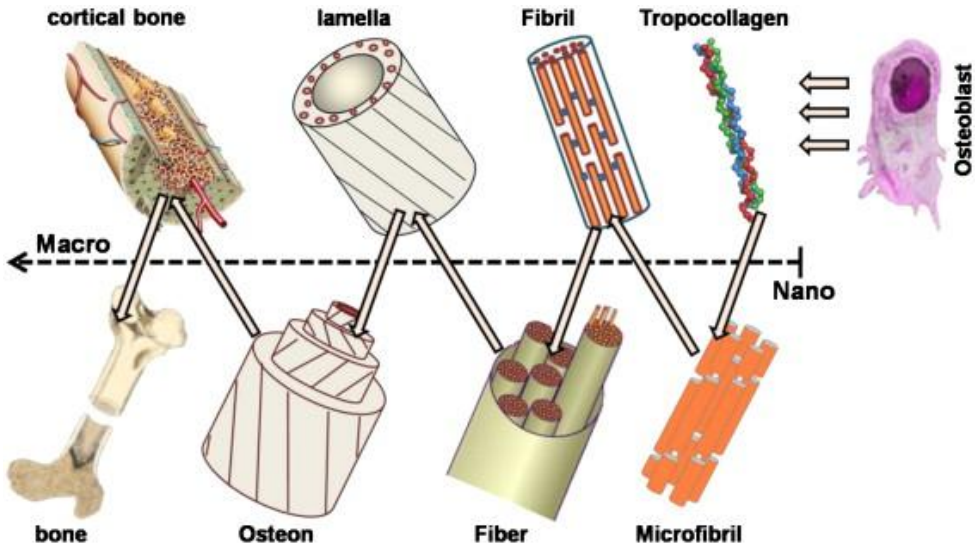

Figure 5.1 The hierarchical structure of cortical bone (Hambli et al. 2012).

Figure 5.2 shows the tropocollagen molecules (~300 nm long and ~1.5 nm wide). These molecules are assembled with irregular shaped nanocrystal platelets of carbonated apatite (3 nm - 5 nm thick and a lateral size of ~50nm) to form the sub-nanostructure level (Rho et al. 1998a). Two tropocollagen molecules form the mineralised collagen fibril with a diameter of around 100 nm (Gupta et al. 2005). Collagen fibres are formed with bundles of fibril and range in size from hundreds of a nanometer to 1 μm.

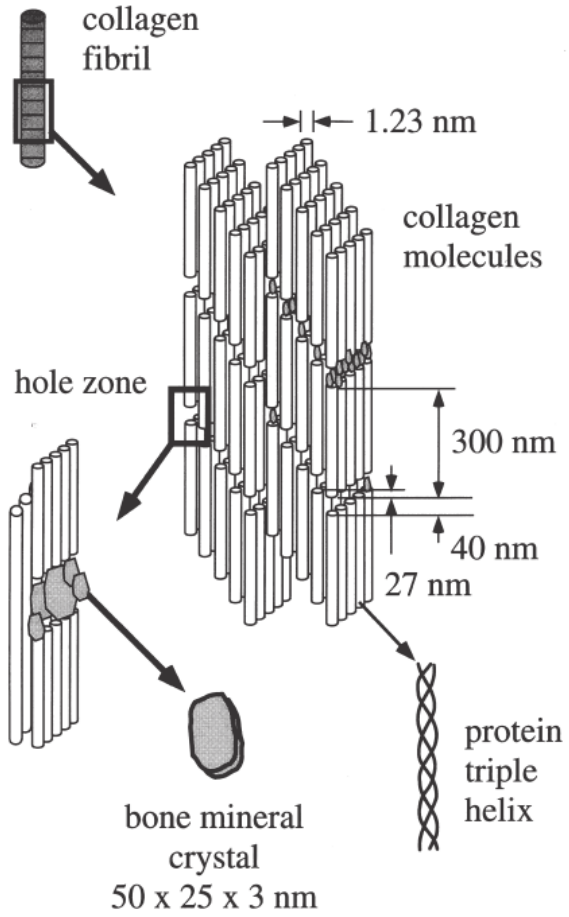

Figure 5.2 A schematic diagram illustrating the assembly of collagen fibrils and fibers and bone mineral crystals. The well known 67 nm periodic pattern results from the presence of adjacent hole (40 nm) and overlap (27 nm) regions of the assembled molecules (Rho et al. 1988a).

Basic Principles

A critical issue encountered in finite element analysis is the generation of the model. Generally, there are two types of analysis: 2-D modeling, and 3-D modeling. 2-D modeling conserves simplicity but tends to yield less accurate results. 3-D modeling, however, produces more accurate result and is modeled by curves and curved surfaces which are controlled by the number of elements used. The more elements used, the smoother and more accurate the representation of the curved parts by straight edges will be (Liu et al. 2003).

The geometrical model of FEA involves a complex system of small elements or cells using a set of grids (meshes) and points (nodes). Figures 5.3 and 5.4 show various type of element shapes (ABAQUS / CAE User's Manual). Each element consists of a number of vertices or nodes. An important pre-process task is mesh generation. Based on the generated mesh, information such as the simultaneous system equations can be formulated for later analysis (Liu et al. 2003). Mesh created with triangular elements is the most flexible and well-established way to model complex geometry and its boundaries. However, the accuracy is lower than quadrilateral elements (Liu et al. 2003). Usually tetrahedral elements are applied to the complicated geometric model.

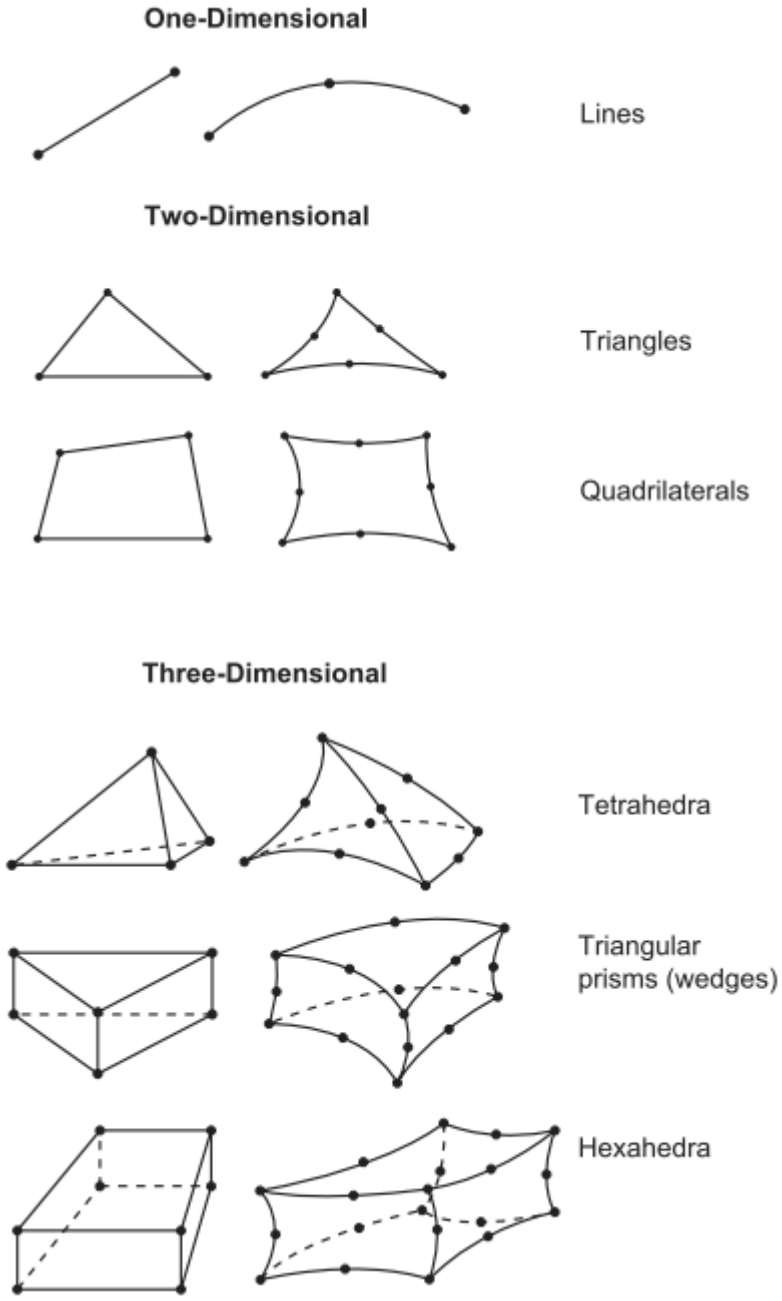

Figure 5.3 Element shapes (Abaqus / CAE User's Manual version 6.5).

Generally, a 3-D solid element can be a tetrahedron or hexahedron in shape, with either flat or curved surfaces. Each node of an element have three translational degrees of freedom (DOFs), thus, the element is able to deform in all three directions (Liu et al. 2003). A basic tetrahedron element is shown in Figure 5.4(a). This element contains four nodes and four surfaces with each node having three DOFs (*u, v* and *w*). Therefore, 12 DOFs can be found in this tetrahedron element. Tetrahedron elements can develop up to 10 and 20 nodes to achieve a high order element. The hexahedron element shown in Figure 5.4(b) contains eight nodes and six surfaces; each having three DOFs (ξ, η and ζ), making the total of 24 DOFs in a hexahedron element (Liu et al. 2003). Table 5.1 summarises various researchers meshing systems.

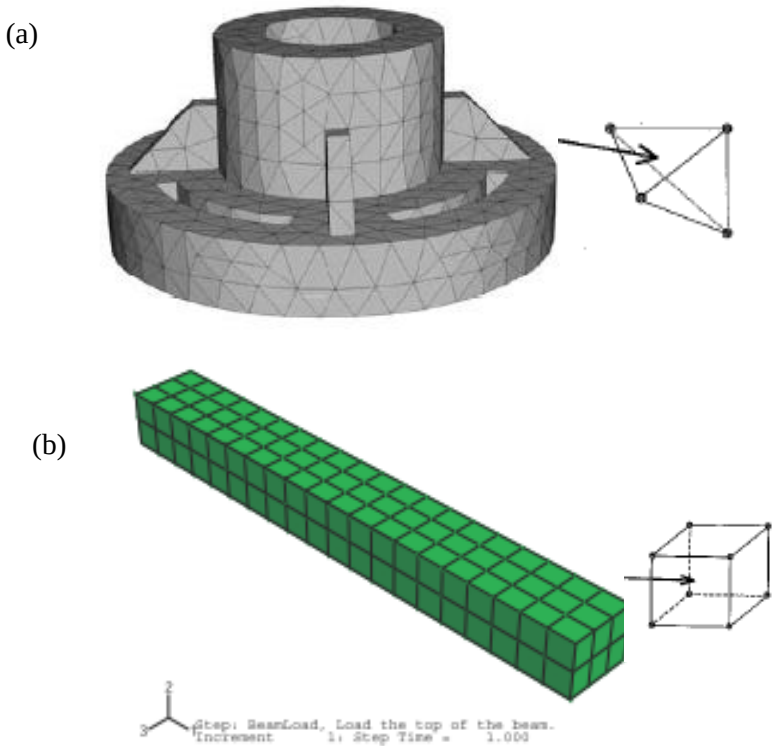

Figure 5.4 (a) mesh generated with tetrahedral elements (b) mesh generated with hexahedral elements (Abaqus / CAE User's Manual version 6.5).

Table 5.1 Summary of meshing system by various researchers

Researchers	Bone Type	Method	Mesh Type	Research Purpose
Chen et al. 2010	Tibia	CT scan image	Tetrahedron elements	Comparison of element types
Yang et al. 2008	Femur	CT scan image	Hexahedral elements	Simulate the inhomogeneity and anisotropy of femur
Baca et al. 2008	Femur	CT scan image	Tetrahedral elements	Compare the inhomogeneous orthotropic and inhomogeneous isotropic material
Helgason et al. 2008	Femur	CT scan image	Tetrahedral elements	Compare the Young's modulus at the strain gauge nodes and the Young's modulus of the elements
Wong et al. 2010	Tiabia	CT scan image	Tetrahedral elements	Simulated the fracture mechanisms
Ulrich et al. 1998	Trabecular	Micro-CT scan image	- Hexahedron meshing - Tetrahedron meshing	Comparison of hexahedron and tetrahedron models
Akhtar et al. 2006	Trabecular	X-ray microtomo-graphy	Hexahedral elements	Simulated the compressive behaviour of trabecular bone
Taylor et al. 2002	Trabecular	Micro-CT scan image	Tetrahedral elements	Simulated the fracture mechanisms
Preusser et al. 2007	Trabecular	Micro-CT scan image	Tetrahedral elements	Simulation of elastic microstructured bone material
Ural et al. 2005	Cortical		Cohesive elements	Simulation of crack propagation
Mullins et al.	Cortical		Hexahedral representative volume element	Analysis the effect of the orientation of the Haversian system
Dong et al. 2008	Mineral-Collagen Composite		2-D Quadrilateral elements	Simulation of microdamage progression in mineral-collagen composite

CT-Computed Tomography

5.2 Finite Element (FE) Model of Cortical Bone Microstructure

5.2.1 Basic Assumptions

According to the images obtained from backscattered electron (BSE) and Sevostianov et al. (2000) as shown in Figure 5.5 (a) & (b), the microstructures of cortical bone are formed by repeating units in which the composition of the material is represented at the macrostructure level (Mullins et al. 2007). A single osteon unit contains sufficient features to capture the physical behavior of the material.

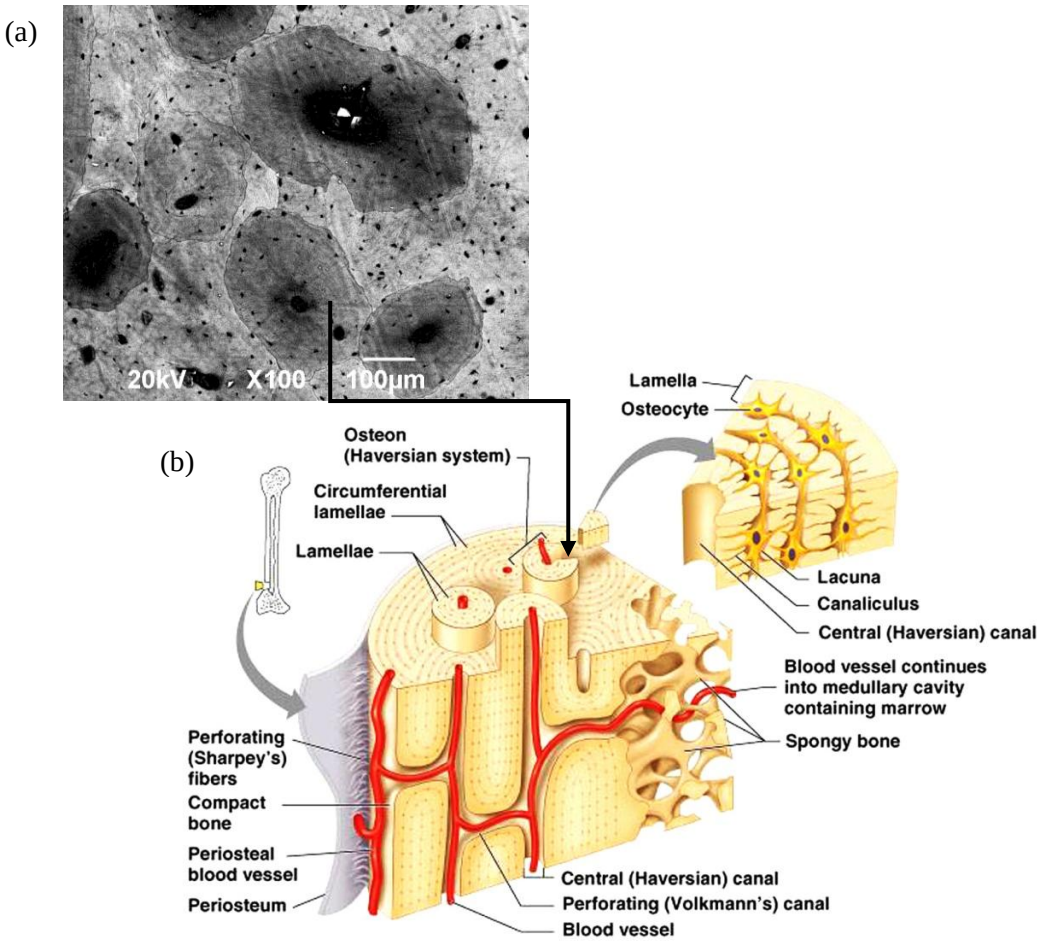

Figure 5.5 (a) BSE scanned image of osteons; (b) microstructure of the osteonal cortical bone, canals and osteons are not to scale (http://hk.image.search.yahoo.com**; viewed on 23/12/2012).**

The average diameter of the Haversian canal (containing blood, lymph and nerve fibers) is 50 μm and is surrounded by concentric lamellae to form an osteon. An osteon is approximately 200 μm - 300 μm in diameter and 3 mm - 5mm in length (Rho et al. 1998a; Sevostianov et al. 2000). The lamellae contain oblate shaped lacunae (bone cells - osteocytes) which measure approximately 5 μm in diameter. Volkman's canals that link the Haversian canal, blood and lymph vessels are much smaller and measure around 5 μm - 10 μm. Both Volkman's canals and canaliculi are randomly oriented and lie in planes perpendicular to Haversian canals (Sevostianov et al. 2000).

The numerical model for this study was developed using the commercial FE service package (ABAQUS/Standard 6.10). Due to the complexity of the cortical bone, only the elastic response along the longitudinal direction was considered. Therefore, a simplified 3-D FE model of the microstructure was generated under the following assumptions:

i) Cortical bone is considered a composite material. The osteon is assumed as the fibres, and the interstitial bone is assumed as the matrix. The porous part of the composite includes the Haversian and Volkman's canals.

ii) Since the Volkman's canals were used to link with the Haversian canals of the osteonal, therefore, more than one Volkman's canals were introduced to obtain a more realistic results.

iii) The biological fluid and soft tissues inside the pores (including blood, lymph vessels, nerve fibres and osteocytes) are ignored in this study.

iv) 3-D FE modelling in this study is assumed to have been generated in idealised geometries. This includes the sizes and arrangement of the osteons, Harversian canals, and Volkman's canals.

v) Linear elastic behaviour is presented in this study.

There were four main steps in setting up the simulation. The first step was to establish a geometric model that could described the shape as closely as the osteon and interstitial bone. The second step was to determine the mechanical properties for all materials. The materials in the model were defined in isotropic and elastic. Then third step was to determine the elements and meshing for the model. The final step was to apply the boundary conditions and loading to the model. In this study, the osteon and interstitial bone was generated in two separate models. A detailed explanation is presented in the following sections.

5.2.2 Model Geometry

Based on the image obtained from BSE, the simplified model of osteons and interstitial bones are illustrated in Figure 5.6 (a-c), it is the key for the FE model as it provide the foundation of the simplified model. The proposed 3-D FE model of an osteon is represented as a cylinder which was composed of Haversian canal and Volkman's canals. The interstitial bone is represented as a block composed of osteon

and Volkman's canals. As lacunae are much smaller, as compared to Haversian canal and Volkman's canals, they are not generated in this model.

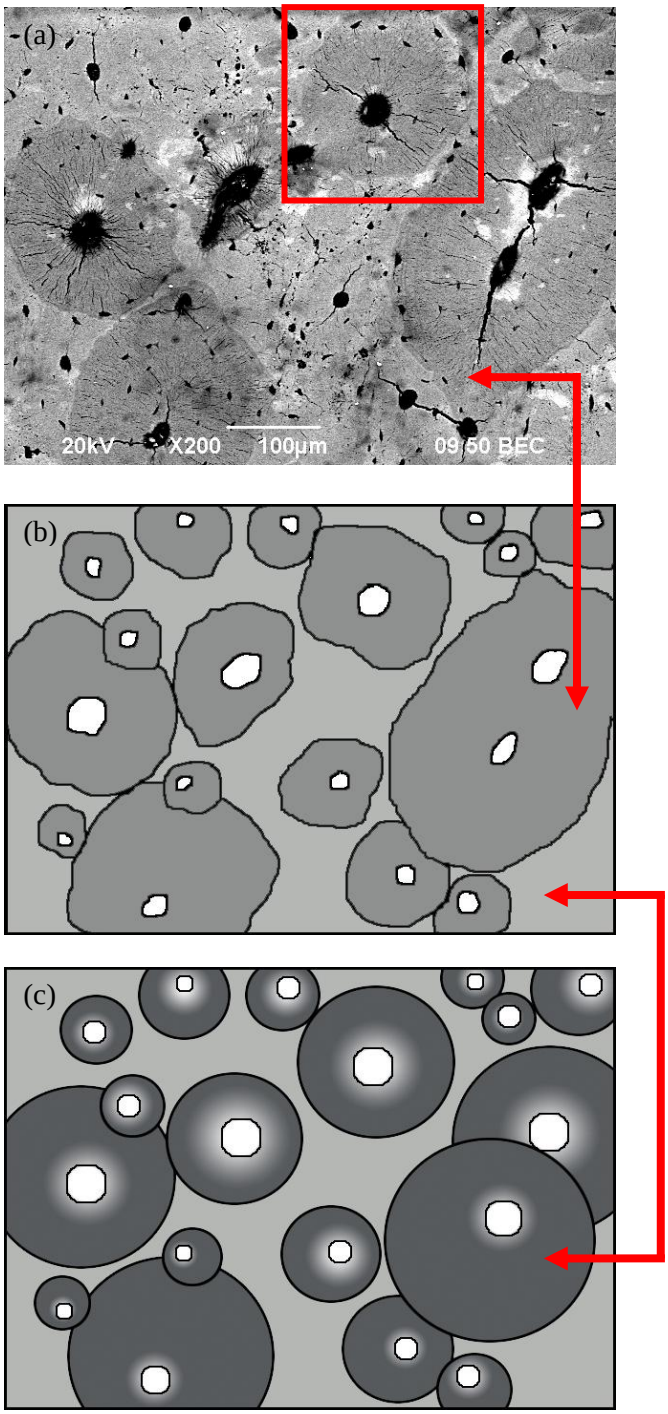

Figure 5.6 (a) BSE image used as a reference to generate the model; the red square shows the osteon and interstitial bone; (b & c) Schematic diagram of simplified model of osteons and interstitial bone from BSE image.

A total of 10 osteon models were generated. The diameter of 200 µm was used in the five osteon models. However, the diameter of the Haversian canal ranged from 40 µm to 60 µm. The Volkman's canals were evenly distributed and perpendicular to Haversian canal at a diameter of 10 µm. A further five osteon models used the same diameter of 200 µm, with the Volkman's canal being randomly distributed. The parameters are summarised in Table 5.2. The top and side views of the osteon models (O3A and B) are illustrated in Figure 5.7 (a-c).

Table 5.2 Summary of the osteon model parameters

Model		Osteon-cylindrical (µm)	Haversian canal (µm)	Volkman's canal (µm)	
Osteon 1 (O1)	A	Ø 200; l: 250	Ø 40; l: 250	Ø 10; l: 200	ED
	B				RD
Osteon 2 (O2)	A	Ø:200; l: 250	Ø 45; l: 250	Ø 10; l: 200	ED
	B				RD
Osteon 3 (O3)	A	Ø:200; l: 250	Ø 50; l: 250	Ø 10; l: 200	ED
	B				RD
Osteon 4 (O4)	A	Ø:200; l: 250	Ø 55; l: 250	Ø 10; l: 200	ED
	B				RD
Osteon 5 (O5)	A	Ø:200; l: 250	Ø 60; l: 250	Ø 10; l: 200	ED
	B				RD

Ø = diameter; l = length; ED = evenly distributed; RD = randomly distributed

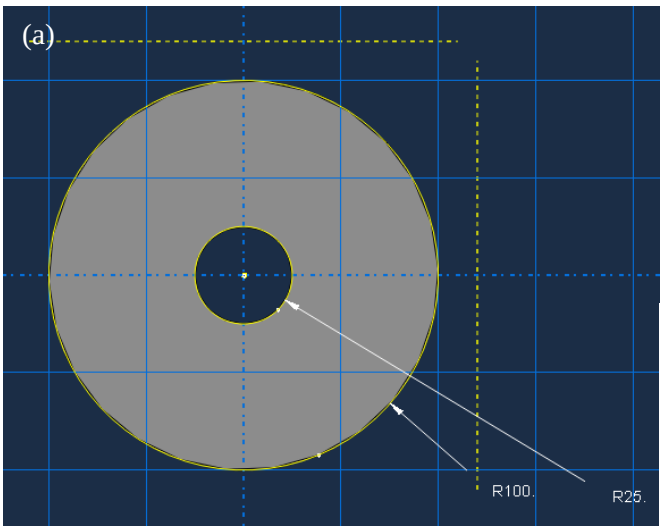

Figure 5.7 (a) Top view of the single osteon model (O3 A and B), the diameter of the Haversian canal is changed from 40 µm to 60 µm.

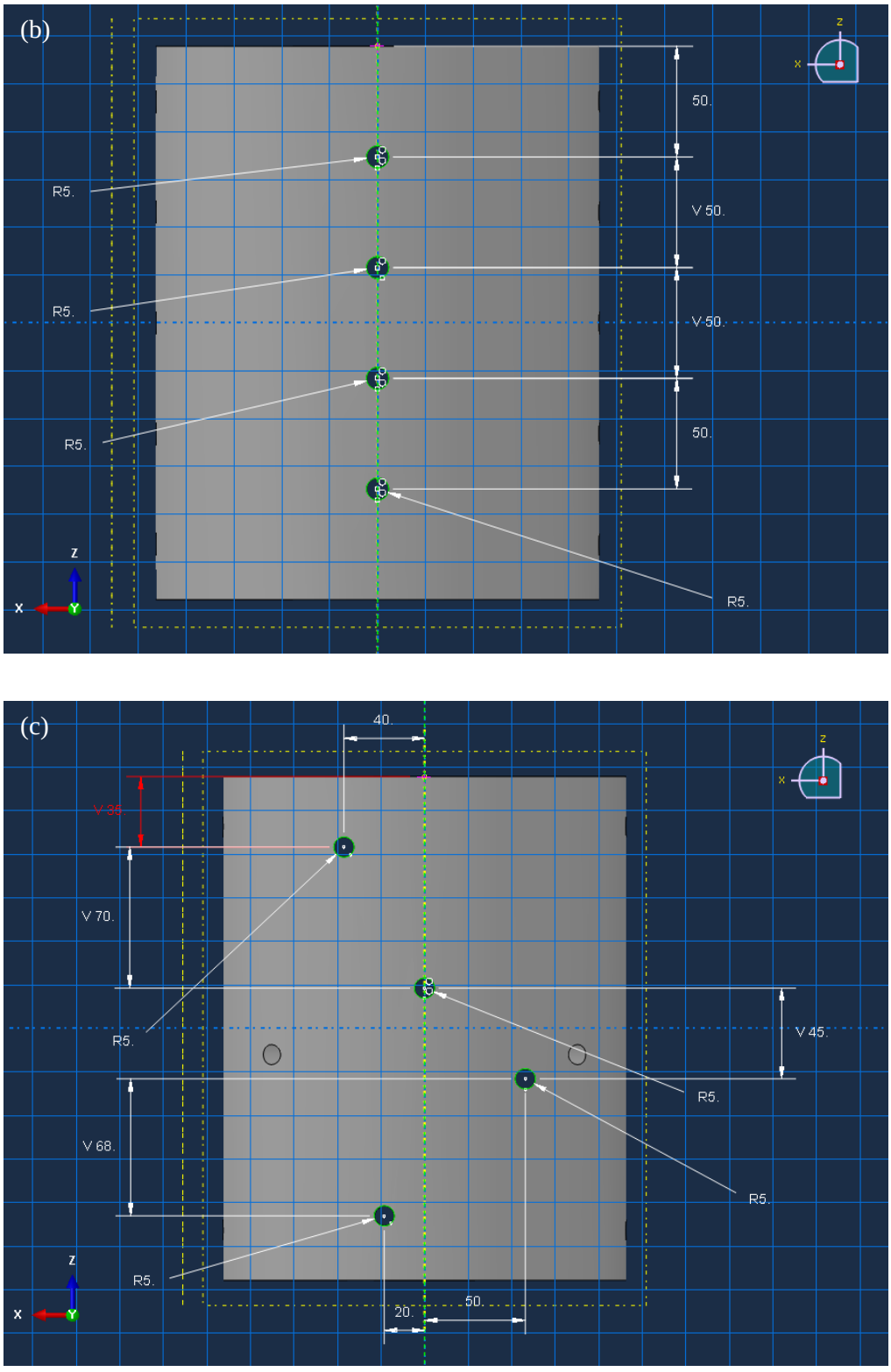

Figure 5.7 (b) Schematic side view of the single osteon model (O3A), Volkman's canals are evenly distributed; (c) side view of the single osteon model (O3B), Volkman's canals are randomly distributed.

A total of ten interstitial bone models were generated in a block form. The osteon was represented as a hollow cylinder with the same diameter. The Volkman's canals diameter ranged from 7 µm to 11 µm; five models were evenly distributed and another five models were randomly distributed around the osteon. Table 5.3 summarises the parameters of the models. Figure 5.8 (a-c) illustrates the top and side views of the model (I4 A and B).

Table 5.3 Summary of the interstitial bone model parameters

Model		Interstitial (µm)	Osteon-cylindrical (µm)	Volkman's canal (µm)	
Interstitial 1 (I1)	A	250 x 250 x250	Ø 200; l: 250	Ø 7; l: 250	ED
	B				RD
Interstitial 2 (I2)	A	250 x 250 x250	Ø:210; l: 250	Ø 8; l: 250	ED
	B				RD
Interstitial 3 (I3)	A	250 x 250 x250	Ø:220; l: 250	Ø 9; l: 250	ED
	B				RD
Interstitial 4 (I4)	A	250 x 250 x250	Ø:230; l: 250	Ø 10; l: 250	ED
	B				RD
Interstitial 5 (I5)	A	250 x 250 x250	Ø:240; l: 250	Ø 11; l: 250	ED
	B				RD

Ø = diameter; l = length; ED = evenly distributed; RD = randomly distributed

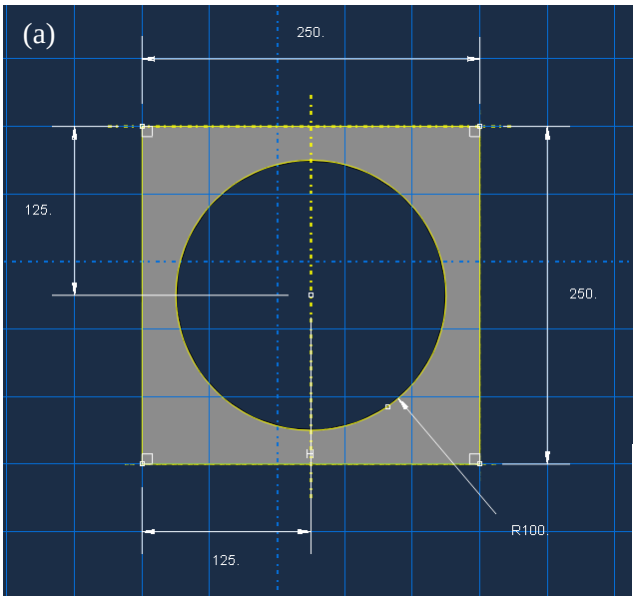

Figure 5.8 (a) Top view of the single interstitial model (I4A and B), the diameter of the osteon is 200 µm.

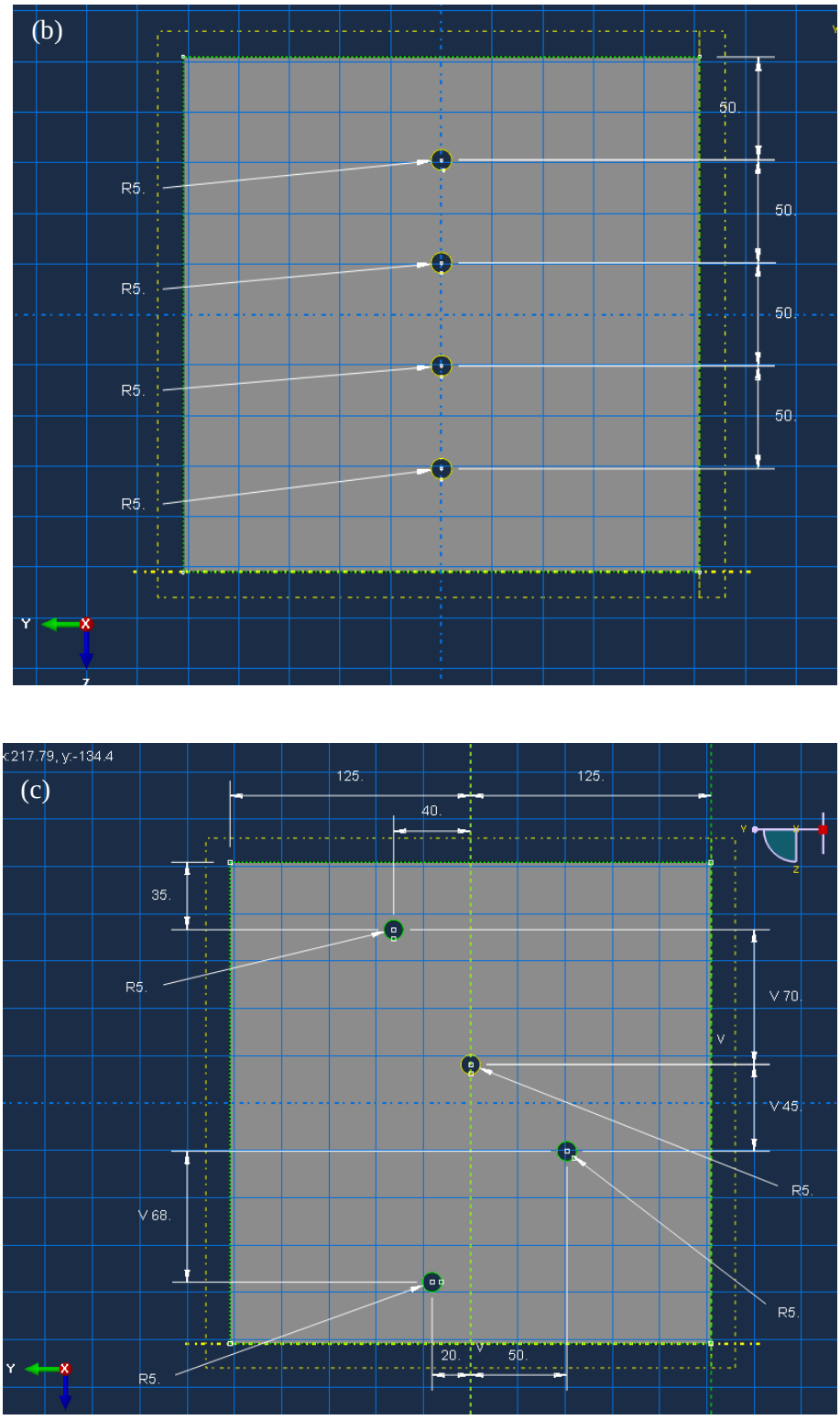

Figure 5.8 (b) Schematic side view of the single interstitial bone model (I4A), Volkman's canals are evenly distributed; (c) side view of the single interstitial bone model (I4B), Volkman's canals are randomly distributed.

Apart from generating the single osteon and interstitial bone model, a group of four osteons were formed as a pattern to further simulate the relationship between the elastic response and the porosity. Therefore, a group of four osteons in same dimension was formed as a pattern. A total of ten models were generated with different diameters of Haversian canal (from 40 ~ 60 μm). All the Volkman's canals were evenly distributed. Among them, five models were in the same diameter (10 μm); while another five models were in different diameters (from 8 ~ 12 μm). Table 5.4 summarises the osteon pattern model parameters. The top and side views of the model (OP3) are shown in Figures 5.9 (a & b).

Table 5.4 Summary of the osteon pattern model parameters

Model		Osteon-cylindrical (μm)	Haversian canal (μm)	Volkman's canal (μm)	
Osteon Pattern 1 (OP1)	A	Ø 200; l: 250	Ø 40; l: 250	Ø 10; l: 200	ED
	B			Ø 8; l: 200	RD
Osteon Pattern 2 (OP2)	A	Ø:200; l: 250	Ø 45; l: 250	Ø 10; l: 200	ED
	B			Ø 9; l: 200	RD
Osteon Pattern 3 (OP3)	A	Ø:200; l: 250	Ø 50; l: 250	Ø 10; l: 200	ED
	B				RD
Osteon Pattern 4 (OP4)	A	Ø:200; l: 250	Ø 55; l: 250	Ø 10; l: 200	ED
	B			Ø 11; l: 200	RD
Osteon Pattern 5 (OP5)	A	Ø:200; l: 250	Ø 60; l: 250	Ø 10; l: 200	ED
	B			Ø 12; l: 200	RD

Ø = diameter; l = length; ED = evenly distributed; RD = randomly distributed

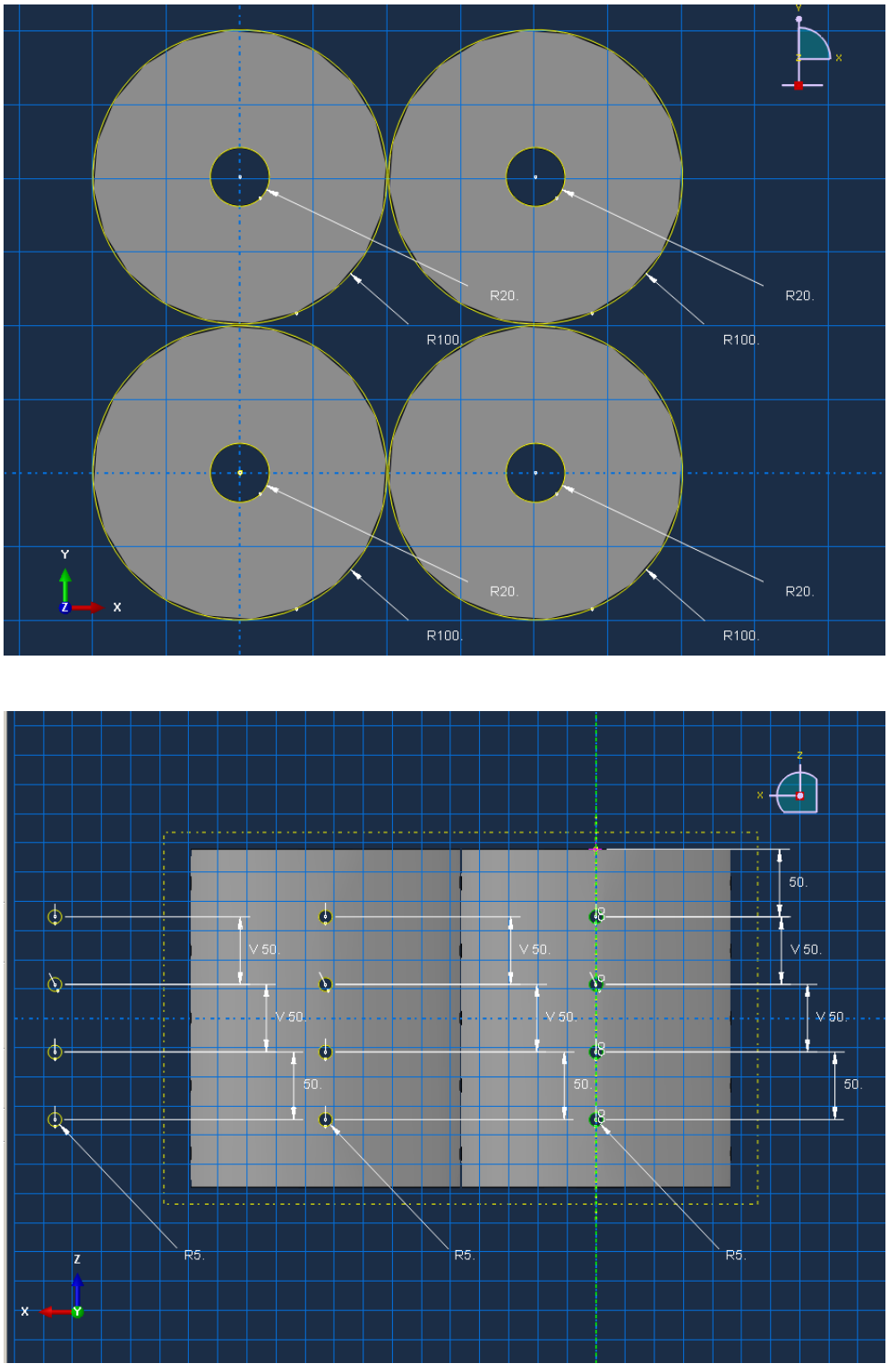

Figure 5.9 (a) Schematic top view of the osteon pattern model (OP3A); (b) side view of the osteon pattern model (OP3A), Volkman's canals are evenly distributed.

In order to understand whether there was any effect in the change in porosity on osteon and interstitial bones, twelve models of interstitial bones were developed with osteon diameter ranged from 200 μm to 240 μm. The Volkman's canals used a diameter of 12 μm in ten models and two models diameters ranged from 10 μm to 12 μm. The Volkman's canals of five models were evenly distributed and another five models were randomly distributed. Table 5.5 summarises the interstitial bone pattern parameters. Figure 5.10 (a-h) illustrates the top and side views of the pattern (IP1A, IP3B, IP6A and IP6B), respectively.

Table 5.5 Summary of the interstitial pattern model parameters

Model		Interstitial (μm)	Osteon-cylindrical (μm)	Volkman's canal (μm)	
Interstitial 1 (IP1)	A	740 x 740 x250	Ø 200; l: 250	Ø 12; l: app.740	ED
	B				RD
Interstitial 2 (IP2)	A	740 x 740 x250	Ø 210; l: 250	Ø 12; l: app.740	ED
	B				RD
Interstitial 3 (IP3)	A	740 x 740 x250	Ø 220; l: 250	Ø 12; l: app.740	ED
	B				RD
Interstitial 4 (IP4)	A	740 x 740 x250	Ø 230; l: 250	Ø 12; l: app.740	ED
	B				RD
Interstitial 5 (IP5)	A	740 x 740 x250	Ø 240; l: 250	Ø 12; l: app.740	ED
	B				RD
Interstitial 6 (IP6)	A	740 x 740 x250	Ø 200~240; l: 250	Ø 10~12; l: app.740	ED
	B				RD

Ø = diameter; l = length; ED = evenly distributed; RD = randomly distributed

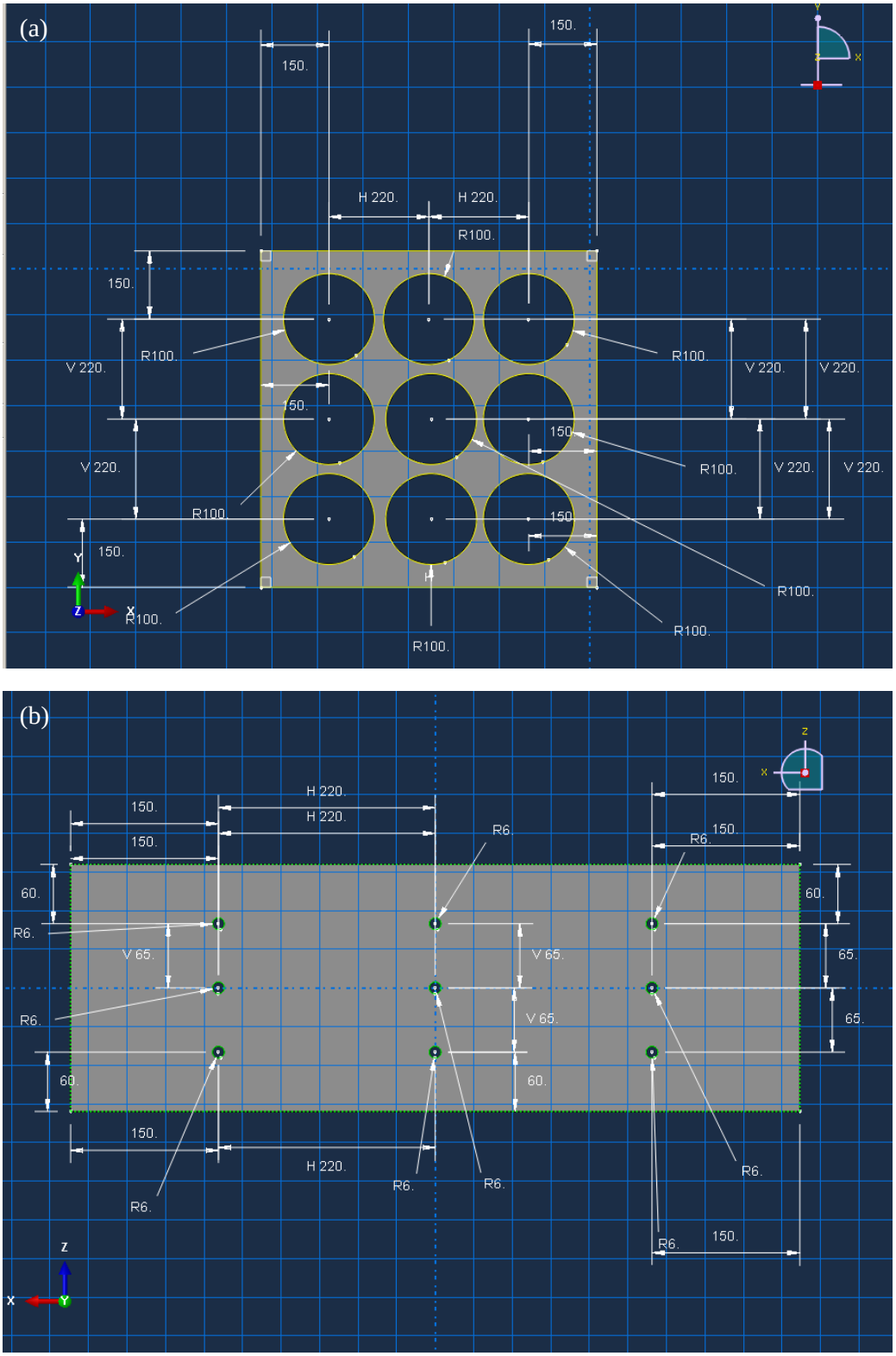

Figure 5.10 (a) Schematic top view of the interstitial pattern model (IP1A); (b) side view of the evenly distributed Volkman's canals.

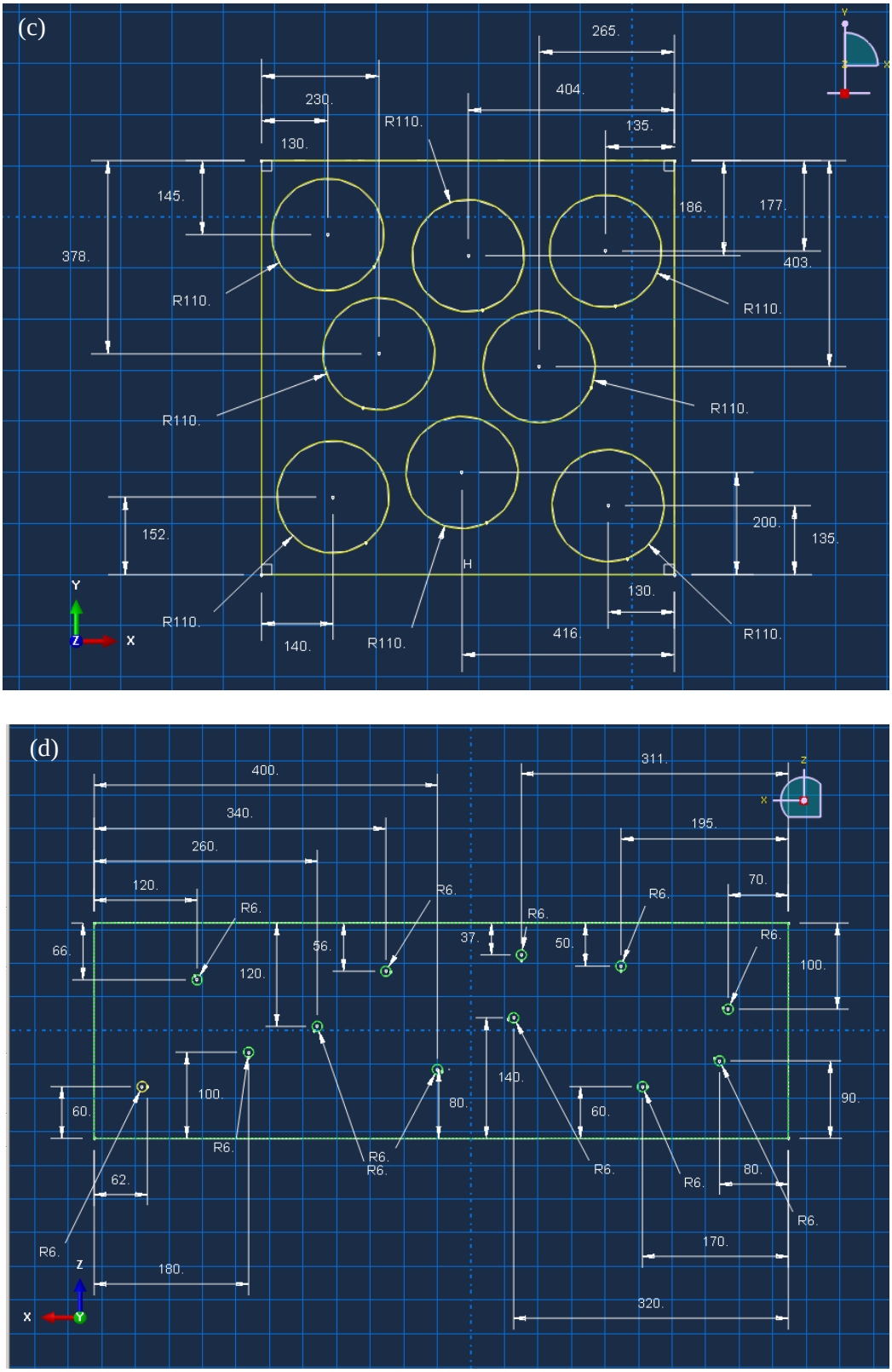

Figure 5.10 (c) Schematic top view of the interstitial pattern model (IP3B); (d) side view of the randomly distributed Volkman's canals.

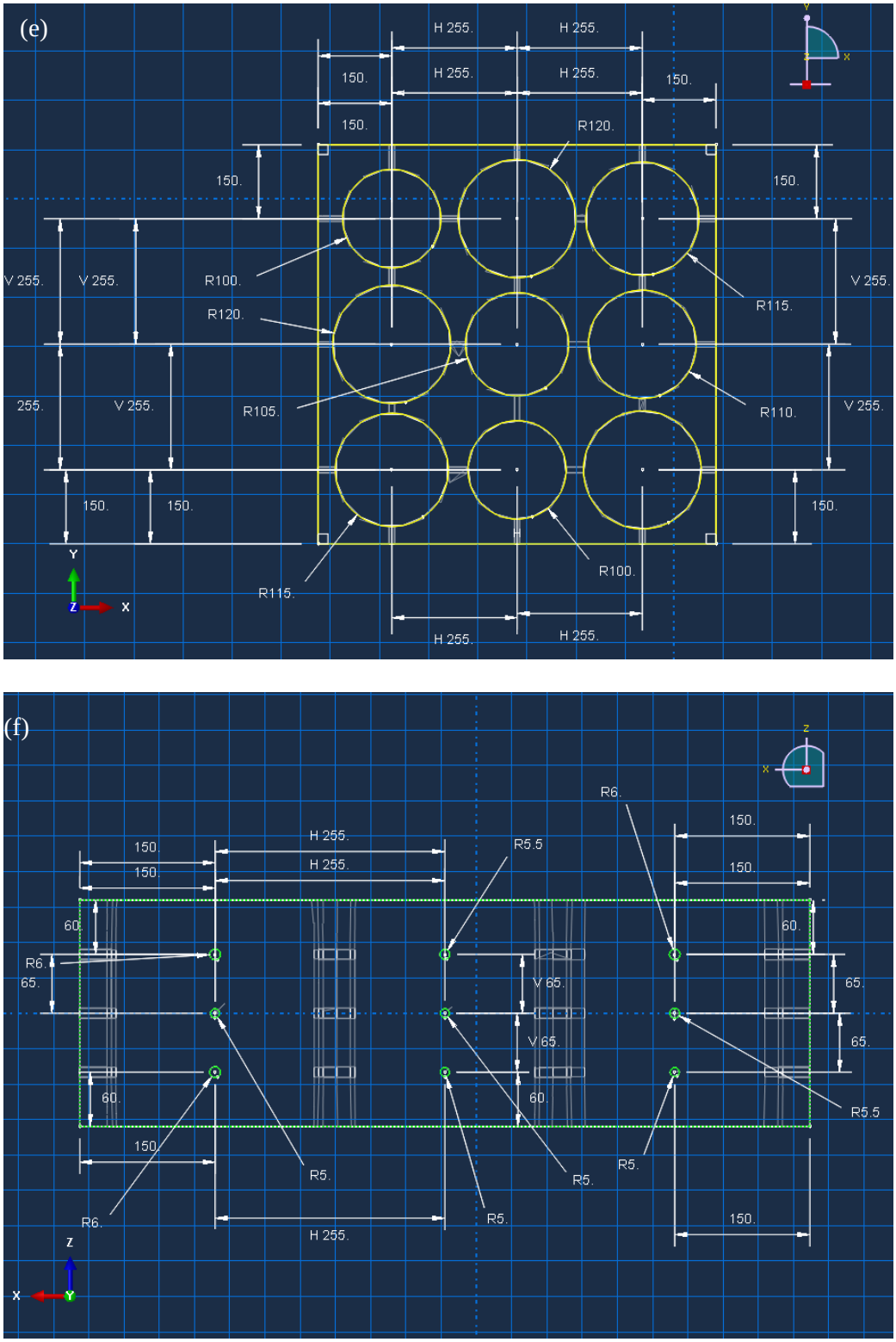

Figure 5.10 (e) Schematic top view of the interstitial pattern model (IP6A), the osteons are evenly distributed and the diameters are set from 200-240 μm in diameter; (b) side view of the evenly distributed Volkman's canals, the diameters are set from 10-12 μm.

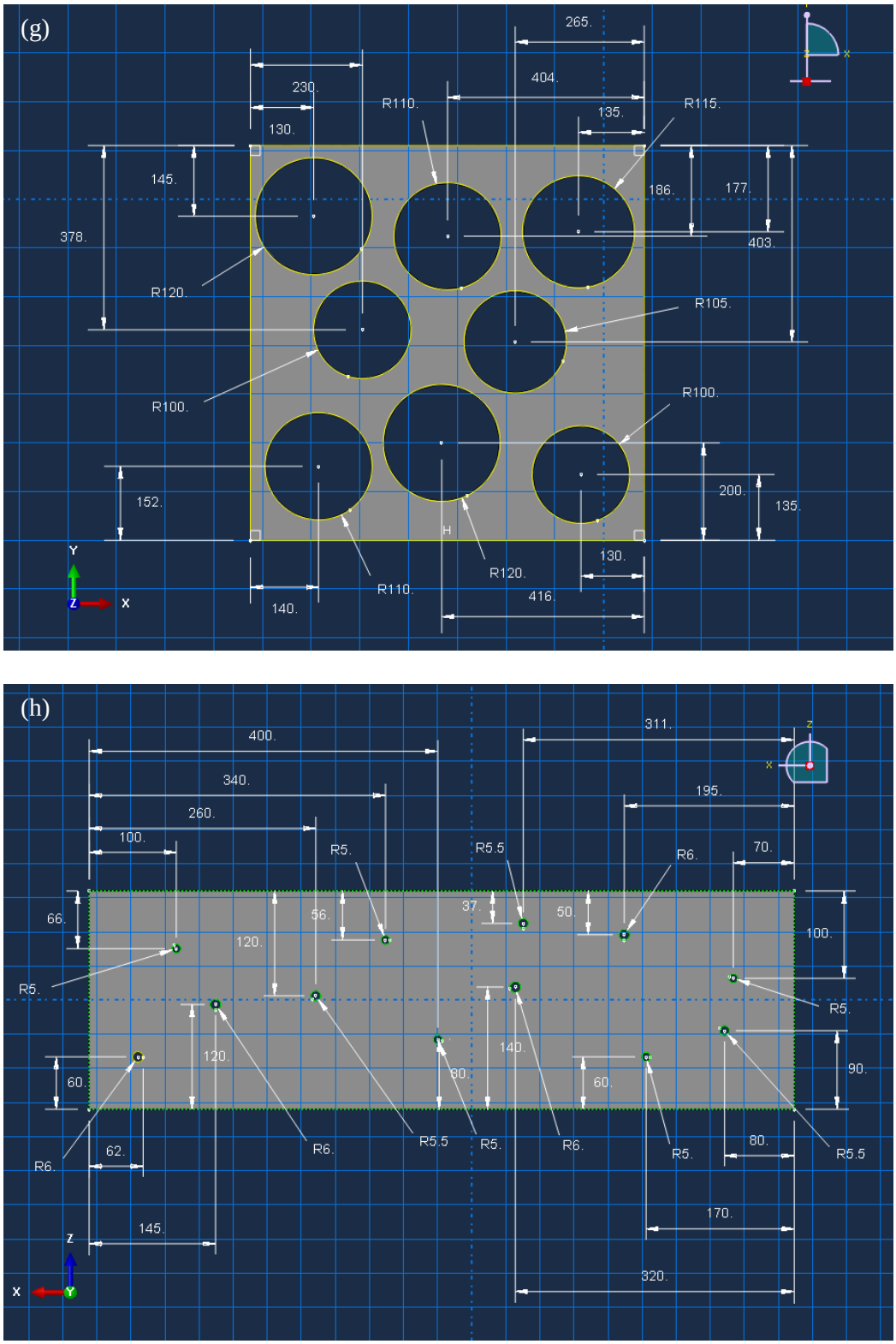

Figure 5.10 (g) Schematic top view of the interstitial pattern model (IP6B), the osteons are randomly distributed and the diameters are set from 200-240 µm in diameter; (h) side view of the randomly distributed Volkman's canals, the diameters are set from 10-12 µm.

5.2.3 Materials Properties

Table 5.6 summarises the values of elastic modulus and Poisson's ratio of human bones used in several FE simulations. The material properties used in this study are according to Mullins et al. (2007). Mullins et al. (2007) based their findings on the study by Fan et al. (2002) which investigated the microstructure of cortical bone of human tibiae using nanoindentation. Based on the dehydration effects reported by Rho and Pharr (1999a & b), a reduction of 15% of the elastic modulus was applied to the results.

Table 5.6 Summary of elastic modulus and Poisson's ration used in several FE simulations

Reference	Material	Elastic modulus, GPa	Poisson's ratio, υ
Ramos et al. 2006	Whole bone	19	0.3
Baca et al. 2008	Whole bone	16	0.3
van Rietbergen et al. 1998	Cancellous bone	10	0.3
Wong et al. 2010	Cortical bone	12	0.3
Carnelli et al. 2010	Cortical bone	20	0.3
Mullins et al. 2007	Interstitial bone	23.03	0.3
	Osteonal bone	21.33	0.3

5.2.4 Elements and Meshing

The osteon was simulated in cylindrical shape. The model mesh was made of quadrilateral tetrahedral elements. The mesh was composed of C3D10 first-order 10-node tetrahedral elements. Table 5.7 shows the elements and nodes of each model. Figure 5.11 shows the typical mesh used to model the effects of Haversian and Volkman's canals porosity.

Table 5.7 Summary of the elements and nodes of the models

Model		Element	Node
O1	A	266566	372638
	B	259031	362815
O2	A	275923	386156
	B	234385	329218
O3	A	265212	371797
	B	220796	310856
O4	A	273087	382619
	B	241283	339529
O5	A	278232	389836
	B	244270	343979
I1	A	286863	413401
	B	372652	535238
I2	A	158515	236288
	B	276654	402427
I3	A	158515	236288
	B	192851	285977
I4	A	117253	179543
	B	144147	218799
I5	A	80471	128450
	B	87157	138048
OP1	A	851266	1191241
	B	1221445	1698375
OP2	A	830693	1164450
	B	985732	1377001
OP3	A	804195	1128705
	B	804195	1128705
OP4	A	791082	1111001
	B	695930	979920
OP5	A	773846	1088201
	B	582502	824102
IP1	A	491698	715312
	B	1293834	1813183
IP2	A	422040	621049
	B	1167577	1642408
IP3	A	378484	562616
	B	1016691	1437754
IP4	A	400501	592516
	B	922245	1309990
IP5	A	509982	744075
	B	1135221	1600707

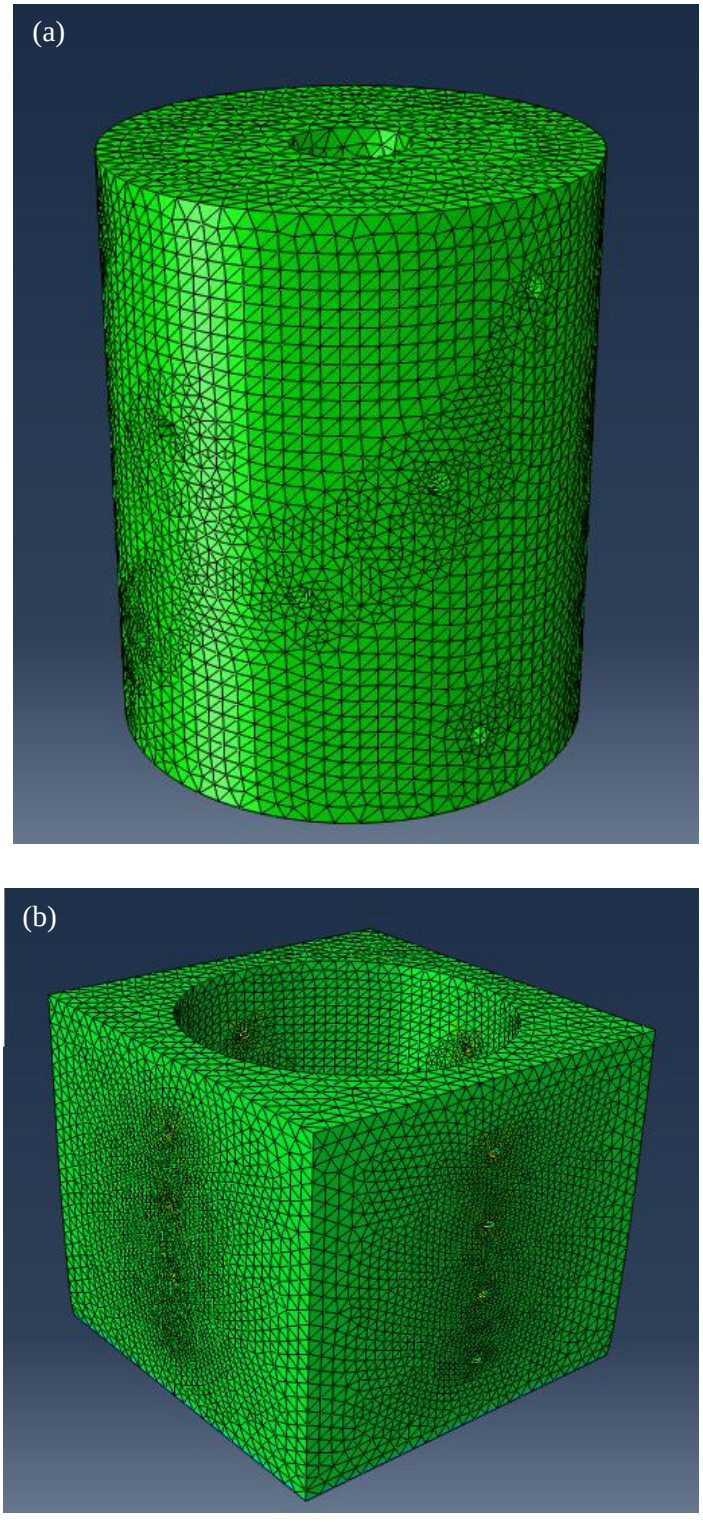

Figure 5.11 Typical mesh showing the single unit cell of osteonal and interstitial bone model. (a) osteon with Haversian canal and randomly distributed Volkman's canal, (b) interstitial bone with osteon and evenly distributed Volkman's canals.

5.2.5 Boundary Conditions

In general, bone is loaded in compression. Therefore, a compressive force is applied on the top surface and the bottom surface is fixed (refer Figure 5.12). Displacement and rotation methodology was employed as the boundary condition for all simulations presented in this study.

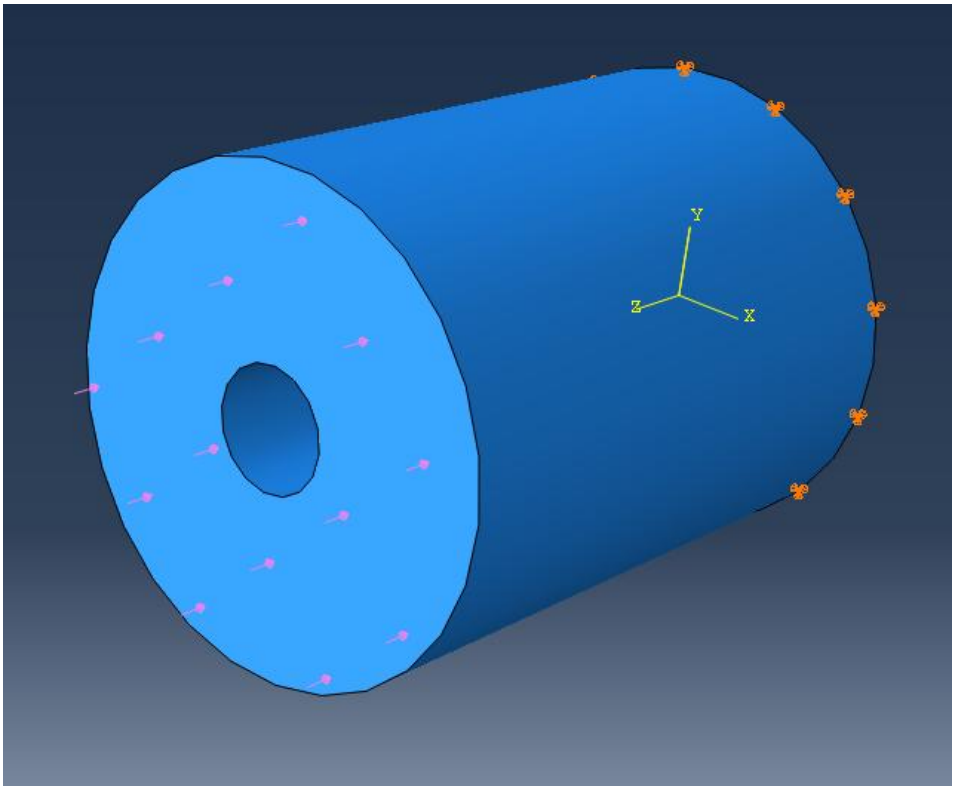

Figure 5.12 Boundary conditions of the compressive simulation. A compressive force is applied on the top surface and bottom surface is fixed.

5.3 FEA Simulation Results

The two main components of cortical bone, osteonal and interstitial bone were assumed to be isotropic materials (Rho et al. 1999b; Fan et al. 2002). This means the materials properties in the plane perpendicular to the long axis are the same while the direction along the axis is different. Rather than presenting all the variation effects on the overall macroscopic properties, two important features, the Haversian and Volkman's canals corresponding to the mechanical properties were assessed in this study. The relationship between mechanical properties and the porosity effect of these features were also evaluated. Table 5.8 summarises the maximum principal stress, Von Mises stress and maximum principal strain of all models.

Table 5.8 Summary of the maximum principal stress, Von Mises stress and maximum strain of all models

Model		Maximum Principal Stress (MPa)	Von Mises Stress (MPa)	Maximum Principal Strain
O1	A	7.12	17.47	2.68
	B	41.5	42.08	13.63
O2	A	3.95	17.94	3.26
	B	33.61	22.33	10.65
O3	A	7.74	18.58	2.76
	B	29.75	23.08	9.39
O4	A	4.86	18.09	3.39
	B	23.99	21.58	8.45
O5	A	3.69	17.61	2.62
	B	10.82	28.09	6.64
OP1	A	6.46	18.24	2.69
	B	8.28	18.31	2.81
OP2	A	7.54	19.31	3.11
	B	8.59	20.66	3.07
OP3	A	6.13	17.87	4.06
	B	7.08	20.09	3.37
OP4	A	7.61	17.4	3.35
	B	7.61	17.4	3.35
OP5	A	8.34	17.96	3.20
	B	7.25	17.59	3.01

Table 5.8 Continued

Model		Maximum Principal Stress (MPa)	Von Mises Stress (MPa)	Maximum Principal Strain
I1	A	11.08	27.41	4.07
	B	8.07	22.75	3.10
I2	A	11.36	28.42	5.44
	B	11.16	37.83	6.61
I3	A	11.09	28.01	6.86
	B	10.95	32.39	6.71
I4	A	11.15	27.52	5.78
	B	11.50	34.27	4.93
I5	A	10.28	27.58	5.80
	B	11.31	31.92	6.66
IP1	A	2.86	17.47	2.91
	B	7.16	34.85	7.44
IP2	A	2.84	17.55	2.60
	B	4.92	41.29	7.75
IP3	A	2.82	18.03	2.74
	B	5.04	29.63	6.49
IP4	A	3.29	17.41	2.53
	B	6.36	31.29	4.89
IP5	A	5.86	19.79	2.89
	B	5.18	41.85	7.05

5.3.1 Osteonal Bone Porosity

A 3-D unit cell of an osteon was used to analyse the effect of the Haversian canal and Volkman's canals at both the macroscopic and microscopic mechanical property level and stress field. In this single osteonal model, the Volkman's canals in diameter of 10 μm represented a porosity of around 2%. Varying the diameter of the Haversian canal from 40 μm to 60 μm represented a porosity of around 4 to 9%. Thus, a total of around 6-11% of the combined porosity associated with the Haversian and Volkman's canals was assumed in the single unit osteonal model. Loading was applied in the longitudinal direction.

Figure 5.13 shows the porosity effect of the Haversian and Volkman's canals on the mechanical properties of a single osteonal unit. In Osteonal Model A (OA), as the diameter of the Haversian canal increased from 40 µm to 60 µm, the maximum principal stress (S max.) decreased from 7.74 MPa to 3.70 MPa. In Osteonal Model B (OB), a greater decrease appeared in S max as the diameter of the Haversian canal changed to 45 µm. However, from 50 to 60 µm, the S max decreased gradually from 33.61 MPa to 23.99 MPa. There was around a 71% decrease in OB.

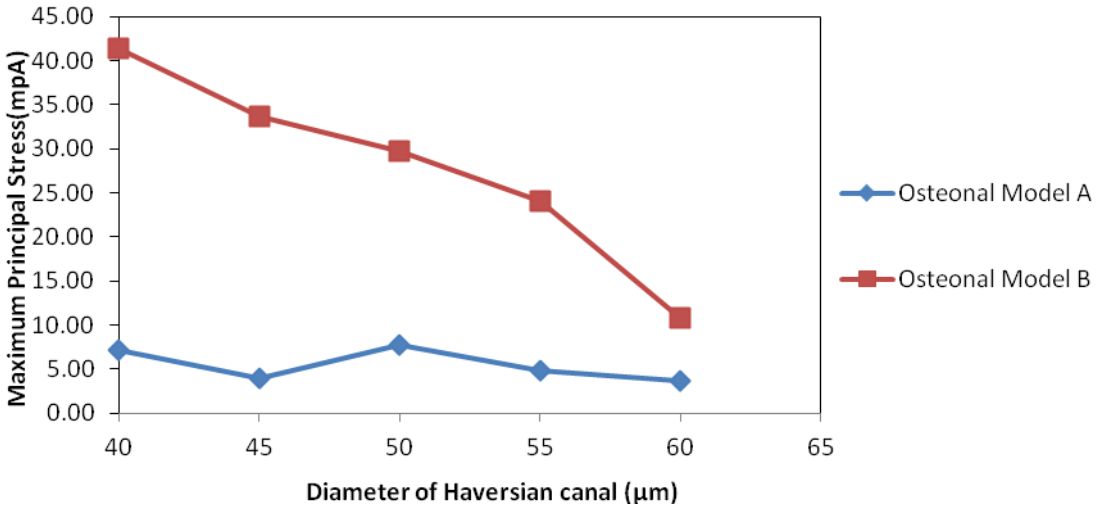

Figure 5.13 shows the maximum principal stress of osteonal model A and B.

5.3.2 Interstitial Bone Porosity

In order to compare the porosity effect of the osteonal bone and interstitial bone, a square unit cell was represented the interstitial bone. The osteon was represented by a circular hollow with a fixed diameter. Since the Haversian canal is generated within the osteonal model, it was not included in the interstitial bone model. Figure 5.14 shows the interstitial bone porosity effect on the mechanical properties.

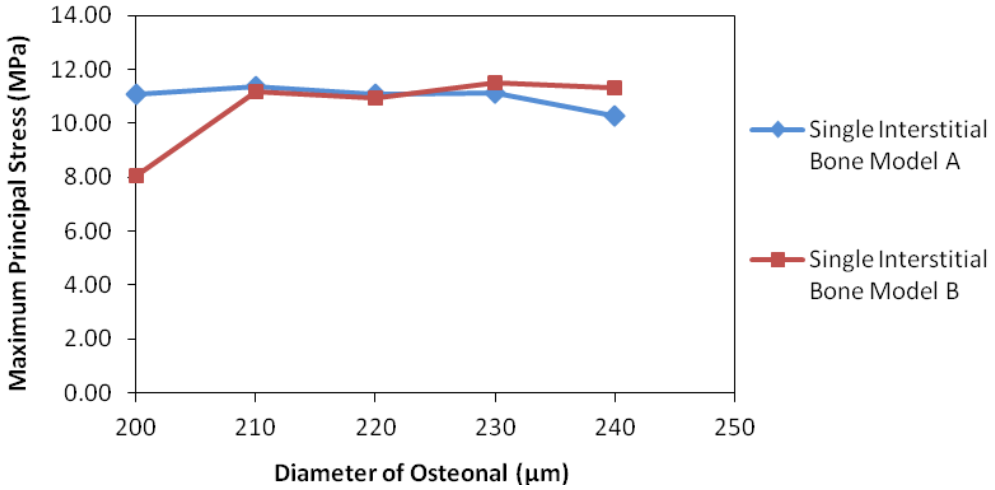

Figure 5.14 shows the maximum principal stress of interstitial model A and B.

5.3.3 Microstructural Stress and Strain Fields

In the present study, the stain contour plots showed that the Haversian and Volkman's canals, particularly in the intersections, indicated high strain concentrations under longitudinal loading. The model simulated the realistic loading on the Haversian system.

Single Osteonal Bone Model

Figures 5.15 and 5.16 shows the stress and strain distributions of model O3A and O4B (single sectioned osteonal). Due to the porosity of Haversian and Volkman's canals, 11% strain concentrations were observed under longitudinal loading.

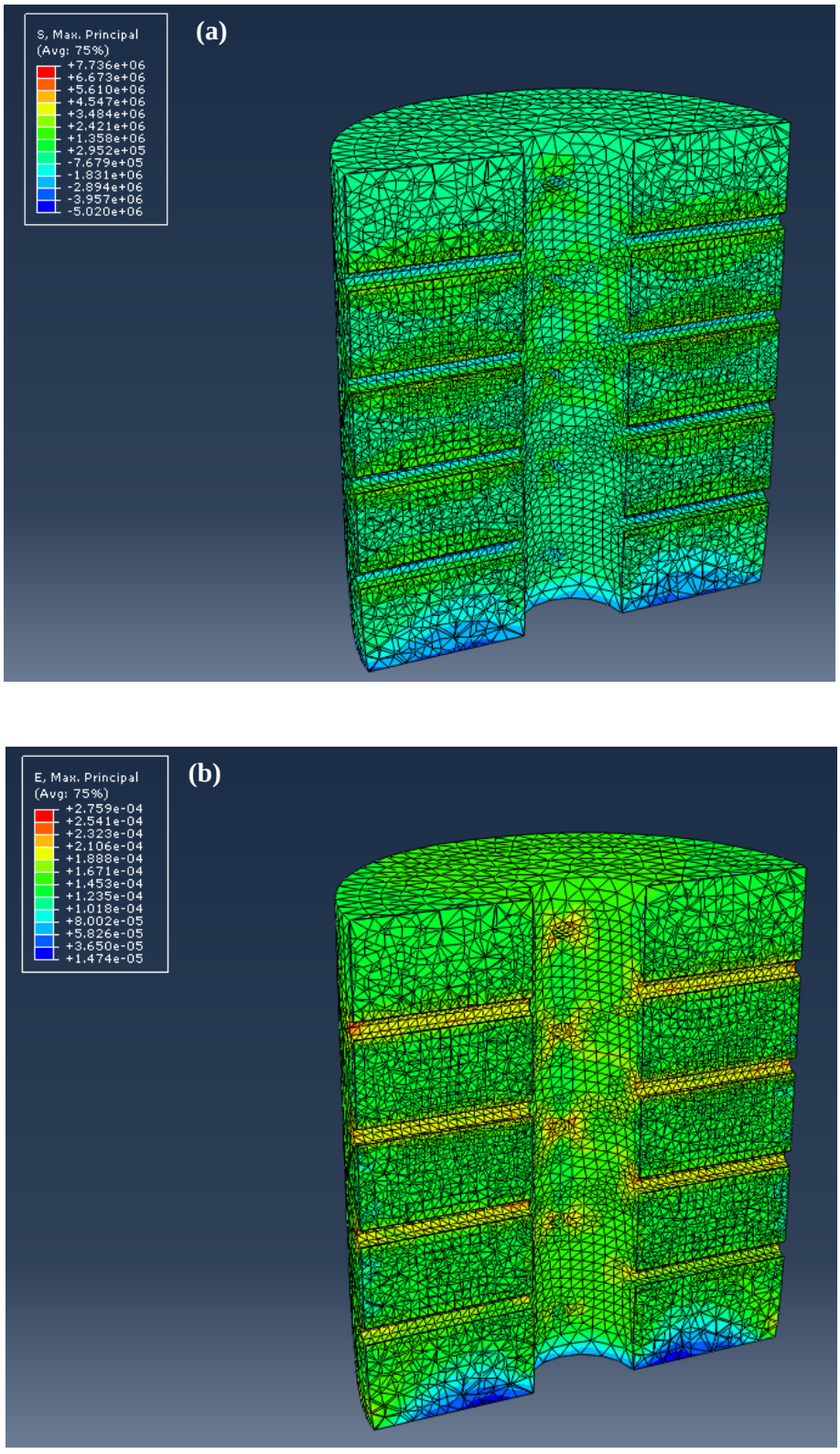

Figure 5.15 Sectioned model O3A, typical stress (a); typical strain (b), found in osteonal bone under compressive loading. The Volkman's canals evenly distributed.

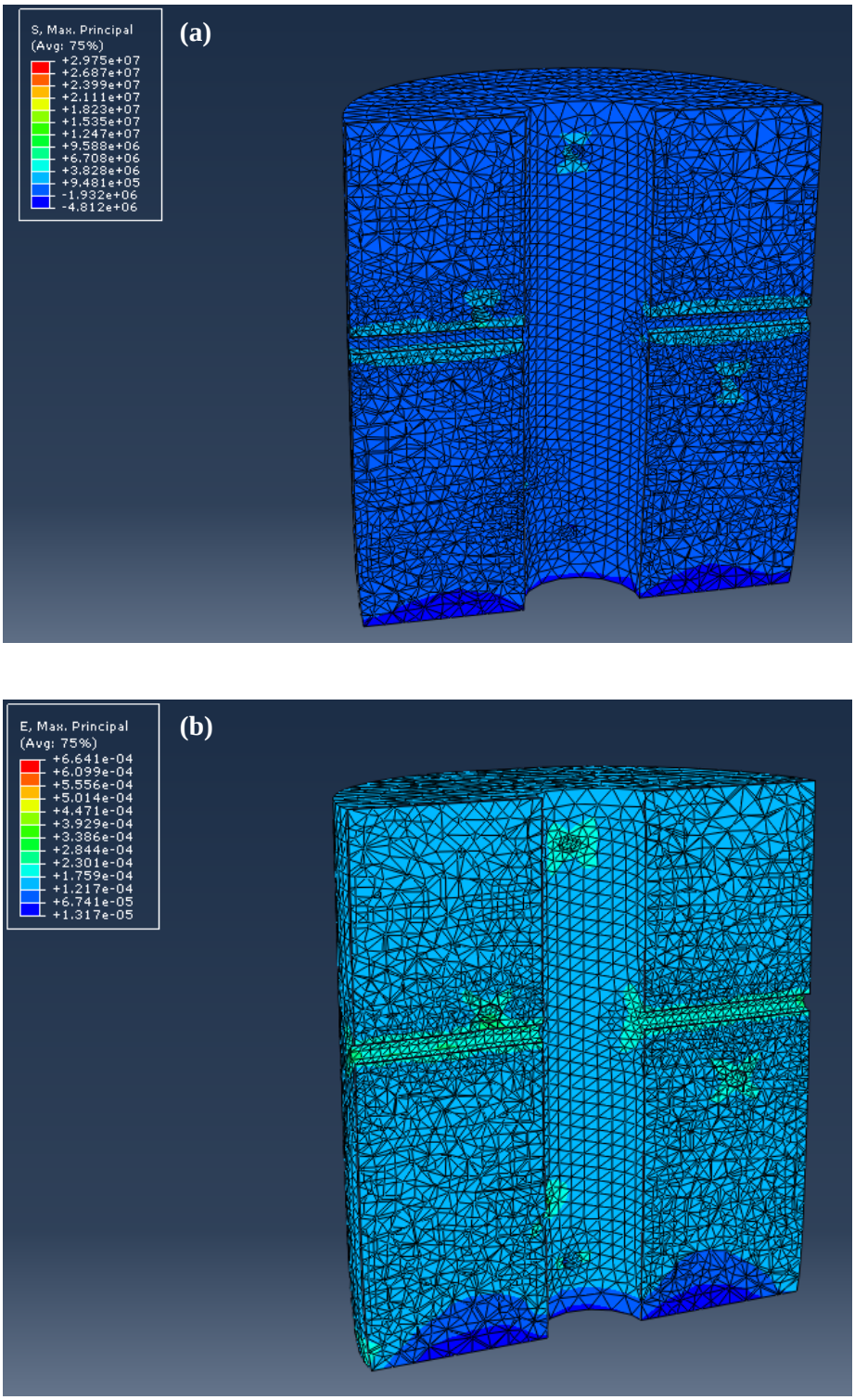

Figure 5.16 Sectioned model O4B, typical stress (a); typical strain (b), found in osteonal bone under compressive loading. The Volkman's canals are randomly distributed.

The S max distribution showed significant variation of stress in regions that were close to the intersections of the Haversian and Volkman's canals. These stresses were found to be around 47% and 71% and increased in OA and OB as the porosity of Haversian and Volkman's canals increased.

Average strain concentrations of 2.9 were observed in OA models, while in OB models, it was up to 9.7. This is due to the randomly distributed Volkman's canals. Figure 5.17 shows the maximum principal strain of the OA and OB models.

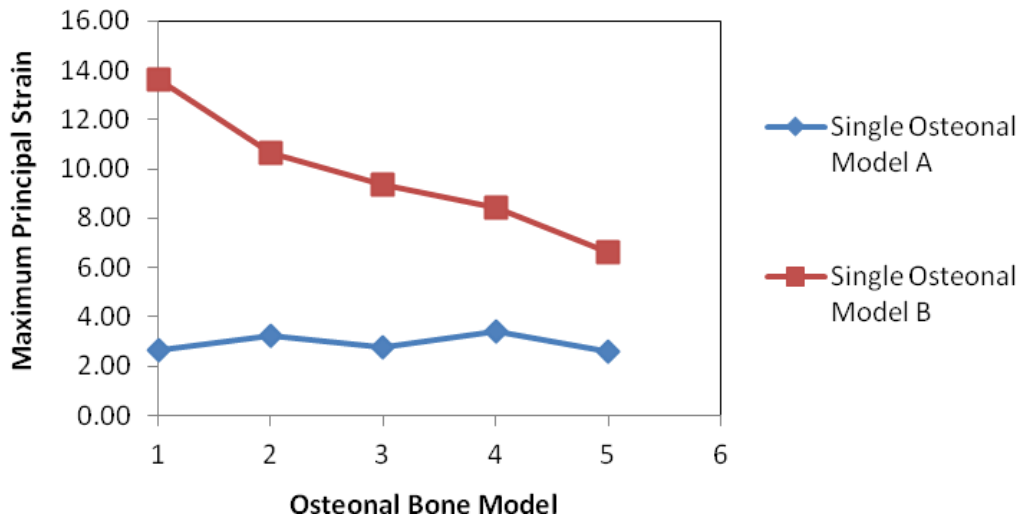

Figure 5.17 Maximum principal strain of osteonal bone model OA and OB

Osteonal Pattern Model

A group of four osteons were formed as a pattern to simulate the stress and strain distributions as a realistic loading on the Haversian system. Osteonal Pattern A (OPA) was formed by varying the diameter of the Haversian canal from 40 µm to 60 µm. The Volkman's canals were fixed at 10 µm and arranged evenly around the Haversian canals. For Osteonal Pattern B (OPB), the diameters of both Haversian

and Volkman's canals were varyied from 40 μm to 60 μm and 8 μm to 12 μm, respectively. Figure 5.18 presents the stress and strain distributions of OP5A.

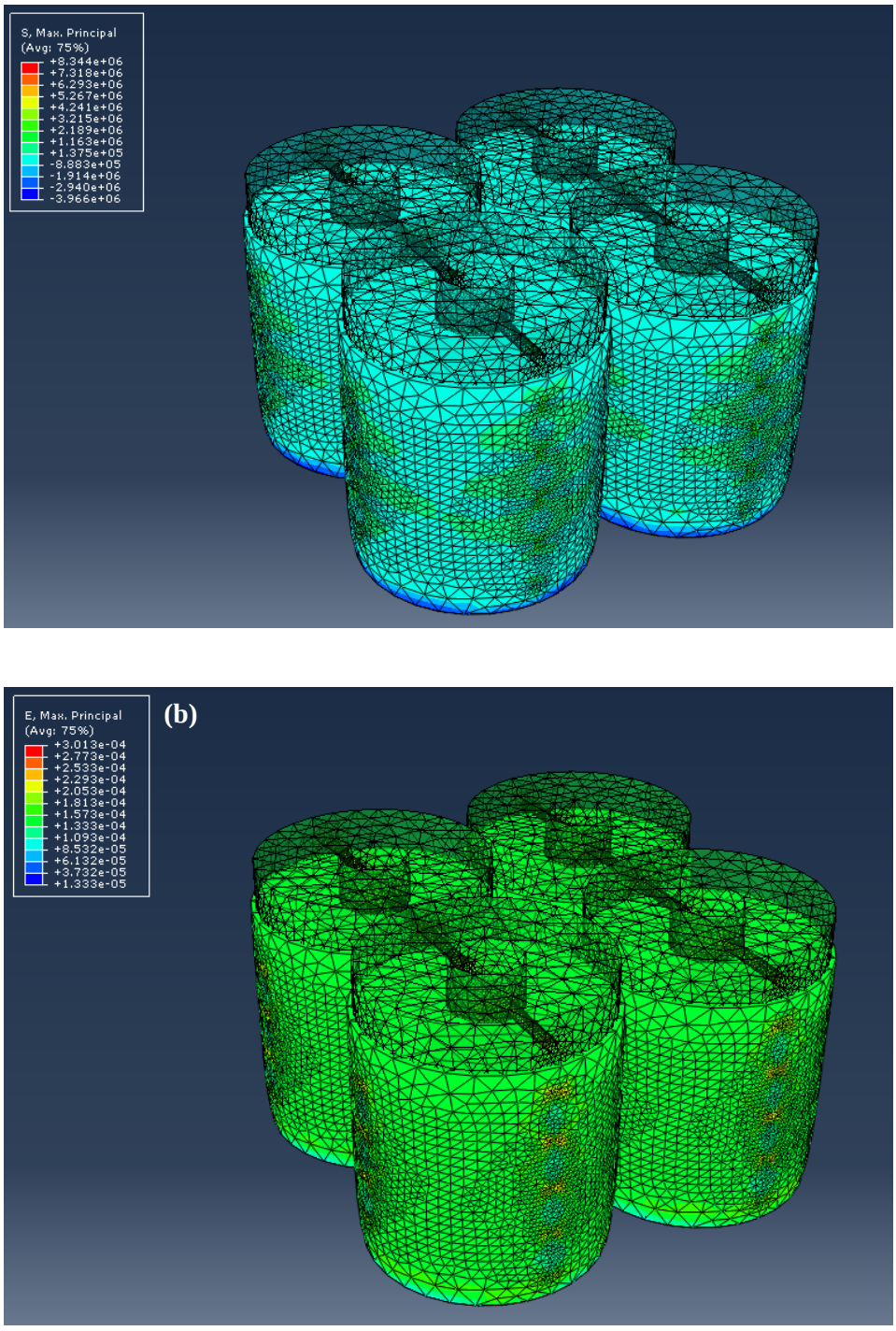

Figure 5.18 Sectioned model OP5A, typical stress, (a) and strain (b), found in osteonal bone under compressive loading. The Volkman's canals are evenly distributed.

In OPA, the average stress was around 7.2 MPa, while in OPB the average was around 7.8 MPa. This represented an increase of 7% in stress between these two models. This demonstrated that the change in the diameter of the Volkman's canals had no significant effect on the mechanical properties.

Average strain concentrations were observed to be 3.14 in OPA models, while in OPB models, it was 3.26. This is due to the different diameter in the generated the model. Figure 5.19 shows the maximum principal strain of OPA and OPB model.

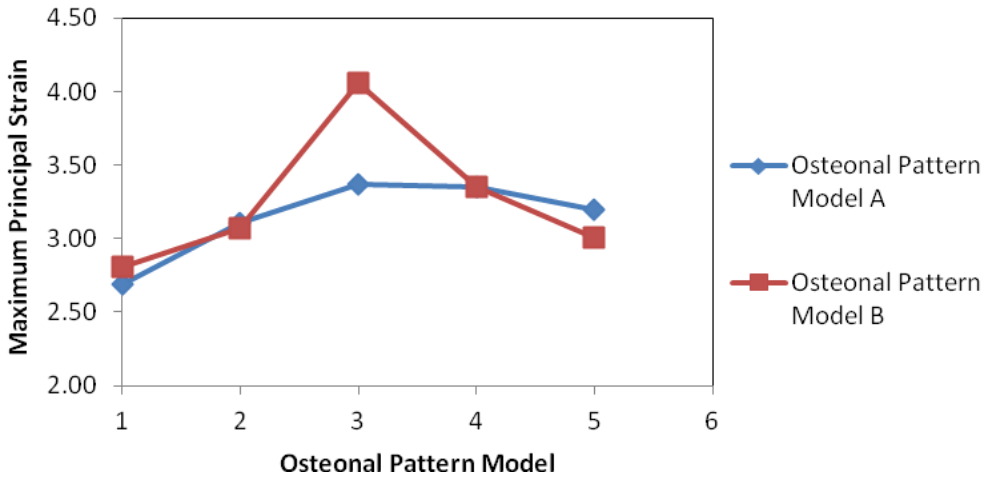

Figure 5.19 Maximum principal strain of osteonal bone model OPA and OPB

Single Interstitial Bone Model

Figures 5.20 and 5.21 show the stress and strain distributions of models I3A and I3B (single sectioned interstitial bone). The circular hollow represents the osteonal which varied in diameter; whilst the Volkman's canal in model A was arranged evenly with differing diameters. In model B, the osteonal and Volkman's canals also varied in diameter, but the Volkman's canals were randomly distributed.

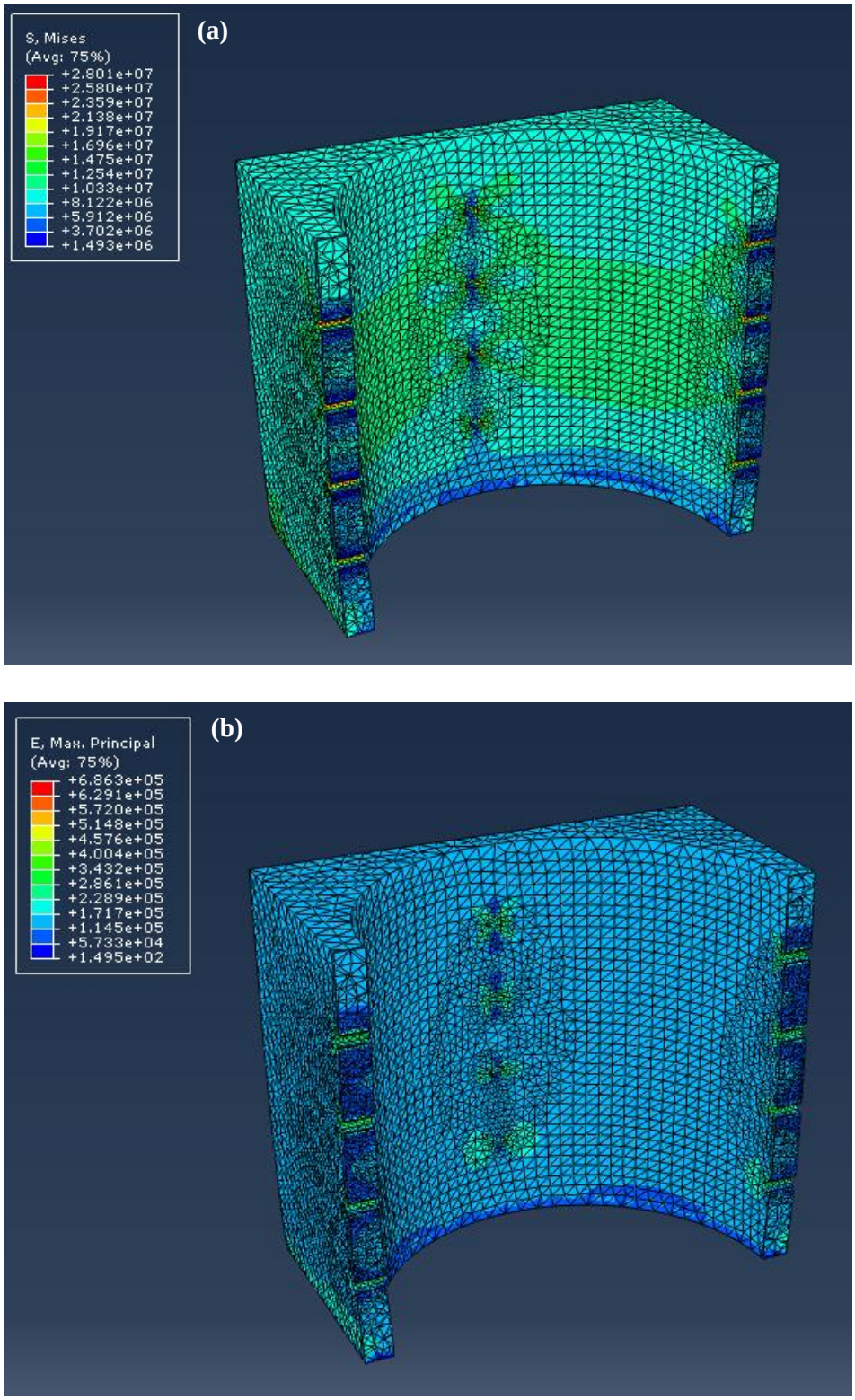

Figure 5.20 Sectioned model I3A, typical stress, (a) and strain (b), found in interstitial bone under compressive loading. The diameter of osteonal and Volkman's canals are varied and Volkman's canals are evenly distributed.

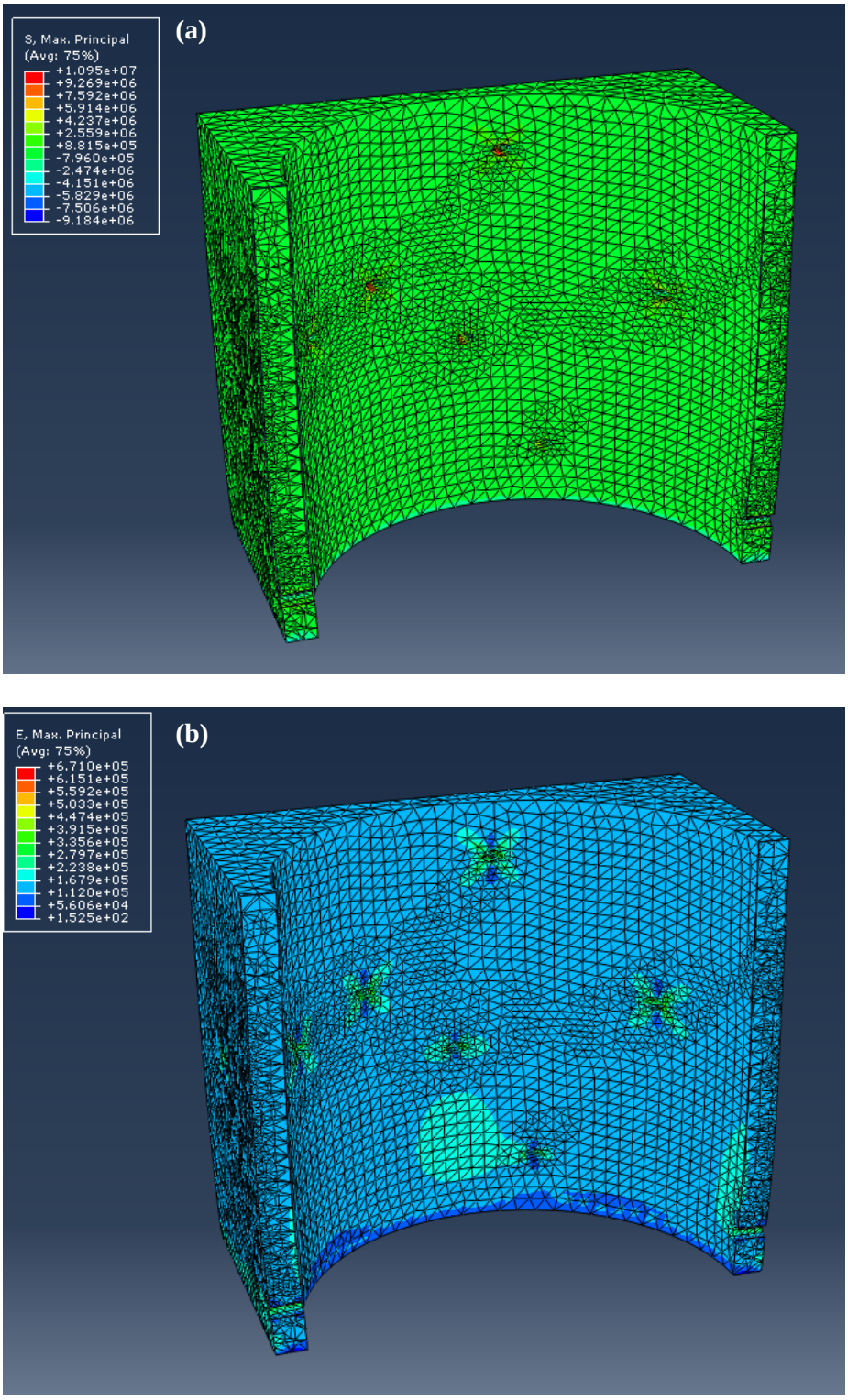

Figure 5.21 Sectioned model I3B, typical stress, (a) and strain (b), found in interstitial bone under compressive loading. Varying diameter in osteonal and Volkman's canals, and Volkman's canals are randomly distributed.

The S max distribution shows paramount variation of stress concentrations in two models. The average stresses observed in these two models are around 11 MPa and 10.5 MPa. The difference is small as the diameter of osteon and Volkman's canal increased.

Average strain concentrations, were observed to be 5.6 in both models, which shows that the influence of the change in diameter is less than models OA and OB. Figure 5.22 shows the maximum principal strain of IA and IB models.

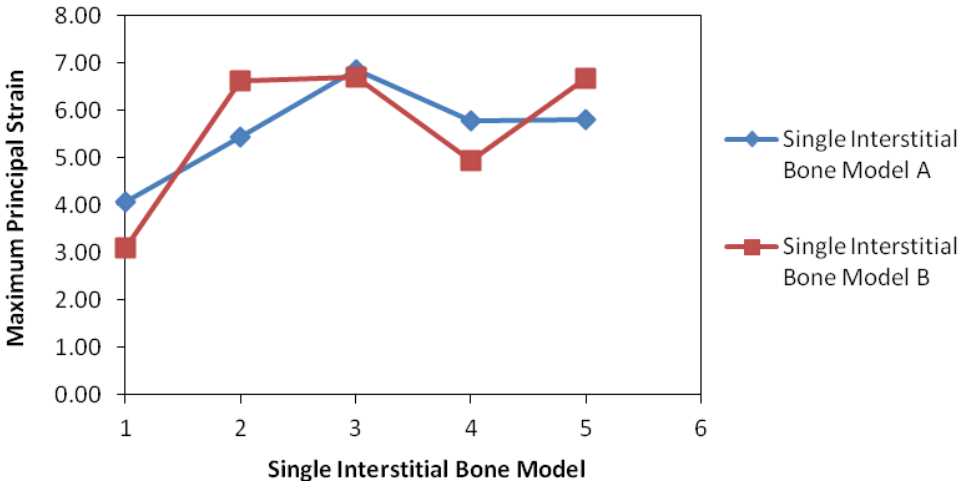

Figure 5.22 Maximum principal strain of single interstitial bone model IA and IB.

Interstitial Bone Pattern Model

In the interstitial bone pattern model, IP1-IP4 (A and B) the diameter of osteon was varied from 200 µm to 230 µm and the diameter of the Volkman's canals were fixed to 12 µm and distributed evenly and randomly perpendicular to the loading direction. In models IP5A and B, the diameter of the osteon and Volkman's canals varied from

200 µm to 240 µm and 10 µm to 12 µm, respectively. Figures 5.23 and 5.24 illustrate the stress and strain concentrations of models IP5A and B.

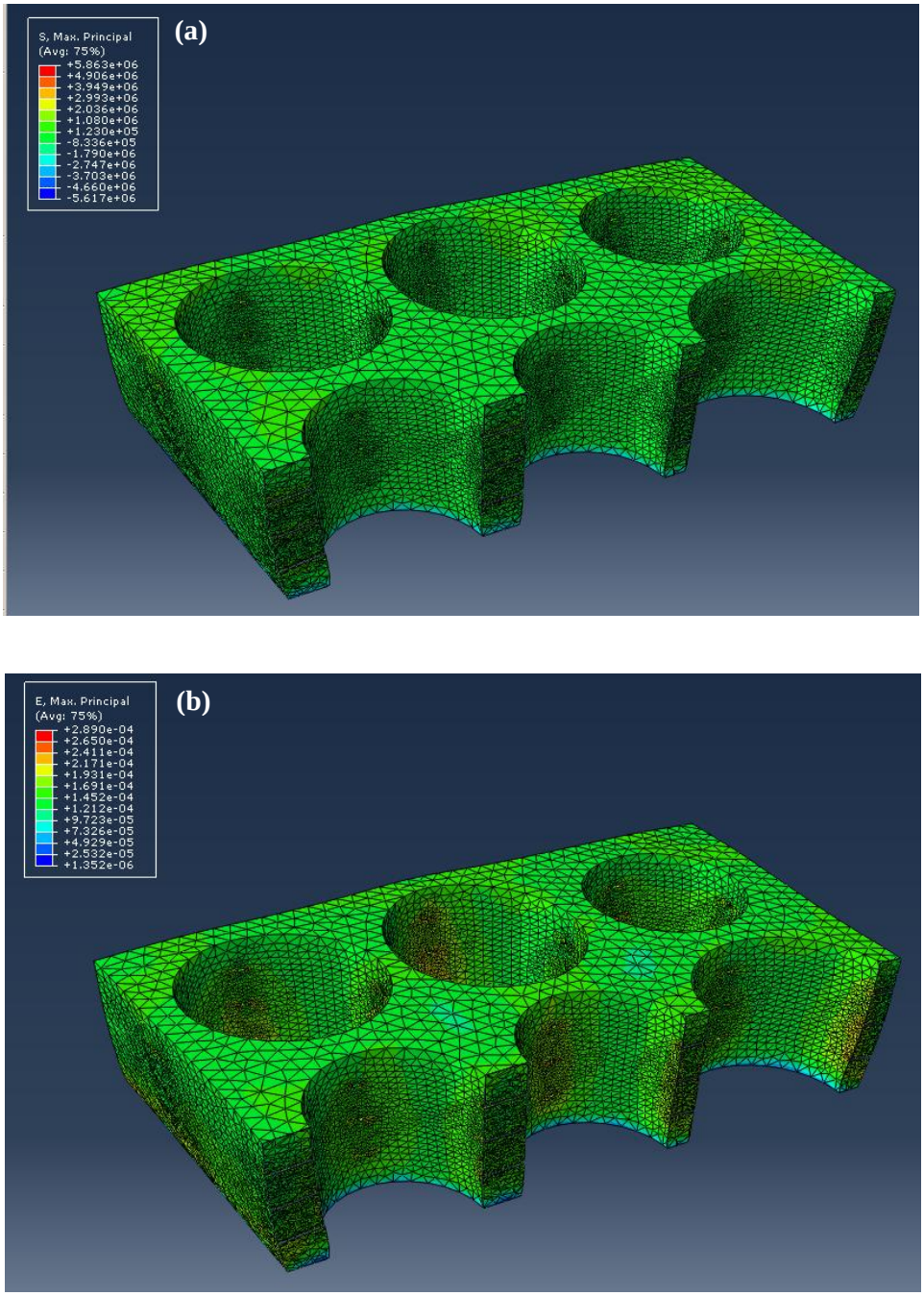

Figure 5.23 Sectioned model IP5A, typical stress, (a) and strain (b), found in interstitial bone pattern under compressive loading. Varying diameter in osteonal and Volkman's canals, and Volkman's canals are evenly distributed.

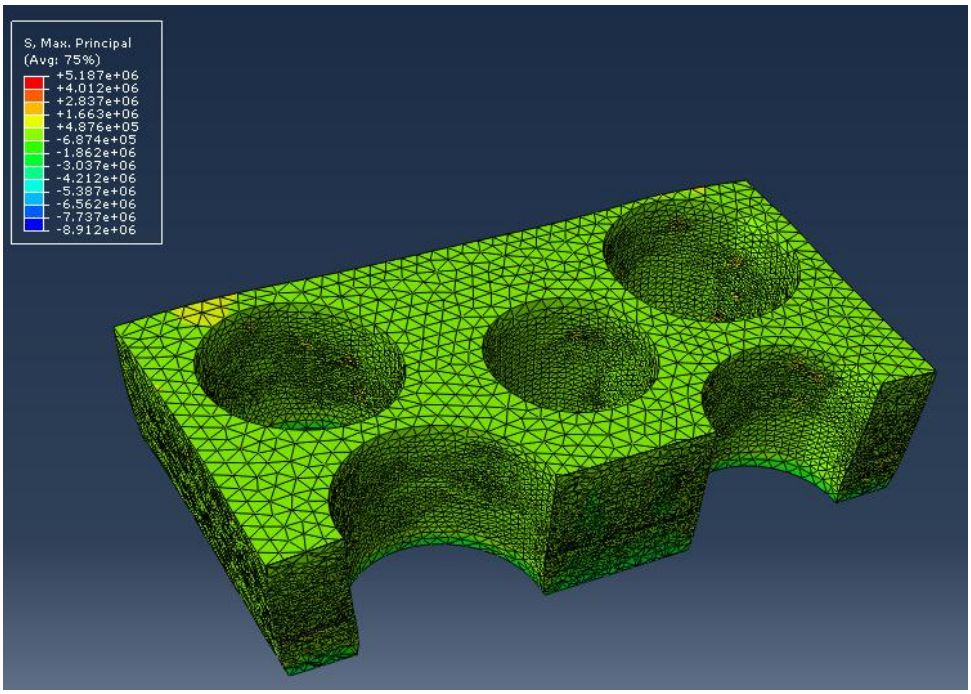

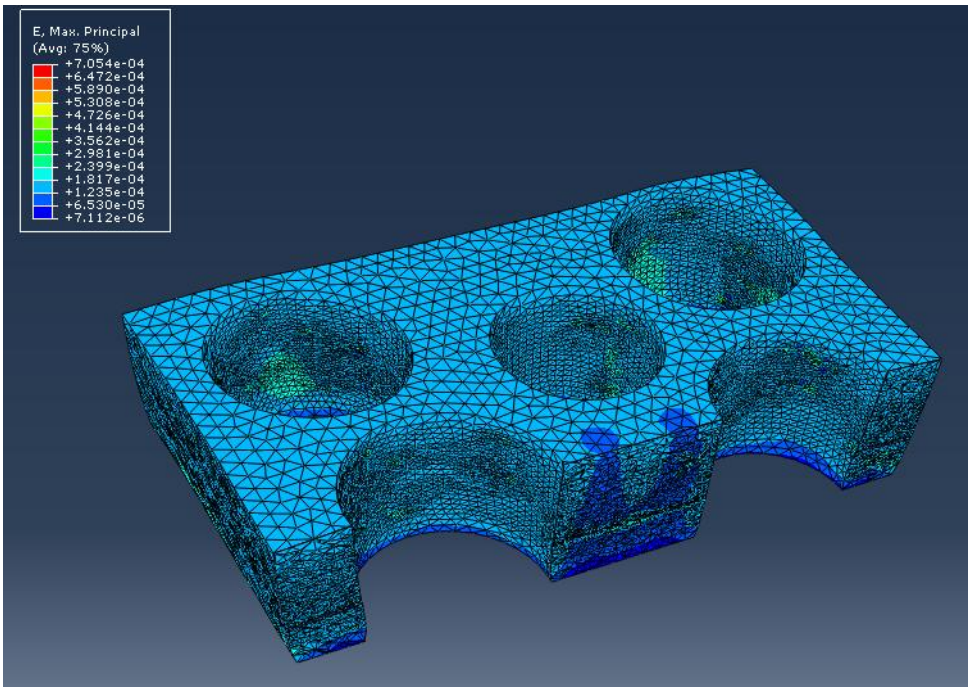

Figure 5.24 Sectioned model IP5B, typical stress, (a) and strain (b), found in interstitial bone pattern under compressive loading. Varying diameter in osteonal and Volkman's canals, and Volkman's canals are randomly distributed.

The average S max observed in model IPA is around 3 MPa, while in model IPB it is around 5.9 MPa. This is nearly 51% higher than in IPA. While in IP5 A and B, the S max is around 5.86 MPa and 5.18 MPa, respectively.

Average strain concentrations, were observed to be 2.7 in IPA, while in IPB it was up to 6.7. This is nearly an increases of 40% compared to IPA. Figure 5.25 shows the maximum principal strain of both models.

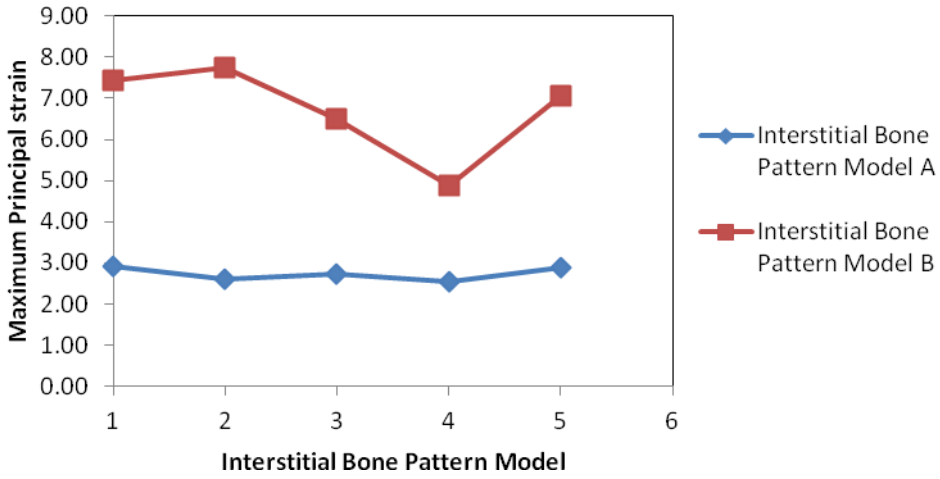

Figure 5.25 Maximum principal strain of interstitial bone pattern model IPA and B.

5.4 FEA Simulation Discussion

The objective of the FEA was to investigate the porosity effects of two main components of cortical bone, the osteonal and interstitial bone. The microstructural properties and its stress and strain fields were also examined. A single osteonal and interstitial bone were employed and simplified as a porous fiber composite to build the FEA models. The simplified osteonal and interstitial bone models were further formed as a pattern in order to observe a more realistic loading on the Haversian system. All the models were simulated under compressive loading in longitudinal direction as the majority of human daily activities are highly related to continuing and cyclic loads in the longitudinal direction.

The Volkman's canals were introduced in two different arrangements. One approach was arranged perpendicular and evenly around osteon. The other was randomly oriented around the osteon. Due to the fact that, the Volkman's canals provided connection between Haversian canals, therefore, in order to obtain a more realistic and accurate result, more than one Volkman's canal was generated in the model. Since no comprehensive studies have documented the variation of Volkman's canals and Haversian canals with increasing levels, this FEA study provides a comprehensive understanding of the relationship between various microstructural parameters and material properties at the microscale.

Varying the diameters of the Haversian canal and the distribution of the Volkman's canals in osteonal bone models (OA and OB) shows a significant difference in stress

and strain. Model OB observed a higher stress under loading in the longitudinal direction, with the average principal stress of OA around 5.5 MPa and around 27.8 MPa in OB. One of the major factors that lead to the differences between these two models was due to the change in diameter in the Haversian canals. As the diameter increased, the porosity within the osteon also increased. However, the differences in principal stress observed in interstitial bone models (IA and IB) are not explicit. The average principal stress shown in IA and IB was 11 MPa and 10.6 MPa, respectively. The influence of varying the diameter of osteon in interstitial bone model was less than the Haversian canal in osteonal bone model.

The increase of the porosity apparently affects the elastic modulus of cortical bone. Numerous researches have observed the significant correlations between porosity and cortical bone in determining the mechanical properties (Currey 1988; Cooper et al. 2004; Martínez-Reina et al. 2011). The findings of this study also well agree with Dong et al. (2004), who reported that the elastic modulus in longitudinal direction decreased significantly with the porosity in cortical bone.

Figure 5.26 shows the results of the maximum principal stress of OPA and OPB. In the OPA model, the Haversian canal is varies in diameters, but the Volkman's canals diameter were fixed. All arrangements were assumed to be evenly distributed. In the OPB model, both the Haversian and Volkman's canals varied in diameter, and the arrangements of Volkman's canals also remain evenly distributed. In the OPB, it was observed that as the diameters of the Haversian and Volkman's canals increased, the

maximum principal stress showed a 12.5% decrease. Since the Haversian and Volkman's canals were generated as cylindrical hollow tubes, an increase in the porosity within osteonal bone resulted in a decrease in modulus.

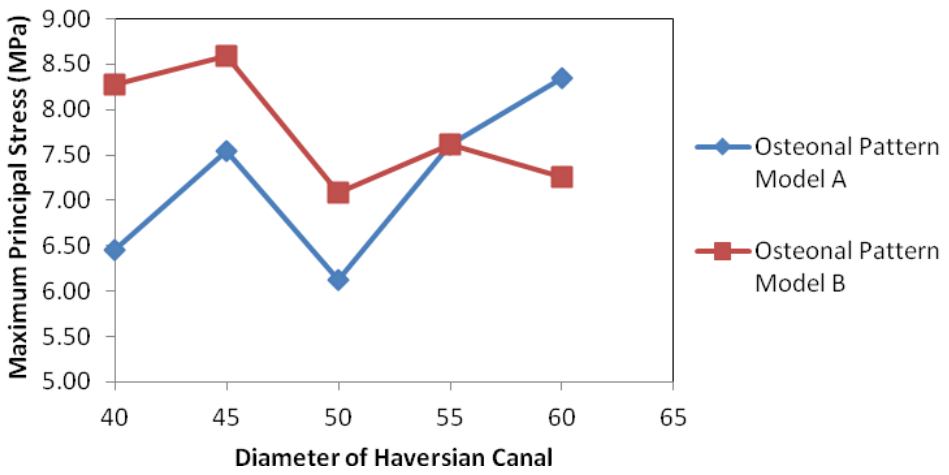

Figure 5.26 Maximum principal stress of osteonal pattern model OPA and B.

Another factor that affected the results was due to the orientation of the Volkman's canals. According to Mullins et al. (2007) randomly oriented arrangements of Volkman's canals can provide more realistic results, because the scattered Volkman's canals may be well explained the actual microstructure. Hence, the Volkman's canals were generated into evenly oriented arrangements and randomly oriented arrangements for comparison. In models IP5A and IP5B, the osteons are represented by cylinders of different diameters. The Volkman's canals were built in varying diameters in two approaches. The first was arranged evenly around the osteons, and the second were randomly arranged around the osteons. This was to generate a more realistic model of the microstructure of cortical bone. The maximum

principal stress obtained in IP5A was 5.86, while in model IP5B was 5.18. The difference between them is small. However, the Von Mises stress obtained in these two models was great with a 53% increase in IP6B as compared to IP6A.

Inspecting strain contour plots in this study indicated a high strain concentration of the Haversian and Volkman's canals, particularly at their intersections, with concentrations ranging from an average of 2.7 up to 9.7 under longitudinal loading. Models with randomly oriented arrangements of Volkman's canals presented higher strain magnification factors than the evenly oriented arrangements. This finding shows a consistency with Mullins et al. (2007), who mentioned that the magnified globally applied strain in regions closed to Haversian, Volkman's canals and their intersections could up to seven.

While this study does provide a framework of the power of microstructural modeling in predicting the porosity effect and oriented arrangements on the mechanical properties of cortical bone, there are several limitations that should be highlighted. Due to the complex hierarchical structure of bone, the motivation in selecting continuum levels which consisted of reliable material data is important. The smallest structural level selected in this study does not consider features such as canniculi, lacunae, individual lamellae and their interfaces; because the porosity proportion of such features is small, thus these features were ignored in this study. Another limitation was the variation of the ostoens material properties. According to Rho et al. (1999c), osteons can vary radically by up to 15% in the material properties. The

effect of such variation was excluded in the models. Since the linear elastic approach was used in this study, decisive conclusions about the fracture or post-yield behavior of the microstructure of cortical bone are not included. Again, the inaccuracies shown in the FE model can arise due to the segmentation and how to define the region for analysis.

In conclusion, this comparative study identified considerable variation of the mechanical properties of the cortical bone in the microstructural level. Two main components of the cortical bone, osteonal and interstitial bone were idealised and simplified as being regular geometries. The randomly oriented arrangements of the Volkman's canals were introduced in the models to yield more realistic results under longitudinal loading. Finally, this study may provide appropriate data to validate the relationship between the mechanical properties and the effect of porosity at the microstructural level. This validated FE model is able to predict the bone properties with the consideration of different bone porosity and its heterogeneous mechanical properties in osteonal and interstitial bone's longitudinal and lateral directions.

Chapter 6

Concluding Remarks and Suggestions for Future Research

6.1 Conclusion

The International Osteoporosis Foundation (IOF-2009) reported that there will be a dramatic increase of hip replacements by the year of 2030 in the USA. Over the past decades, an increase of hip fractures of 300% has been reported in Hong Kong. In fact, bone fractures have increased in importance as a health concern globally and continue to be burden among the aged population. The necessity of suitable grafting materials has become more and more significant.

Autograft bone is commonly used for bone replacement. However, it is limited in volume and additional surgery is often needed. Allograft and xenograft bone have been proposed as a substitute transplant material. Conventional sterilization methods such as autoclaving, gamma irradiation and ethylene oxide are associated with the

destruction of collagen and influence the quality of bone. Alternatively, heat-treatment of bone has been shown to be a promising sterilization method which can maintain both the mechanical and biological properties of bone.

The mechanical properties of bone at the micro-structural level and after heat-treatment are addressed in this study. The surface nanoindentation technique was employed to measure the localised mechanical properties of heat-treated bovine cortical bones along the long axis in both longitudinal and transverse directions. In the longitudinal direction, the E and H values of rib specimens were generally much higher than those in the transverse direction at all temperature ranges. These finding shows a significant correlation between the structural orientation of the collagen network and mechanical properties. As the temperature increased, the experimental results of both rib and femur specimen showed an increased in E and H values compared to the pristine specimen. While the E and H values showed a slight decrease when the specimen was heated at 160°C. Heat treatment from 90°C to 150°C was deemed to be acceptable from the biological and biomechanical points of view to be a practical bone graft substitutes.

Global mechanical properties of bovine cortical bone were conducted by compressive testing. The elastic modulus (E) of bone specimen in the compressive tests showed a slight increase of 11.4% in stiffness as the bone specimen was heat-treated to 90°C, and a significant increase of 60% in stiffness as it was heated-up to 150°C.

To understand the change of the composition of bovine cortical bone and how it relates to bone strength, backscattered electron (BSE) imaging was employed to examine the mineral content of the nanoindentation regions of bovine cortical bone. Although the weight percentage of calcium and phosphorous showed a slight decrease as temperature was increased to 150°C, however, this change might be due to the local variations and lower mineral contents existed in the BSE imaged region. In this study, the changes were not severe (with P content increasing and Ca/P ratio decreasing) and the measurements were localised.

Thermal gravimetric analysis (TGA) was employed to further observe the weight loss from rib and femur bone specimens from room temperature (23°C) to 850°C. The TGA results showed the organic components such as collagen, fat tissues and proteins were removed as the specimens were heated up to 200°C and completed at approximately at 600°C. The results clearly show a higher weight loss in rib specimens than that of the femur cortical bone specimens.

Preliminary studies of bovine cortical bone from present the relationship between the mineral content and the mechanical properties after heat-treated at different temperature ranges. In order to further investigate the effect of porosity and the mechanical properties of the microstructural level of cortical bone, various osteonal bone models and interstitial bone models were generated in this study. Varying the diameters of the Haversian and Volkman's canals represented an increased in porosity, which highly related to the decrease of the maximum principal stress. High

strain concentrations were observed around the Haversian and Volkman's canals and their intersections. The orientation arrangements of the Volkman's canals also played a paramount important role to the mechanical properties of the cortical bone.

In conclusion, it was demonstrated that heat-treated cortical bone is a promising bone grafting material. With the advantages obtained in the biological and mechanical properties of the heat-treatment of bone, it is proposed that this is a reliable and simple sterilisation method to overcome the risk of rejection and disease transfer form allograft and xenograft.

6.2 Suggestions for Future Research

There is a great need for additional research in the mechanical properties of the cortical bone, especially in conducting heat-treatment as a possible sterilisation method. There are limited experiments in investigating the mechanical properties of the microstructural level after heat-treatment. The experimental data of the mechanical properties in literature varies in a huge range. Variable such as the type of test, specimen size, individual characteristic (sex, age, weight, geometry, etc.), and location and section level can all affect the results of the experiments. It is difficult to define which parameters may affect the mechanical properties.

Since autograft and allograft bone grafts are limited in supply, xenograft bone is a possible substitute material for bone transplantation. However, the selection of the desired sterilisation methods is significant. The main concern of using xenograft bone is possible disease transmission during transplantation. Most of the sterilisation methods result in the destruction of collagen and affect the bone quality. Therefore, developing a better sterilisation method is essential and urgent.

For a better analysis of the mechanical behaviour of the microstrucutural level of cortical bone, accurate constitutive models would be required. The combinstion of advanced techniques such as micro-computed tomography and magnetic resonance can allow quantitative analysis of the geometries in the microstructural level of cortical bone to yield more realistic results.

Last but not the least, further studies in structures, mineral content, and material properties of heat-treated cortical bone are needed, both experimentally and theoretically, in order to gain further insight in the usage of bone grafting applications.

REFERENCES

Akhtar R, Morse S, Mummery PM. (2005), 'Nanoindentation of Bone in a Physiological Environment', *Mater. Res. Soc. Symp. Proc*, vol. 844, Y2.9.1-6.

Akhtar R, Eichhorn SJ, Mummery PM. (2006), 'Microstructure-based finite element modeling and characterization of bovine trabecular bone', *Journal of Bionic Engineering*, vol. 3, no. 1, pp. 003-009.

An Yuehuei H, Draughn RA. (2000), *Mechanical Testing of Bone and the Bone-Implant Interfacre*, CRC Press LLC.

Augat P, Schorlemmer S. (2006), 'The role of cortical bone and its microsturcture in bone strength', *Age and Ageing*, vol. 35, no. S2, pp.ii27-ii31.

Behari J. (2009), 'Biophysical Bone Behavior Principles and Applications', *John Wiley & Sons (Asia) Pte Ltd., Singapore*.

Bloebaum RD, Skedros JG, Vajda EG, Bachus KN, Constantz BR. (1997), 'Determining mineral content variations in bone using backscattered electron imaging', *Bone*, vol. 20, no.5, pp. 485-490.

Boccaccio A, Lamberti L, Pappalettere C. (2008), 'Accuracy of finite element predictions on bone/implant interface contact pressures for models reconstructed from CT scans', *J Mech Med Biol*. vol. 8, no. 2, pp. 161-82.

Boccaccio A, Ballini A, Pappalettere C, Tullo D, Cantore S, Desiate A. (2011), 'Finite element method (FEM), mechanobiology and biomimetic scaffolds in bone tissue engineering', *International Journal of Biological Sciences,* vol.7, no.1, pp. 112-132

Boskey AL, Wright TM, Blank RD. (1999), 'Collagen and bone strength', *J. Bone and Mineral Reseach*, vol.14, no. 3, pp. 330-335.

Bowman SM, Zeind J, Gibson LJ, Hayes WC, McMahon TA. (1996), 'The Tensile behavior of demineralized bovine cortical bone', *Journal of Biomechanics*, vol. 29, no. 11, pp. 1497-1501.

Buehler MJ. (2006), 'Nature design to tough collagen: explaining the nanostructure of collagen fibrils', *PNAS*, vol. 103, no. 33, pp. 12285-12290.

Burr DB. (2002), 'The Contribution of the organic matrix to bone's material properties', *Bone,* vol.31, no. 1, pp. 8-11.

Catanese III J, Featherstone JD, Keaveny TM. (1998), 'Characterization of the mechanical and ultrastructural properties of heat-treated cortical bone for use as a bone substitute', *J. Biomed. Mater. Res*, vol. 45, pp. 327-336.

Carter DR, Hayes WC. (1976), 'Bone compressive strength. The influence of density and strain rate.' *Science*, vol. 1174, pp. 194-195.

Carter DR, Hayes WC. (1997), 'The compressive behavior of bone as a two-phase porous structure', *J. Bone Jt. Surg*, vol. 59a, pp. 954-62.

Carter DR, Schwab GH, Spengler DM. (1980), 'Tensile fracture of cancellous bone', *Acta Orthop Scaned* vol. 51, pp. 733-41.

Chen G, Schmutz B, Epari D, Rathnayaka K, Ibrahim S, Schuetz MA, Pearcy MJ. (2010), 'A new approach for assigning bone material properties from CT images into finite element models', *Journal of Biomechanics*, vol. 43, pp. 1011-1015.

Chevalier Y, Pahr D, Allmer H, Charlebois M, Zysset . (2007), 'Validation of a voxel-based FE method for prediction of the uniaxial apparent modulus of human trabecular bone using macroscopic mechanical tests and nanoindentation', *Journal of Biomechanics*, vol. 40, pp. 3333-3340.

Choi K, Kuhn JL, Ciarelli MJ, Goldstein SA. (1990), 'The elastic moduli of human subchondral trabecular, and cortical bone tissue and the size-dependency of cortical bone modulus', *J Biomech*, vol. 23, pp. 1103-13.

Choi K, Goldstein SA. (1991), 'The fatigue properties of bone tissues on a microstructural level'. *Trans. 37th Orthop. Res. Soc*, vol. 16, pp. 485.

Cooper DML, Matyas JR, Katzenberg MA, Hallgrimsson B. (2004), 'Comparison of Microcomputed Tomographic and Microradiographic Measurements of Cortical Bone Porosity', *Calcified Tissue International*, vol. 74, pp. 437-447.

Cowin SC. (2001), *Bone Mechanics Handbook*. 2nd Edn, CRC Press, Washington, D.C.

Currey JD. (1988), 'The effect of porosity and mineral content on the Young's modulus of elasticity of compact bone', *Journal of Biomechanics*, vol. 21, no. 2, pp. 131-139.

Currey JD. (2001), 'Bone Strength: What are we trying to measure?', *Calcified Tissue International*, vol. 68, pp. 205-210.

Deng HW, Liu YZ. (2005), *Current Topics in Bone Biology*, World Scientific, Singapore.

Dong XN, Guda T, Millwater HR, Wang X. (2009), 'Probabilistic failure analysis of bone using a finite element model of mineral-collagen composites', *Journal of Biomechanics*, vol. 42, no. 3, pp. 202-209.

Donnelly E, Williams R M, Downs SA, Dickinson ME, Baker SP, van der Meulen MCH. (2006), 'Quasistatic and dynamic nanomechanical properties of cancellous bone tissue relate to collagen content and organization', *J. Mater. Res*., vol. 21, no.8, pp. 2106-2117.

Dunsmuir RA, Gallacher G. (2003), 'Microwave Sterilization of Femoral Head Allograft', *Journal of Clinical Microbiology*, vol. 41, no.10, pp. 4755-4757.

Fan.Z, Swadener JG, Rho JY, Roy ME, Pharr GM. (2002), 'Anisotropic properties of human tibial cortical bone as measured by nanoindentation', *Journal of Orthopaedic Research*, vol. 20, pp. 806-810.

Fan Z, Rho JY, Swadener JG. (2004), 'Three-dimensional finite element analysis of the effects of anisotropy on bone mechanical properties measured by nanoindentation', *J. Mater. Res*. vol. 192, no. 1, pp. 114-122.

Fan Z, Smith PA, Eckstein EC, Harris GF. (2006), 'Mechanical properties of OI type III bone tissue measured by nanoindentation', *J. Biomed. Mater. Res.* vol.79A, pp.71–77.

Fan ZF, Smith P, Rauch F, Harris GF. (2007), 'Nanoindentation as a means for distinguishing clinical type of osteogenesis imperfecta', *Composites: Part B*, vol. 38, pp. 411-415.

Fantner GE, Birkedal H, Kindt JH, Hassenkam T, Weaver JC, Curtroni JA, Bosma BL, Bawazer L, Finch MM, Cidada GAG, Morse DE, Stucky GD, Hansma PK. (2004), 'Influence of the degradation of the organic matrix on the microscopic fracture behavior of trabecular bone', *Bone*, vol.35, pp. 1013-1022.

Ferreira F, Vaz MA, Simões JA. (2006), 'Mechanical properties of bovine cortical bone at high strain rate', *Material Characterization*, vol. 57, pp. 71-79.

Finkemeier CG. (2002), 'Bone-grafting and bone graft substitutes', *Journal of Bone and Joint Surgery*, vol. 84-A, no. 3, pp. 454-464.

Fisher-Cripps AC. (2004), *Nanoindentation*, 2nd Edn. Springer.

Gray H. (1977), *Gray's anatomy*, New York, Bounty Books.

Gunn C. (2007), *Bones and Joints A Guide for Students*, 5th Edn. Churchill Livingstone, Edinburgh.

Gupta HS, Wagermaier W, Zickler GA, Aroush DRB, Funari SS, Roschger P, Wanger HD, Fratz P. (2005), 'Nanoscale deformation mechanisms in bone' *Nano Letters*, vol. 5, no. 10, pp. 2108-2111.

Gupta HS, Zioupos P. (2008), 'Fracture of bone tissue: The "hows' and the 'why" *Medical Engineering & Physics*, vol. 30, pp. 1209-1226.

Hambli R, Barkaoui A. (2012), 'Physically based 3D finite element model of a single mineralized collagen microfibril', *Journal of Theoretical Biology*, vol. 301, pp. 28-41.

Hamer A J, Stockley I, Elson RA. (1999), 'Changes in allograft bone irradiated at different temperatures', *The Journal of Bone and Joint Surgery*, vol. 81-B, pp. 342-4.

Helgason B, Taddei F, Pálsson H, Schileo E, Cristofolini L, Viceconti M, Brynjólfsson S. (2008), 'A modified method for assigning material properties to FE models of bones', *Medical Engineering & Physics*, vol. 30, pp. 444-453.

Hengsberger S, Enstroem J, Peyrin F, Zysset PK (2003), 'How is the indentation modulus of bone tissue related to its macroscopic elastic response? Avalidation study', *Journal of Biomechanics*, vol. 36, pp. 1503-150.

Hoc T, Henry L, Verdier M, Aubry D, Sedel L, Meunier A. (2006), 'Effect of microstructure on the mechanical properties of Haversian cortical bone', *Bone*, vol. 38, pp. 466-474.

Hoffler CE, Moore KE, Kozloff K, Zysset PK, Brown MB, Goldstein SA. (2000), 'Heterogeneity of bone lamellar-level elastic moduli', 'Bone', vol. 26, no. 6, pp. 603-609.

Holden JL, Clement JG, Phakey PP (1995), 'Age and Temperature Related Changes to the Ultrastructure and Composition of Human Bone Mineral', *Journal of Bone and Mineral Research*, vol. 10, no. 9, pp. 1400-1409.

Ionescu I, Conway T, Schonning A, Almutairi M, Nicholson DW. (2003), 'Solid modeling and static finite element analysis of the human tibia', *Summer Bioengineering Conference*, Florida.

Jämsä T, Rho J.Y, Fan Z, MacKay CA, Marks Jr SC, Tuukkanen J. (2002), 'Mechanical properties in long bones of rat osteopetrotic mutations', *Journal of Biomechanics* vol. 35, pp. 161–165.

J. Periodontol (2001), "Tissue banking of bone allografts used in periodontal regeneration", vol.72, no.6, pp.834-838.

Khan K, McKay H, Kannus P, Bailey D, Wark J, Bennell K. (2001), *Physical Activity and Bone Health*. Human Kinetics, United States of America.

Kenley RA, Yim K, Abrams J, Ron E, Turek T, Marden LJ, Hollinger JO. (1993), 'Biotechnology and bone graft substitutes', *Pharmaceutical Research*, vol. 10 no. 10, pp. 1393-1401.

Keller TS, Mao Z, Spengler DM. (1990), 'Young's modulus, bending strength, and tissue physical properties of human compact bone', *J Orthop Res*.,vol. 8, pp. 592-603.

Kotha SP, Guzelsu N. (2005), 'Tensile behavior of cortical bone: Dependence of organic matrix material properties on bone mineral content', *Journal of Biomechanics*, vol. 40, pp. 36–45.

Labastida-Pólito A, Piña-Barba C, Romero-Valdovinos MG, Tello-Solís SR. (2009), 'Physicochemical properties of collagen sheet from bovine femur', *Journal of Applied Biomaterials & Biomechanics*, vol.7, no.3, pp. 200-204.

Lau EMC, Ho SC, Leung S, Woo J. (1997), *Osteoporosis in Asia Crossing the Frontiers*. World Scientific Publishing Co. Pte. Ltd.

Laurencin CT, Khan Y. (2009), 'Bone graft substitute materials'. *eMedicine Clinical Procedures*. pp. 1-17 ((http://emedicine.medscape.com/article; viewed on 15 October, 2010)

Leikina E, Mertts MV, Kuznetsova N, Leikin S. (2002), 'Type I collagen is thermally unstable at body temperature'. *PNAS*, vol. 99, pp. 1314-1318.

Liu GR, Quek SS. (2003), *The Finite Element Method: A Practical Course*, Butterworth-Heinemann.

Lozano LF, Peña-Rico MA, Heredia A, Ocotlán-Flores J, Gómez-Cortés A Velázquez R. Belío IA, Bucio L. (2003), 'Thermal analysis study of human bone', *Journal of Materials Science*, vol. 38, pp. 4777-4782.

Martin RB, Burr DB, Sharkey NA. (1998), *Skeletal Tissue Mechanics*, Springer.

Martínez-Reina J, Domínguez J, García-Aznar JM. (2011), 'Effect of porosity and mineral content on the elastic constants of cortical bone: a multiscale approach', *Biomech Model Mechanobiol*, vol. 10, pp. 309-322.

Massaro EJ, RJM. (2004), *The skeleton biochemical, genetic, and molecular interactions in development and homeostasis*, in Human Press Inc., New Jersey.

Mkukuma LD, Skakle JMS, Gibson IR, Imrie CT, Aspden RM, Hukins DWL. (2004), 'Effect of the proportion of organic material in bone on thermal decomposition of bone mineral: an investigation of a variety of bones from different species using thermogravimetric analysis coupled to mass spectrometry, high-temperature X-ray diffraction, and fourier transform infrared spectroscopy', *Calcif Tissue Int.* vol. 75, pp. 321-328.

Mithal A, Lau E. (2009), *The Asian Audit Epidemiology, costs and burden of osteoporosis in Asia 2009*. International Osteoporosis Foundation Report.

Mullins LP, McGarry JP, Bruzzi MS, McHugh PE. (2007), 'Micromechanical modelling of cortical bone'. *Computer methods in Biomechanics and Biomedical Engineering*, vol. 10, no.3, pp. 159-169.

Murugan R, Ramakrishna S. (2005), 'Development of nanocomposites for bone grafting', *Composites Science and Technology*, vol. 65, pp. 2385-2406.

Nalla RK, Kinner JH, Ritchie RO. (2003), 'Mechanistic fracture criteria for the failure of human cortical bone', *Nat Mater* vol. 2, pp. 164-8.

Oliver WC, Pharr GM. (1992), 'An improved technique for determining hardness and elastic modulus using load and displacement sensing indentation experiments', *J. Mater. Res.*, vol. 7, pp. 1564-1583.

Ooi CY, Hamdi M, Ramesh S. (2007), 'Properties of hydroxyapatite produced by annealing of bovine bone', *Ceframics International*, vol. 33, pp. 1171-1177.

Ortiz M, Pandolfi A. (1999), 'Finite deformation irreversible cohesive elements for three-dimensional crack-propagation analysis', *Internal Journal for Numerical Methods in Engineering*, vol. 44, pp. 1267-1282.

Oyen ML. (2006), 'Nanoindentation hardenss of mineralized tissues', *Journal of Biomechanics*, vol. 39, pp. 2699-2702.

Parikh SN. (2002), 'Bone graft substitutes: past, present, future', *Journal of Postgrad. Med.*, vol. 48, no 2, pp. 142-8.

Raspanti M, Guizzardi S, De Pasquale V, Martini D, Ruggeri A, 'Ultrastructure of Heat-Deproteinated Com- pact Hone', *Biomaterials,* vol. 15, no. 6, 1994, pp. 433- 437.

Reilly DT, Burstein AH. (1974), 'The mechanical properties of cortical bone', *JBJS*, vol. 56, pp. 1001-1022.

Rho JY, Ashman RB, Turner CH. (1993), 'Young's modulus of trabecular and cortical bone material: ultrasonic and microtensile measurements', *J Biomech,* vol. 26, pp. 111-9.

Rho JY, Tsui TY, Pharr GM. (1997), 'Elastic properties of human cortical and trabecular lamellar bone measured by nanoindentation', *Biomaterials*, vol. 18, pp. 1325-1330.

Rho JY, Kuhn-Spearing L, Zioupos P. (1998a), 'Mechanical properties and the hierarchical structure of bone. Medical Engineering and Physics', vol. 20, pp. 92-102.

Rho JY, Tsui TY, Pharr GM. (1998b), 'Elastic properties of osteon and trabecular bone measured by nanoindentation', *Journal of Biomechanics*, pp. 31:21.

Rho J.Y., Tsui T.Y. Pharr G.M. (1998c), 'Elastic properties of osteons and trabecular bone measured by nanoindentation'. *11th Conference of the ESB, France.*

Rho. JY, Pharr GM. (1999a), 'Effects of drying on the mechanical properties of bovine femur measured by nanoindentation', *Journal of Materials Science: Materials in Medicine*, vol. 10, pp. 485-488.

Rho.JY, Roy II ME, Tsui TY, Pharr GM. (1999b), 'Elastic properties of microstructural components of human bone tissue as measured by nanoindentation', *J. Biomed. Mater. Res,* vol. 45, pp. 48-54.

Rho JY, Zioupos P, Currey JD, Pharr GM. (1999c), 'Variations in the individual thick lamellar properties within osteons by nanoindentation', *Bone* vol. 25, pp. 295-300.

Rho JY, Zioupos P, Currey JD, Pharr GM. (2002), 'Microstructural elasticity and regional heterogeneity in human femoral bone of various ages examined by nano-indentation', *J Biomech,* vol. 35, pp. 189-198.

Rice J.C, Cowin S.C., Bowman J.A. (1998), 'On the dependence of the elasticity and strength of cancallous bone on apparent density', *J Biomech*, vol. 21,pp.155-68.

Ritchie RO, Kinney JH, Kruzic JJ, Nalla RK. (2004), 'A fracture mechanics and mechanistic approach to the failure of cortical bone', *Fatigue Fract Engng Mater Struct*. vol. 28, pp. 345-371.

Roschger P, Paschalis EP, Fratzl P, Klaushofer K. (2008), 'Bone mineralization density distribution in health and disease', *Bone*, vol. 42, pp. 456-466.

Roylance D. (1999), 'Stress Strain Curve', Department of Mate-rials Science and Engineering, Massachusetts Institute of Technology, Cambridge, http://ocw.mit.edu/courses/materials-science-and-engineering/3-11-mechanics-of-materials-fall-1999/modules/ss.pdf

Schaffler MB, Burr DB. (1988), 'Stiffness of compact bone:effects of porosity and density', *J. Biomechanics*, vol.21, no. 1, pp. 13-16.

Shin S, Yano H, Fukunaga T, Ikebe S, Shimizu K, Kaku N, Nagatomi H, Masumi S. (2005), 'Biomechanical properties of heat-treated bone grafts', *Arch. Orthop. Trauma Surg*, vol.125, pp.1–5.

Stanishevsky A, Chowdhury S, Chinoda P, Thomas V. (2008), 'Hydroxyapatite nanoparticle loaded collagen fiber composites: Microarchitecture and nanoindentation study', *J. Biomed. Mater. Res*. vol. 86A, pp. 873-882.

Sevostianov I, Kachanov M. (2000), ' Impact of the porous microstructure on the overall elastic properties of the osteonal cortical bone', *J. Biomechanics*, vol.33, pp. 881-888.

Taddei F, Cristofolini L, Martelli S, Gill HS, Viceconti M. (2006), 'Subject-specific finite element models of long bones: An in vitro evaluation of the overall accuracy', *Journal of Biomechanics*, vol.39, no.13, pp. 2457-2467.

Tai K, Qi HJ, Ortiz C. (2005), 'Effect of mineral content on the nanoindentation properties and nanoscale deformation mechanisms of bovine tibial cortical bone', *Journal Materials Science: Materials in Medicine*. vol. 16, pp. 947-959.

Tatarinov A, Sarvazyan N, Sarvazyan A. (2005), 'Use of multiple acoustic wave modes for assessment of long bones: Model study', *Ultrasonics*, vol. 43, pp. 672-680.

Todoh M, Tadano S, Imari Y. (2008), 'Effect of heat densturation of collagen matrix on bone streng', *ICBME Proceedings*, vol. 23, pp. 2034-2037.

TriboScratch®user manual 2006, Hysitron, Inc., Minneapolis, MN.

Turner CH, Rho JY, Takano Y, Tsui TY, Pharr GM. (1999), 'The elastic properties of trabecular and cortical bone tissues are similar: results from two microscopic measurement techniques', *Journal of Biomechanics*, vol. 32, pp. 437-441.

Ural A, Vashishth D. (2006), 'Cohesive finite element modeling of age-related toughness loss in human cortical bone', *Journal of Biomechanics*, vol. 39, pp. 2974-2982.

Ural A, Vashishth D. (2007), 'Anisotropy of age-related toughness loss in human cortical bone: A finite element study', *Journal of Biomechanics,* vol. 40, pp. 1606–1614.

Ulrich D, van Rietbergen B, Weinans H, Rüegsegger P. (1998), 'Finite element analysis of trabecular bone structure: a comparison of image-based meshing techniques', *Journal of Biomechanics,* vol. 31, pp. 1187-1192.

Ulrich H, Zioupos P, Simpson R, Currey JD, Hynd D. (2008), 'The effect of strain rate on the mechanical properties of human cortical bone', *Journal of Biomechanical Engineering,* vol. 130, pp. 11011-8.

van Rietbergen B, Weinans H, Huiskes R, Odgaard A. (1995), 'A new method to determine trabecular bone elastic properties and loading using micromechanical finite-element models', *Journal of Biomechanics,* vol. 28, pp. 69-81.

van Rietbergen B, Majumdar S, Pistoia W, Newitt DC, Kothari M. (1998), 'Assessment of cancellous bone mechanical properties frome micro-FE models based on micro-CT, pQCT and MR images', *Technology and Health Care,* vol. 6, pp. 413-420.

Wang X, Bank RA, Teloppele JM, Athansiou KA, Agrawal CM. (1999), 'Effect of Collagen Denaturation on Bone Biomechanical Integrity', *45th Annual Meeting, Orthopaedic Research Society*, California, pp. 782

Wang X, Bank RA, TeKoppele JM, Agrawal CM. (2001), 'The role of collagen in determining bone mechanical properties', *Journal of Orthopaedic Research,* vol.19, no. 6, pp.1021-1026

Wang XJ, Chen XB, Hodgson PD, Wen CE. (2006), 'Elastic modulus and hardness of cortical and trabecular bovine bone measured by nanoindentation', *Transactions of Nonferrous Metals Society of Chin.* vol. 16, pp. 744-748.

Yang HS, Guo TT, Wu JH, Ma X. (2008), 'Finite element simulation of inhomogeneity and anisotropy of femur', *Proceedings of the 5th International Conference on Information Technology and Application in Biomedicine, in conjunction with the 2nd International Symposium & Summer School on Biomedical and health Engineering,* pp. 437-440.

Yeni YN, Fyhrie DP. (2001), 'Collagen-bridged microcrack model for cortical bone tensile strenght', *ASME Bioeng Conf,* vol.50, pp. 293-4.

Zioupos P, Currey JD, Hamer AJ. (1999), 'The role of collagen in the declining mechanical properties of aging human cortical bone', *J Biomed Mater Res,* vol. 45, pp. 108–116.

Zysset PK, Guo XE, Hoffler CE, Moore KE, Goldstein SA. (1999), 'Elastic modulus and hardness of cortical and trabecular bone lamellae measured by nanoindentation in the human femur', *Journal of Biomechanics*, vol. 32, pp. 1005-1012.

Reference from Website

http://www.feppd.org/ICBDent/campus/biomechanics_in_density/1dv_data/mech/basic_bone.htm; viewed on 15 January, 2011

http://hk.image.search.yahoo.com/search/images;_ylt=A2oKmKVNCmlQ4HcAd8uzygt.?p=collagen+fibrils+fibers&fr=FP-tab-web-t&fr2=piv-web; viewed on 15 January, 2011

http://www.iofbonehealth.org; viewed on January, 2013

http://www.hkosc.org/eng/osteoporosis05.html; viewed on 08 February, 2013

http://www.niams.nih.gov/health_info/bone/osteogenesis_imperfecta/default.asp; viewed on October, 2010

http://www.orpha.net/data/patho/GB/uk-OI.pdf; viewed on October, 2010

http://www.training.seer.cancer.gov/module_anatomy/unit3_1_bone_functions.html (National Cancer Institute); viewed on 15 January, 2011

http://www.spine.org/Documents/bone_grafts_2006.pdf; viewed on 16 May, 2011

http://www.hkosc.org/eng/osteoporosis05.html; viewed on 08 February, 2013

APPENDIX 1

Mechanical Properties of Bovine Cortical Bones Tested by compression, Tensile, Torsional, and Bending Testing (all at the tissue level) (An et al. 2000)

Bone	Specimen Dimensions (mm)	Strength (MPa)	Elastic Modulus (GPa)	Reference
Compressive Test				
Femur	3.8 x 2.3 x 7.6 dumbbell	133	24.1-27.6 [a]	McElhaney 1964
	2 x 2 x 6 dumbbell	240-295[a]	21.9-31.4 [a]	Reilly 1974
Tibia	4 x5 rectangular	165	23.8±2.2	Simkin 1973
	2 x 2 x 6 dumbbell	228±31	20.9±23.26	Reilly 1974
	Ø 3 cylindrical dumbbell	217±27	-	Cezaayirlioglu 1985
Tensile Test				
Femur	3.8 x 2.3 x 7.6 dumbbell	92	20.5	McElhaney 1964
	2 x 2 x 6 dumbbell	129-182 [a]	23.1-30.4 [a]	Reilly 1974
	Ø 3 cylindrical dumbbell	162 ±14 [a]		Cezaayirlioglu 1985
Tibia	4 x 5 x 30 dumbbell	136	7.1±1.1	Simkin 1973
	2 x 2 x 6 dumbbell	152±17	21.6±5.3	Reilly 1974
	2 x 2 x 6 dumbbell	188±9	28.2±6.4	Burstein 1975
Torsional Test				
Femur	3 x 3 x 6 dumbbell	62-67 [a]	-	Reilly 1975
	Ø 3 cylindrical dumbbell	76±6	-	Cezaayirlioglu 1985
Bending Test				
Femur	2 x 3.5 x 30 beam	-	18.5±2.8	Curry 1988
	2 x 4 x 35 beam	228±5	19.4±0.7	Curry 1988
	2 x 30.4 beam	209±13	18.1±0.5	Curry 1995
Tibia	4 x 4 x 35 beam	-	14.1	Simkin 1973
	4 x 10 x 80 beam	230±18	21.0±1.9	Martin 1993

[a] Range of average values